

Technical Report

Warwick Mobile Robotics: Urban Search and Rescue Robot

ES410 Group Project

15th March 2012

0709552

0803265

0816930

0816964

0819250

0818908

0823710

0826804

Abstract

The stimulus behind developing the field of Search and Rescue Robots is to save lives. Inspiration for specific robot design and capability however, depends on their potential tasks. Warwick Mobile Robotics (WMR) competes in the RoboCup Rescue League competition to demonstrate proficiency in search and rescue operations. The 2012 WMR team aims to improve the functionality and reliability of the Tele-Operated robot to exceed the results previously achieved.

Identification and evaluation of the specific problems from 2011 has highlighted the main robotic areas which require innovation and improvement. Specific design changes have been made to eradicate the functional problems recognised and pursue the target of greater reliability. Re-engineering, rather than pursuing a new design has been the focus of the changes made, which is particularly evident in the major mechanical part of the project – designing a robotic arm.

The results of the modifications can only be fully evaluated during the competition. This scenario tests all capabilities of our robotic system. A direct comparison of the success in 2011 compared to 2012 can only then be truly measured. However, some conclusions from the detailed design and theoretical application of the Mechanical Arm have resulted in reduced levels of backlash and mass as shown:

- Mass of the Mechanical Arm was reduced by 45%, with a 1kg mass relocation from the end effector position to the base joint
- Backlash in the Shoulder Joint has been reduced to a level where the only 'play' in the joint is caused by the distance between the tooth thickness and space width in any gearing transmission

Table of Contents

Abstract.....	I
Table of Figures.....	VI
1 Introduction	1
2 Literature Review	2
3 Product Improvement Methodology.....	5
3.1 SWOT Analysis of Previous Robot.....	5
3.1.1 Mechanical Investigation	5
3.1.2 Software and Systems Investigation.....	7
3.1.3 Electronic Investigation.....	8
3.2 Identified Improvements	8
3.2.1 Mechanical.....	8
3.2.2 Software.....	11
3.2.3 Electronics.....	13
3.3 Prioritised Improvements	13
3.3.1 Mechanical Arm	14
3.3.2 Head	15
3.3.3 Flippers.....	15
3.3.4 Chassis.....	15
3.3.5 Software and Systems.....	15
3.3.6 Electronics.....	16
4 Mechanical Arm	17
4.1 Objectives.....	17
4.2 Requirements.....	17
4.3 Formal Specification.....	18
4.4 Mechanical Breakdown.....	19
4.5 Design Intent.....	20
4.5.1 Fully Supported Motor Shaft.....	20
4.5.2 Modular Design of Joints	21
4.5.3 Mass Re-distribution	22
4.5.4 Shoulder Joint Loading.....	22
4.5.5 Concentric Mounting of Base Rotation.....	23
4.5.6 Potentiometers	24

4.6.	Design Calculations	25
4.7.	Joint and Link Design.....	27
4.7.1	Base Joint	27
4.7.2	Shoulder Joint	28
4.7.3	Elbow Joint	29
4.7.4	Wrist Joint	31
4.7.5	Head Joint	31
4.7.6	Rigid Links.....	32
4.8.	Post Design Analysis.....	32
4.8.1	Shoulder joint analysis	33
4.8.2	Elbow joint analysis.....	34
4.9.	Manufacture	36
4.9.1	Design for Manufacture	36
4.9.2	Machining.....	37
4.9.3	Rapid Prototyping	38
4.10.	Testing.....	38
4.10.1	Packaging of the Base Joint.....	38
4.10.2	Elbow Joint	39
4.10.3	Shoulder Joint	39
5	Head.....	40
5.1	Objectives.....	40
5.2	Requirements.....	40
5.3	Formal Specification.....	41
5.4	Design Intent.....	41
5.4.1	Integration of Sensors.....	41
5.4.2	Mounting.....	42
5.4.3	Material.....	42
6	Flippers.....	44
6.1	Objectives.....	44
6.2	Requirements.....	44
6.3	Formal Specification.....	45
6.4	Process Flowchart	45
7	Software and Systems.....	47
7.1	Objectives.....	47

7.2	Requirements.....	48
7.3	Formal Specification.....	49
7.4	Design Intent.....	49
7.4.1	Mapping	49
7.4.2	Inverse Kinematics	57
7.4.3	QR Code Reading.....	58
7.4.4	Centre of Mass	59
7.5	Testing.....	61
7.5.1	Mapping	61
7.5.2	Inverse Kinematics	62
7.5.3	QR Code Reading.....	62
7.5.4	Centre of Mass	63
8	Electronics.....	63
8.1	Objectives.....	63
8.2	Requirements.....	63
8.3	Formal Specification.....	64
8.4	Design Intent.....	64
8.4.1	Absolute Encoders	64
8.4.2	Battery Sensor.....	66
8.4.3	Stack Configuration.....	67
8.4.4	Wiring.....	68
9	Critical Review.....	71
9.1	Chassis Design.....	71
9.2	Flipper Design	71
9.3	Mechanical Arm Design	71
9.4	Head Design	72
9.5	Software and Systems.....	72
9.6	Electronics.....	73
10	Conclusions	73
11	References	75
	Appendices.....	79
A	Mechanical Arm.....	79
A.1	Analysis of 2010/2011 arm	79
A.2	Motor shaft straightening jig	83

A.3	Efficiency calculations.....	84
A.4	Speed calculations.....	85
A.5	Tangential loading calculations.....	85
A.6	Worm gears and backlash.....	86
A.7	Technical Drawings	88
B	Head.....	101
B.1	Analysis of Design	101
C	Flippers.....	102
C.1	Distorted Flipper Components.....	102
C.2	Static force exerted onto motors due to robot weight	102
C.3	Loading due to step field fall.....	103
C.4	Analysis of force distribution on the flipper motor shaft	104
D	Software.....	106
D.1	Camera Pixel Mapping	106
D.2	Java centre of gravity calculation classes.....	109
E	Electronics.....	111
E.1	Hall Effect Theory.....	111

Table of Figures

Figure 1: Mind Map of Mechanical Arm Ideas.....	9
Figure 2: Mind Map of Head Ideas.....	9
Figure 3: Mind Map of Flipper Ideas.....	10
Figure 4: Mind Map of Chassis Ideas	11
Figure 5: Mind Map of Software and Systems Ideas	12
Figure 6: Mind Map of Electronics Ideas	13
Figure 7: Decision Parameters	14
Figure 8: (shown left) Front View of Arm	17
Figure 9: (shown right) Rear View of Arm.....	17
Figure 10: Five Revolute Joints of the Arm	19
Figure 11: Thrust Spigot and Ball Bearing.....	20
Figure 12: Centre Distance altered by adding and removing shims	21
Figure 13: Router in the Base Joint.....	22
Figure 14: Shoulder Joint Motor Positioning and Accurate Meshing of Teeth.....	23
Figure 15: Cross-section of sleeve and Shoulder Bolt with Teeth Mesh	24
Figure 16: Mounting of Potentiometer.....	24
Figure 17: Torque Requirement Diagram	25
Figure 18: Exploded Diagram of the Base Joint	27
Figure 19: (shown left) Rear View of Motor	28
Figure 20: (shown right) Front View of Motor.....	28
Figure 21: Driven Joint (Shoulder Joint).....	28
Figure 22: Exploded Diagram of Shoulder Joint.....	29
Figure 23: Exploded Diagram of the Elbow Joint	30
Figure 24: Wrist Joint (Housing RX-64 servo-motor)	31
Figure 25: Head Joint	31
Figure 26: Advantages of Dual Tube Design	32
Figure 27: Shoulder Link Analysis (Abaqus)	33
Figure 28: Section View through FEA Analysis of the Shoulder Joint	33
Figure 29: FEA Analysis of Ball Bearing Housing	34
Figure 30: Section View through the FEA Analysis of the Ball Bearing Housing.....	35
Figure 31: FEA Analysis of the Keyway Uprights.....	35
Figure 32: Section View of Elbow Joint Upright.....	36
Figure 33: Base Plate - Two Set-ups and Three Tool Changes	37
Figure 34: Bridgeport Series II Interact 4 - CNC Milling Machine ⁽²²⁾	37
Figure 35: Support Motor Plate - Difference in Machined Part vs. Rapid Prototyped Equivalent	38
Figure 36: Router in the Machined Base.....	39
Figure 37: (shown left) Arm Structure	39
Figure 38: (shown right) Complete Elbow Joint Assembly	39
Figure 39: (shown left) Base Joint Construction	40
Figure 40: (shown right) Shoulder Joint Gearing Construction	40
Figure 41: Axis M1054 Security Webcam ⁽²⁴⁾	42
Figure 42: (shown left) Net Shape of Head.....	43
Figure 43: (shown right) CAD Image of Head Base Plate	43

Figure 44: Head Hood Cover	43
Figure 45: Process Flowchart of Flipper Design Process.....	46
Figure 46: The Hokuyo URG-04LX and xSens MTi mounted for positional agreement.....	51
Figure 47: LiDAR orientation definitions.....	51
Figure 48: LiDAR pulse angles	52
Figure 49: Simultaneous Localisation and Mapping (SLAM) using a LiDAR module.....	53
Figure 50: Large 2D map produced by Duke University's DP-SLAM	55
Figure 51: Map produced by tinySLAM.....	56
Figure 52: An example QR code, containing WMR's homepage URL.....	58
Figure 53: Final rotational transformation	60
Figure 54: Robot centre of gravity geometry.....	60
Figure 55: A 3D point cloud of the project leader, created by new LiDAR software.....	61
Figure 56: The textured point-cloud resulting from a Kinect (RGBD camera) scan of the teleoperated chassis	62
Figure 57: Melexis MLX90316 (42)	65
Figure 58: Encoder PCB.....	65
Figure 59: Vishay Model 357 (43)	66
Figure 60: Battery with attached LiPo warning circuit.....	67
Figure 61: Stack Configuration.....	67
Figure 62: Harwin Connectors (44)	68
Figure 63: Stack Arrangement by Component.....	69
Figure 64: Wiring Diagram	70
Figure 65: The cantilever loading on an unsupported motor shaft.....	79
Figure 66: The damaged thrust bearing housings	80
Figure 67: The router in the head	80
Figure 68: The complex geometry from the arm joints.....	81
Figure 69: Shoulder joint motor position.....	82
Figure 70: Section through the base joint.....	82
Figure 71: Cross section of a bent worm gear	83
Figure 72: The motor shaft straightening jig	83
Figure 73: Diagram of worm and worm wheel gear transmission	87
Figure 74: Anti-backlash gear design	88
Figure 75: Stress on the head design from a 100N force.....	101
Figure 76: Displacement of head structure due to impact on side and front faces	101
Figure 77: Distortion in flipper motor housing	102

1 Introduction

Urban Search and Rescue Robots represent a significant opportunity to increase the speed at which searching for survivors is carried out in response to disaster sites. Tackling ruins poses great difficulty and complexity, which is amplified in the immediate aftermath of events. One of the considerable advantages of robot use in this situation is a social benefit; robots can enter dangerous environments without putting humans at risk.

At a high level the purpose of this report is to enhance knowledge in the field of Urban Search and Rescue Robots, but more explicitly, it details the evolution of the Warwick Mobile Robotics (WMR) Tele-Operated Robot. The WMR Search and Rescue Robot project is now in its fifth year of operation, and each year the main objective is to improve the robot with new and innovative solutions that demonstrate quality engineering ingenuity. The design changes and implementations derived by the WMR Team of 2011/2012 are described and explained in this report.

The organisation and scope of the report follows a simple structure, which begins by analysing the final robot developed by the WMR Team in 2010/2011. Preliminary examination to identify areas of improvement was carried out using the Strengths, Weaknesses, Opportunities and Threats (SWOT) technique used for strategic planning. The adaptations conform to the over-riding objectives set as,

- Re-engineering the 2010/2011 robot to deliver a greater level of performance in terms functionality and reliability
- Successfully competing in the 2012 German RoboCup Rescue Competition

The scope of the project meant that it was only feasible to embark upon a small number of robotic features identified, which were chosen based on a range of factors including time, cost and the skills of the human resource available. The logical process of initiating the design specification for each individual area and the delivery of design changes with supporting theory is outlined. Analysis of the design changes complements our theoretical approach and a critical review highlights mistakes and

alternative approaches that could have made our improvements more successful. Hence, future work recommendations and conclusions of the 2011/2012 changes can be made.

2 Literature Review

Research in the field of Search and Rescue Robotics can be divided into two individual areas, Tele-Operation and Autonomy. Tele-Operation necessitates a human operator, often in a remote location, whereas an Autonomous robot is purely controlled by its own intelligence. All robots in this field have a need for physical proficiency, for example advanced locomotion, and a need for an intelligent system on board, whether this is purely a perception facility or a combination of functions that include mapping or autonomy for example⁽¹⁾.

There are many different platforms for Search and Rescue Robots, designed depending on the environments they are likely to be deployed in. Sandin describes the various platforms of robot mobility, and defines them in four subcategories as wheeled, tracked, walking and special cases⁽²⁾. In Search and Rescue Robot applications terrain can often be unconventional and demanding, therefore requiring a highly accomplished locomotive system. Sandin states that six tracked robots (two flippers at each end with a central driving track) as having 'truly impressive mobility'⁽²⁾. Mobility in Search and Rescue can be seen to be making even greater inroads at the pinnacle of technology in example robots such as the Bari Bari and IRS Soryu. The Bari Bari supports rubble while moving slowly moving underneath it towards the person in trouble⁽³⁾ while the IRS Soryu is made up of individual bodies which can twist and crawl through narrow spaces⁽⁴⁾.

Detection of human life or unsafe conditions in rescue missions highlights the importance of on board perception/sensory equipment in carrying out successful operations. Burion states that the most commonly used sensor types for human detection are infra-red imaging cameras⁽⁵⁾. However this is not the only sensor type which can be considered. A range of sensors for Search and Rescue

Robot victim identification are considered in Table 1 below (summarised from Burion ⁽⁵⁾ and RoboCup Federation ⁽⁶⁾).

Sensor Type	System	Sensing method	Typical range	Advantages	Disadvantages
Visible Light Sensor	Webcam	RGB CCD	Variable field of view with lenses. Support HD quality video streaming	High quality image capture in real time	Limited with fixed lenses. Multiple lens solutions cost extra money
Stereoscopic Cameras	Dual CCD	RGB CCD	Variable field of view with lenses.	Allows geometry mapping	Computationally challenging
Infra-Red Sensor	Infra-Red Camera module	Wavelengths between CCD	5-14 μm	Live feed image capture with false colour image calibration	Higher quality pixel solutions increase cost
Pyroelectric sensor	Infra-Red sensor tailored to body heat	Detects heat signatures by using motion sensing	5 - 14 μm detection	Small, durable low cost. Commonly used for human detection	Require motion, however moving the sensor relative to object is an option
CO2 Sensor	Gas detection Module	Chemical detection	0-10000 ppm CO2 detection	Low cost	Subject to external noise (CO2 from other sources)
Natural Gas Sensor	Gas Detection	Chemical Detection	300-50000 ppm natural gas detection	Low cost	Not suitable for detecting life

Table 1: Human Identification Sensors

Sensors are not only used for victim identification. They can also aid autonomous capabilities and mapping functionality. For example, LiDAR sensors are used to map the disaster environment, producing a replication of where the robot has travelled ⁽⁷⁾. Mapping capability is a very current research issue in this field, with 3D mapping and SLAM techniques at the forefront of innovation. SLAM techniques aim to resolve issues where a robot does not have prior knowledge of the configuration of the world and it must generate a map as it travels, while also tracking its location in

the map generated so far ⁽⁸⁾. New families of algorithms are being developed to perfect this ambition reliably, accurately and in ‘real’ time as described by Kleiner and Dornhege ⁽⁹⁾. A comparison of such algorithms can be found in section 7.4.1.2 of this report.

Robotic arms are an important feature of Search and Rescue Robots. They allow sensors to be positioned in areas which are difficult to reach (e.g. at heights) and can be used to deliver human essentials or physically aid a mission. Table 2 below summarises some of the common robotic arm concepts.






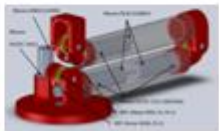
Arm Method	Advantages	Disadvantages	Image
Woodstock joint - Hyper Redundant Arm	High DOF, Low Cost	Poor reliability	
Ball Screw Joint - Hyper Redundant Arm	High DOF	Poor reliability, Expensive	
Pneumatic actuation	High power output, light weight, Capable of high accuracy	Pneumatic systems needs to be implemented	
Linear Servo Actuation	High Power output, readily available	Complex linkage systems may be required to transmit useful power	
Rotary Servo Actuation	High Power Output, Cheap	Possibility of high load on small gears	
Electric motor with gear assembly actuation	Many design options	Weight in comparison to other options. Revolute joint robots require more programming than other robot types	

Table 2: Robotic Arm Concepts ^{(10) (11) (12) (13) (14) (15) (16) (17)}

3 Product Improvement Methodology

3.1 SWOT Analysis of Previous Robot

A series of SWOT analysis matrices were used to assess the advantages and disadvantages of specific areas of the Tele-Operated Robot before any changes were made. By evaluating each area individually, thoughts could be directly focussed on developing specific goals (design changes/improvements) to meet the high level objectives set. It should also be noted that the RoboRescue League competition rules for 2012 were taken into account when considering potential opportunities.

3.1.1 Mechanical Investigation

Table 3, 4, 5 and 6 illustrate the SWOT Analyses carried out for the Mechanical components of the robot.

STRENGTHS	WEAKNESSES
<ul style="list-style-type: none"> • Some functionality, ability to move in independent joint motions • Reach length of 1m • Support of sensors in Head 	<ul style="list-style-type: none"> • Backlash in joints • Unsupported shafts led to bent motor shafts • 'Top Heavy' robot arm • Joints 'over-engineered' and needed 5-axis machining • Constant high torque needed to move arm (shoulder joint), leading to motor failure
OPPORTUNITIES	THREATS
<ul style="list-style-type: none"> • Decreasing joint movement and backlash improves rigidity • Support the motor shafts to prevent bending allows accurate meshing of the gears • Modular design will facilitate accurate meshing and facilitate the ease of manufacture • Reduce mass by using different materials and rapid prototyped parts • Used to 'pick and place' objects e.g. water bottles 	<ul style="list-style-type: none"> • Motor shafts need to be repaired and straightened, hence affecting any future use • Distribution of mass of the arm will have an effect on Robot's overall Centre of Mass as the arm changes position

Table 3: SWOT Analysis for the Mechanical Arm

STRENGTHS	WEAKNESSES
<ul style="list-style-type: none"> • Effective gripper • Contains and protects the sensors from impact • Cheap material and simple manufacturing process 	<ul style="list-style-type: none"> • Spare Volume (not packaged efficiently) • Router in Head increases weight • Difficult to access Head sensors for maintenance • Gripper ends have sharp corners • Fixing methods use Glue and Tape (not reliable)
OPPORTUNITIES	THREATS
<ul style="list-style-type: none"> • Move router out of head to reduce weight • Mechanically fasten sensors to Head structure for reliability • Integrate sensors and use a lighter material to reduce weight 	<ul style="list-style-type: none"> • Sensors in the Head are at the Front = Front Heavy Head • Many sensors make the load furthest away from the base relatively heavy

Table 4: SWOT Analysis of the Head

STRENGTHS	WEAKNESSES
<ul style="list-style-type: none"> • Enables robot to climb up/down slopes and over step fields • Spreads robot weight over a greater area 	<ul style="list-style-type: none"> • Chain slack makes actual position of flippers in space difficult to be known • Motor housing experiencing significant deformation despite improvements • Rear Flipper unable to raise robot
OPPORTUNITIES	THREATS
<ul style="list-style-type: none"> • Reduce slack in Flippers and use absolute position encoders for accuracy • Reduce the force transferred through the Flippers to prevent bending of the housing • Enable Flippers to lift robot 	<ul style="list-style-type: none"> • Strengthening housing may lead to damage in other areas (e.g. chassis, screw holes & motor) • Flipper modifications will have an impact on chassis design • Inability to climb complex terrain

Table 5: SWOT Analysis of the Flippers

STRENGTHS	WEAKNESSES
<ul style="list-style-type: none"> • 'Best Mobility' in the RoboCup Competition • Houses the motors and electrical stack well • Tracks are effective over many terrains 	<ul style="list-style-type: none"> • Motors are all mounted in cantilever fashion • Mounting bolts go through thin sheet • Large amounts of mass located at the rear of the body
OPPORTUNITIES	THREATS
<ul style="list-style-type: none"> • Smaller Chassis to manoeuvre through smaller gaps • Weatherproof the Chassis 	<ul style="list-style-type: none"> • Chassis damage when driving over step fields • Centre of mass of the chassis towards the rear, likely toppling on inclines

Table 6: SWOT Analysis of the Chassis

3.1.2 Software and Systems Investigation

STRENGTHS	WEAKNESSES
<ul style="list-style-type: none"> • Java’s modular, object orientated style is very effective for prototyping changing code on changing hardware • Rich code history stored on SVN <ul style="list-style-type: none"> - Attempts at SLAM - IR image heat-spot finding • Functional operator interface • Robust low latency connection between robot and interface 	<ul style="list-style-type: none"> • Java’s relatively low computational speed • Redundant code slowing development • No inverse kinematics, only direct joint-control • Operator interface robot visual representation incomplete: <ul style="list-style-type: none"> - Flipper motion relative, often wrong - No tilt representation - Arm outdated • Interface IR stream non-functional • Duplex audio non-functional • 2D SLAM non-functional • 3D SLAM non-existent • Not a fully Tele-Operational system
OPPORTUNITIES	THREATS
<ul style="list-style-type: none"> • Competition point-scoring: <ul style="list-style-type: none"> - Satisfy new QR code rules - Implement IR feed for visual victim identification - Implement IR hotspot for automated victim identification - Implement 2D SLAM for improved arena navigation - Implement 3D SLAM for judging • Migrate code to C • Strip out redundant code • Implement inverse kinematics, improving controllability and facilitating head-mounted sensor use 	<ul style="list-style-type: none"> • Loss of competition points: <ul style="list-style-type: none"> - Failure to read QR codes - Failure to identify victims by heat - Failure to produce 3D (GeoTIFF) map • Poor arena navigation • Hardware damage due to non-intuitive, unchecked arm control • Hardware damage due to toppling

Table 7: SWOT analysis of Software and Systems

3.1.3 Electronic Investigation

STRENGTHS	WEAKNESSES
<ul style="list-style-type: none"> • Good drive power • Already have all sensors needed for competition • Stack is already set up with correct layout of components 	<ul style="list-style-type: none"> • Reliability of power-boards • Encoders don't give absolute positioning • Underpowered motor-boards (AX500) • Lack of battery monitor • Bad wiring without diagram – wires do not maintain a single colour from head to base • Connections made by glue
OPPORTUNITIES	THREATS
<ul style="list-style-type: none"> • Increasing robot stability • Make wiring easy to follow throughout the robot (caused blowouts last year) • Increasing power of motor-boards will provide power needed to lift the arm • Increasing reliability of power-board will prevent camera drop-outs and sensor malfunctions • Prevent over-discharging batteries 	<ul style="list-style-type: none"> • Unreliable power-board may cause catastrophic failure during use • If flippers are not set up before use the robot could damage itself by causing the flippers to force themselves into each other • Batteries can be easily over-discharged • Electronics are critical in making the robot operate

Table 8: SWOT Analysis of the Electronics

3.2 Identified Improvements

Improvement ideas were based on complementing the acknowledged strengths, maximising the opportunities highlighted, while eradicating the notable weaknesses and reducing the impact of possible threats.

3.2.1 Mechanical

3.2.1.1 Mechanical Arm

At a high level, Figure 1 details ideas which were identified as a by-product of the initial SWOT analysis. As described in Table 1, major improvement areas were identified as reducing the overall mass of the arm and reducing backlash in joints to generate a greater degree of functionality and reliability. Several ideas and concepts, as shown, were assessed in order to meet this objective.

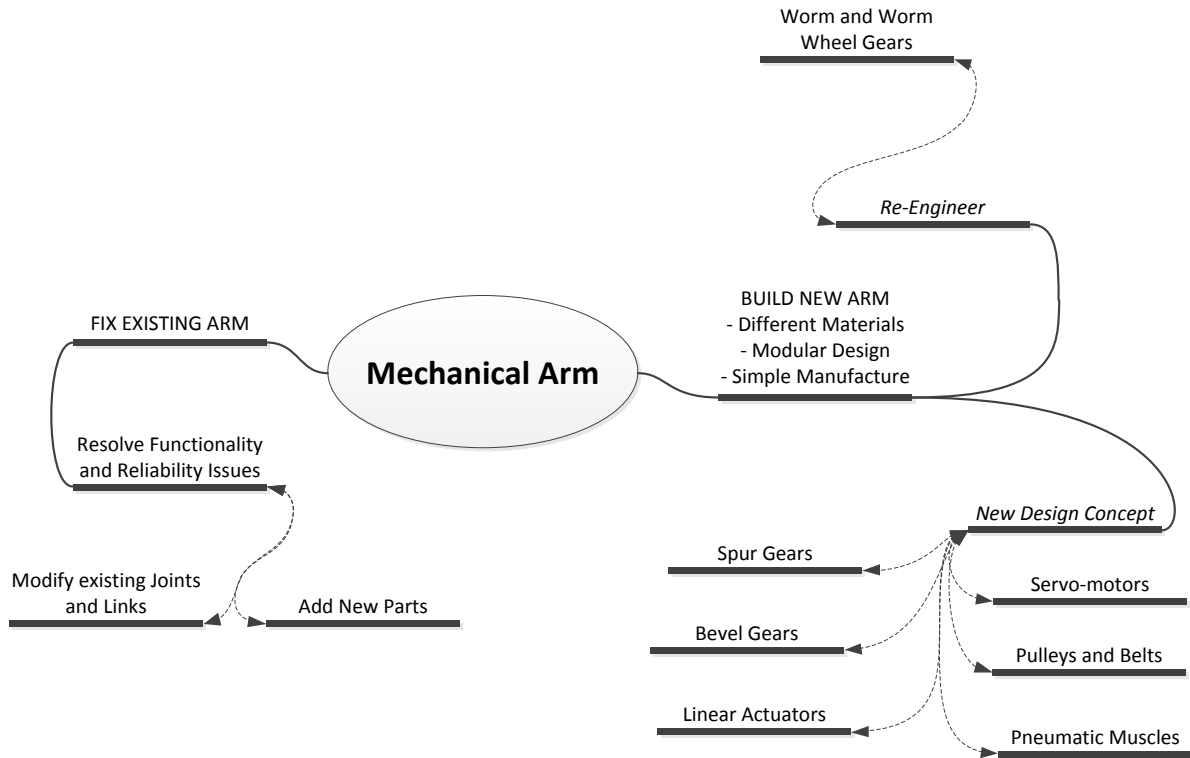


Figure 1: Mind Map of Mechanical Arm Ideas

3.2.1.2 Head

Objectives realised by completing a SWOT analysis are such that, the Head needs to be reduced in mass and volume, as well as securely mounting an array of sensors. Figure 2 indicates how these objectives could be met.

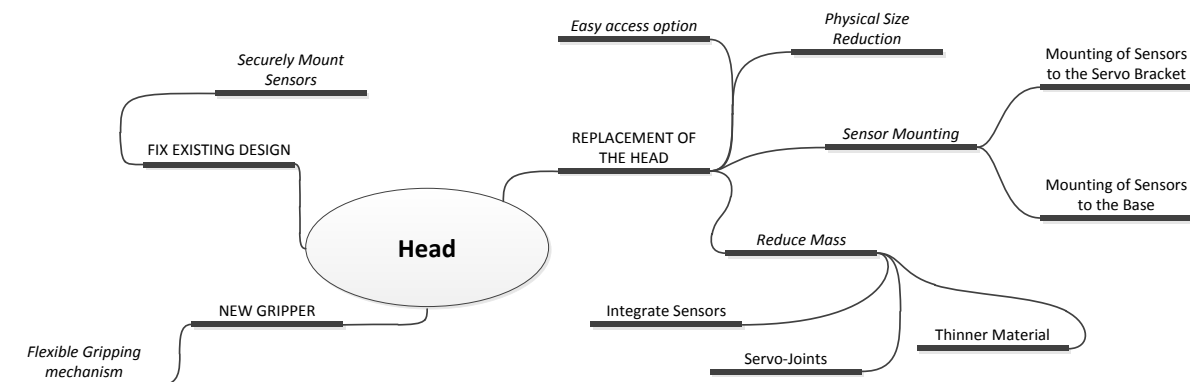


Figure 2: Mind Map of Head Ideas

3.2.1.3 Flippers

The SWOT analysis in section 3.3.1 (Table 5) shows how the reduction in chain 'slack' is of high importance. This is so that the actual position of the Flippers can be accurately known. Also highlighted, is the goal of reducing or transferring the level of force exerted on the Flipper motors, as this is causing deformation. Figure 3 considers numerous solutions to resolve these issues.

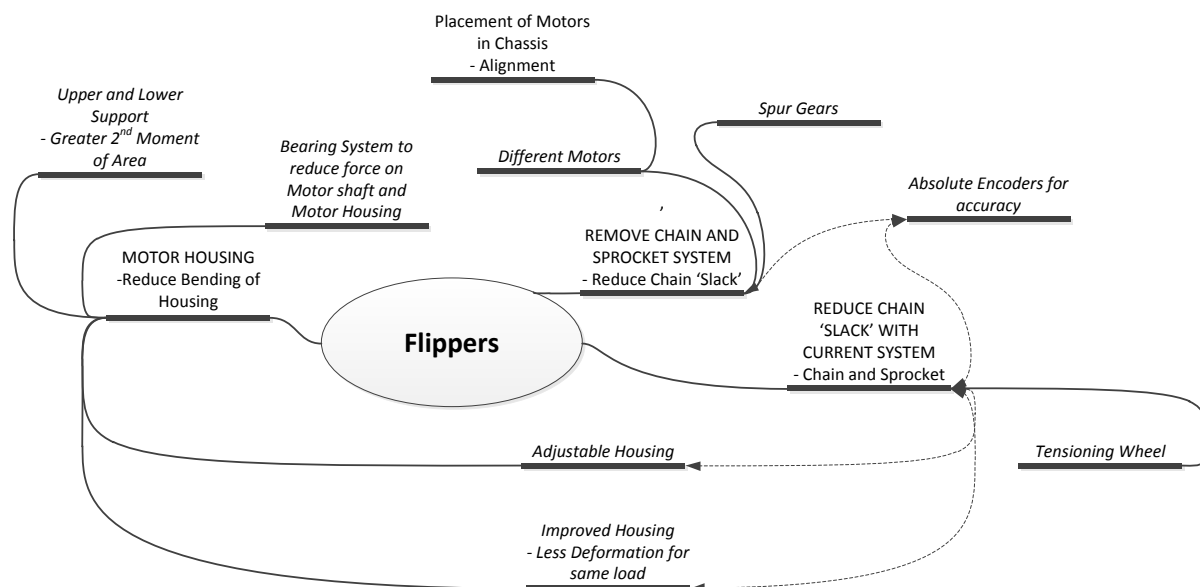


Figure 3: Mind Map of Flipper Ideas

3.2.1.4 Chassis

Counteracting the weaknesses as shown in section 3.3.1 (Table 6) could be achieved by replacing the current body with a space frame concept. Figure 4 shows how a completely new concept could be beneficial to the robots functionality and reliability, yet it should be noted that mobility has been a strong attribute of the robot in the past, so other improvement ideas were also considered.

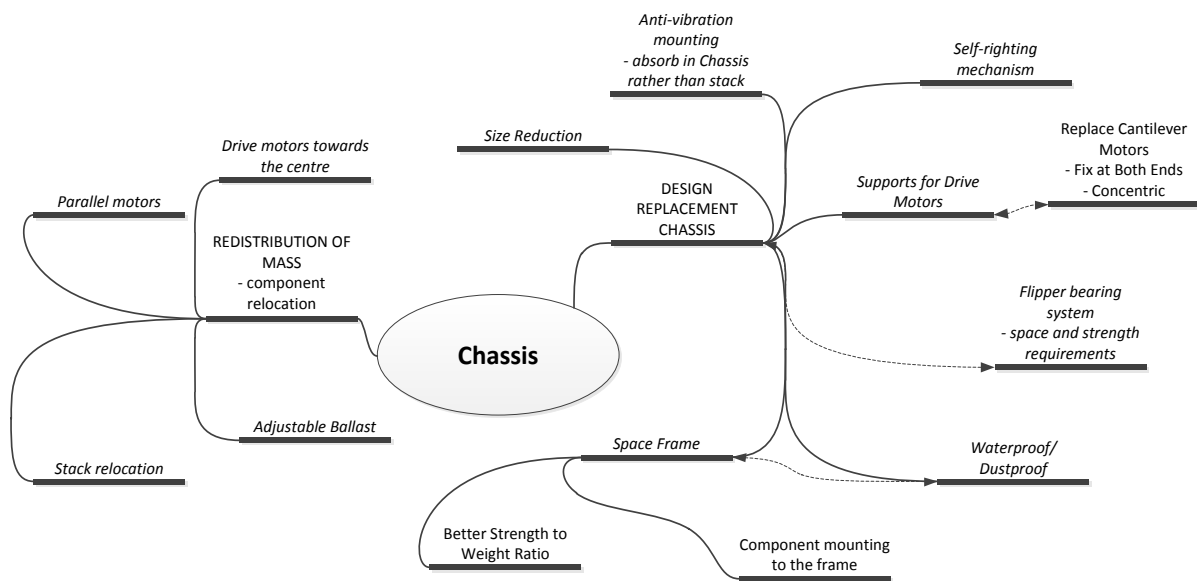


Figure 4: Mind Map of Chassis Ideas

3.2.2 Software

Figure 5 highlights a range of improvement ideas considered from the initial SWOT analysis shown in Table 7. The complexity and scale of software development can be appreciated by the detailed thought process which initially stems from the objectives of ‘Software Optimisation’, ‘Mapping Improvements’, ‘QR Code Reading’, ‘IR Camera Interface Feed’, ‘CO₂ Concentration Recording’ and ‘Improvement to the Operator Controls’.

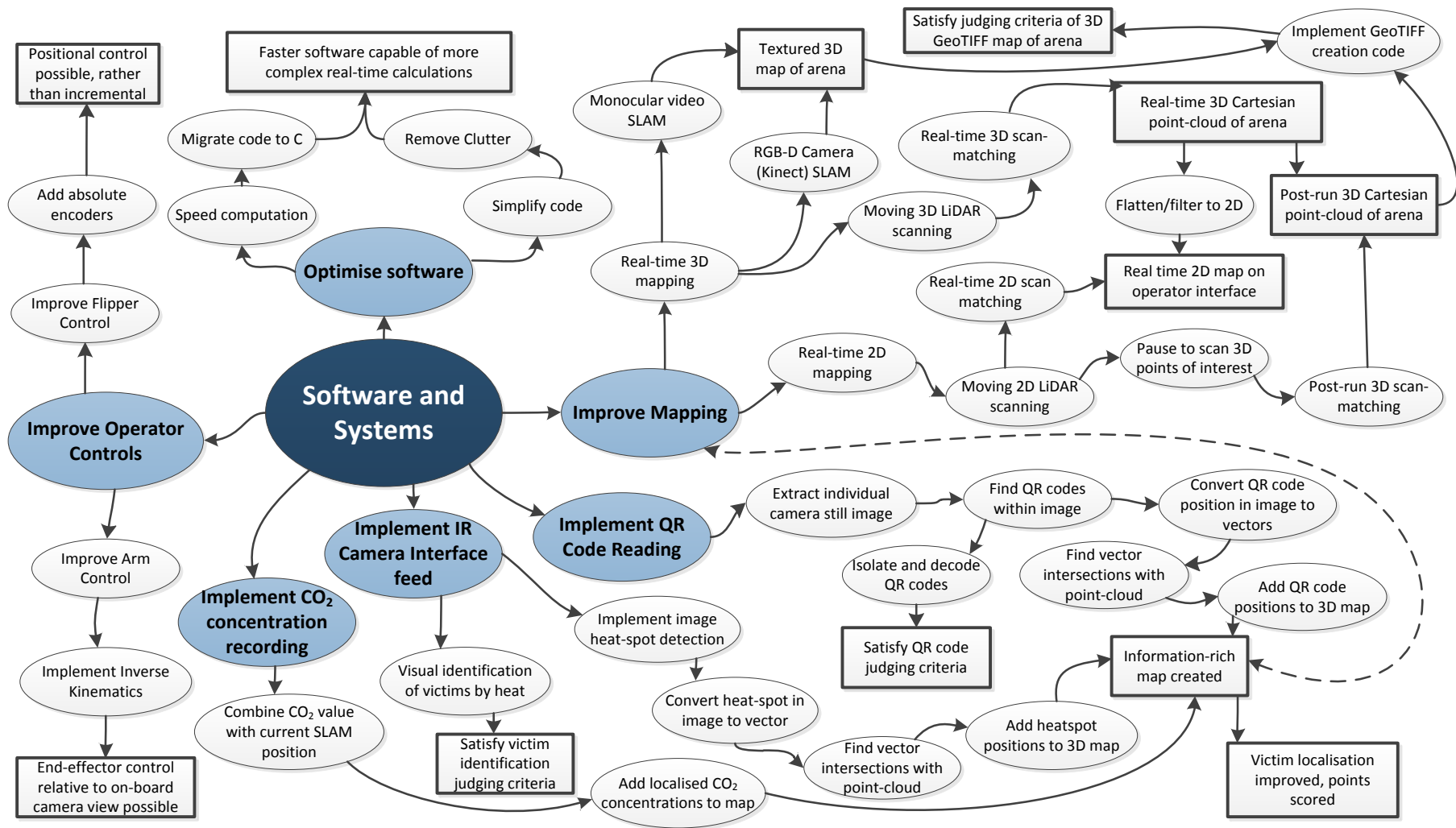


Figure 5: Mind Map of Software and Systems Ideas

3.2.3 Electronics

The SWOT analysis in Table 8 recognises the criticality of the Electronics; even a minor electronics failure could have system-wide repercussions. Hence, functionality and reliability of this area is highly important as it has knock on effects to the capacity at which the robot operates. Figure 6 identifies some of the important improvements needed to meet the objectives set, notably the use of appropriate connections, capable power-boards and correct encoder selection.

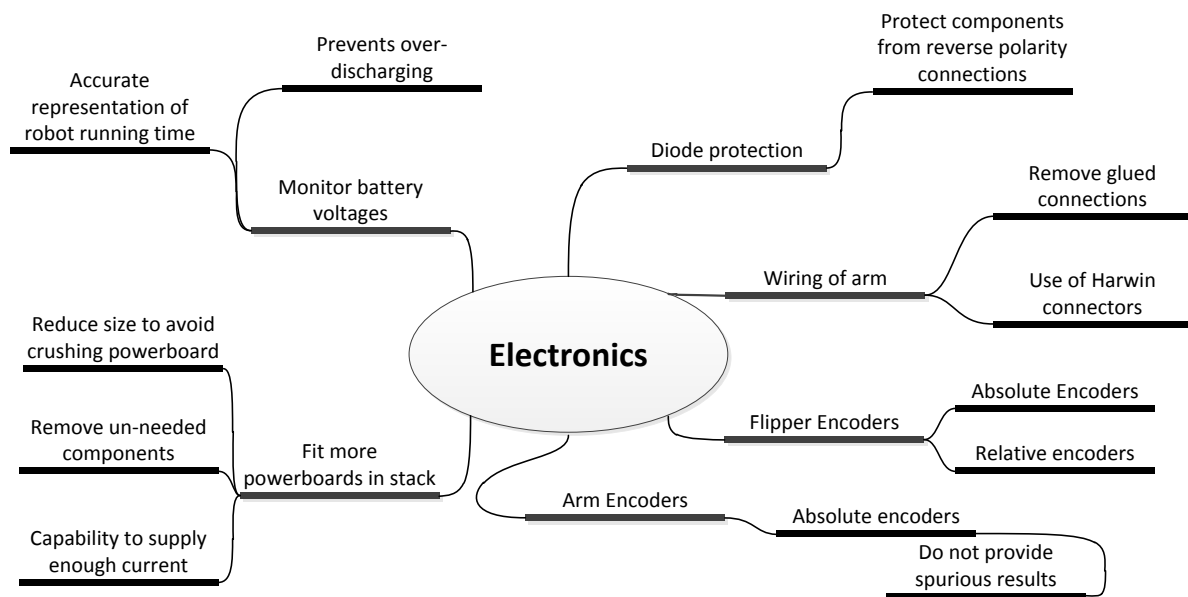


Figure 6: Mind Map of Electronics Ideas

3.3 Prioritised Improvements

The information from the SWOT examinations in section 3.1 and the mind maps in section 3.2 were combined to form a subjective, yet fully reasoned approach to selecting the most appropriate areas of the robot to improve. Qualitative observations and information were also used to decide which methods of improvement should be implemented for the individual robotic areas.

A range of factors were considered in determining both of the criteria outlined. These are shown in Figure 7.

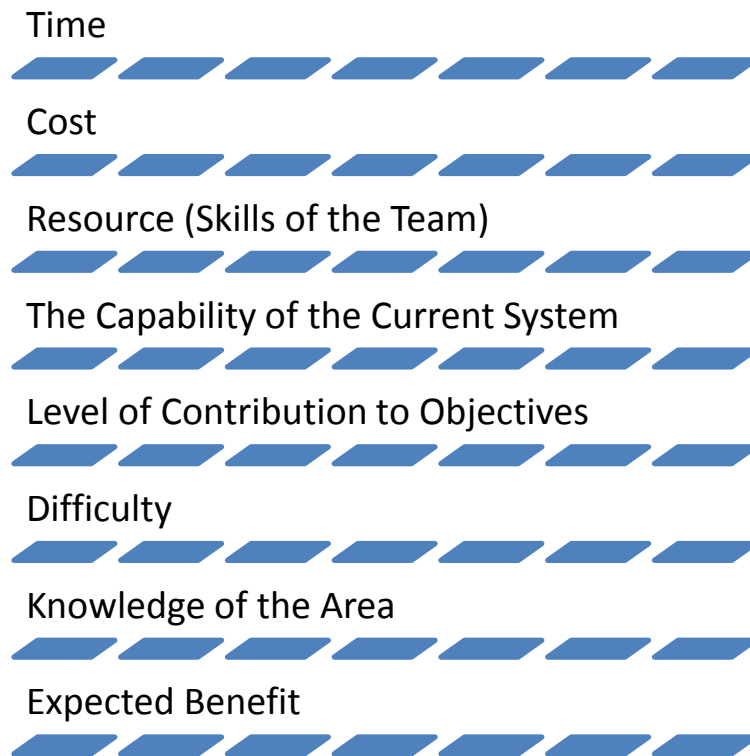


Figure 7: Decision Parameters

3.3.1 Mechanical Arm

Concept: *Build New Arm: based on re-engineering worm and worm wheel gear design*

Reasoning: As described in section 3.1.1 the functionality of the previous design was very limited. The option of re-engineering means specific functionality and reliability problems can be targeted for improvement. The knowledge gained from analysing the previous design and the documentation provided by previous WMR teams means there is ample information available to optimise the worm and worm wheel gear concept, far outweighing any knowledge of other robotic arm ideas. This approach also accounts for several high cost components, such as motors and gears, being re-used in an attempt to reduce expenditure and waste. A mechanically justified improvement was deemed to have a high expected benefit as the competition requires robots to pick and place objects, while searching for victims above ground level.

3.3.2 Head

Concept: *Build New Head*

Reasoning: As described in section 3.2.1.2, a replacement head design has a greater number of advantages than simpler alternatives. A reduction in mass effectively aids the capability and optimal design of the mechanical arm because its end load will be lower and secure fixing of sensors contributes to greater reliability. These scenarios could only be fully achieved by re-designing.

3.3.3 Flippers

Concept: *Reduce 'Slack' in Chain*

Reasoning: The level of 'slack' in the chain needs to be reduced so that encoders can be used to inform the operator of their 'real' position, succeeding in delivering a fully integrated Tele-Operational robot as described in section 3.1.2. A stronger housing complements this desire because deformation leads to greater 'slack'. Yet, there is an inherent design problem which is causing deformation, therefore in implementing a desired solution the root cause must be understood.

3.3.4 Chassis

Concept: *Keep Existing Chassis*

Reasoning: The Chassis has demonstrated very good capability to date and importantly, it functions relatively well. Completely re-designing the Chassis would have been a time consuming task, which could not be achieved whilst carrying out the large scale project of re-designing the mechanical arm. The mechanical arm was judged a more important improvement area because of the perceived additional benefit to the robot as an entire entity.

3.3.5 Software and Systems

Concept: *Implement Inverse Kinematics, Simultaneous Localisation and Mapping, QR code reading, Centre of Gravity calculations and improve Visual Representation*

Reasoning: Existing arm control relies on the operator's knowledge of joint angles and their effects. It is slow and cumbersome and improper joint angles risk mechanical damage/victim injury. Inverse kinematics will allow the operator to move the robot head relative to its current position, observing video feedback. Joint angles are calculated and enacted automatically, after being checked for self-collision scenarios.

Currently, the robot scores no competition points for 3D mapping, nor returns any map to the operator interface to aid in navigation and collision avoidance. This lack of mapping also limits autonomous navigation in signal drop-out zones.

QR code reading is a fairly simple, modular addition to the code; it affects little else, and requires no extra hardware, yet will score additional points in the competition.

Last year's competition failure was largely due to a toppling incident, and the resulting damage to sensors. Centre of gravity calculations will provide warning of impending toppling. Whilst this functionality is added to the current visual representation, both flipper position and arm will be updated to make use of new encoders/arm hardware.

3.3.6 Electronics

Concept: *Stabilise Current Systems and Integrate Design Changes from other Areas*

Reasoning: The electronic network does not require a complete overhaul. Functionality has been proven in the robots success to operate the necessary robot functions. Reliability of the network is the greatest issue and is highlighted in section 3.2.3 as a major threat to the overall operation of the Search and Rescue Robot. Securing connections, using appropriate technologies, and making minor adjustments in an already functional system are most beneficial. In stabilising the current system, devices which integrate mechanical mechanisms to deliver functionality can be chosen and embedded. The electronic network is critical to all parts of the robot working successfully so the expected benefit is unrivalled.

4 Mechanical Arm

Figures 8 and 9 illustrate the finalised WMR Mechanical Arm for 2012.

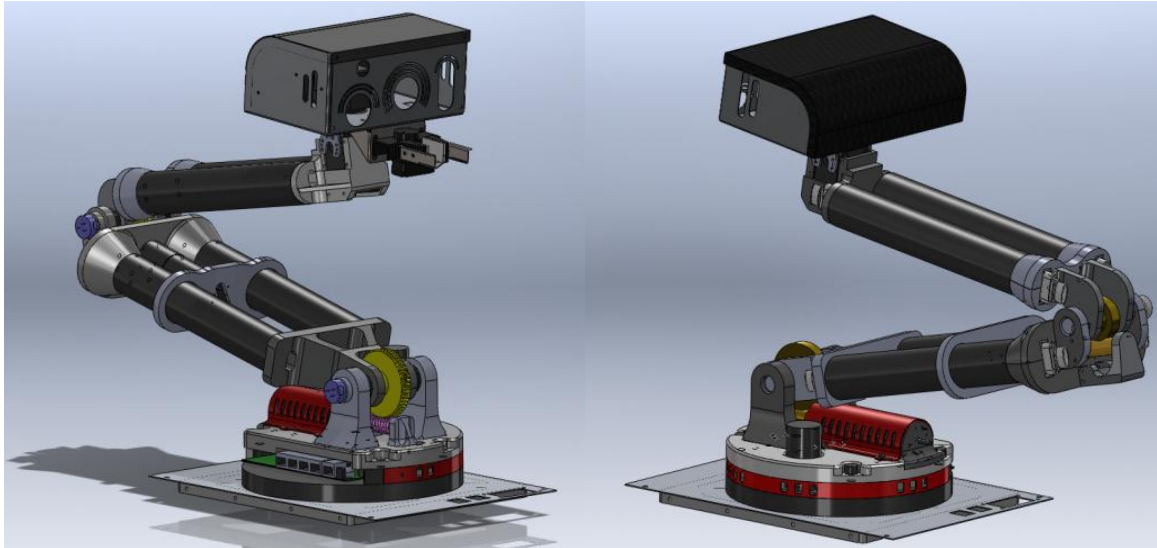


Figure 8: (shown left) Front View of Arm

Figure 9: (shown right) Rear View of Arm

4.1.Objectives

To meet the purpose of being functional and reliable the Mechanical Arm needs to:

- Remain in a settled and balanced orientation while the robot is in motion
- Satisfactorily contribute to lowering mass of the robot to prevent toppling when climbing ramps
- Be of adequate strength in order to adequately lift the Head and prospective payload (water bottle)
- Move into a range of positions and fully extend to 0.7m

4.2.Requirements

To fulfil the objectives stated, the robot must have a high degree of freedom in order to suitably partake in Search and Rescue activities. Unintentional movement in individual joints must be kept minimal by ensuring there is accurate meshing of teeth in the transmission of the joints and full

support of motor shafts is implemented to reduce backlash. The mass of the arm needs to be reduced using high strength low density materials, and mass must be relocated from the end effector position to ensure motors are capable of lifting the required loads. The centre of mass should be kept as close to the robot chassis as possible. Mechanical parts should be designed for rapid and straightforward manufacture to satisfy unpredictability and optimisation in the design and manufacturing processes.

4.3. Formal Specification

SPECIFICATION: MECHANICAL ARM

Strength	<ul style="list-style-type: none"> ▪ The arm needs to be strong enough to lift its own mass easily along with a combined head and payload of 2kg ▪ Motors must be capable of running without burning out due to torque requirements outside of their capability
Reach	<ul style="list-style-type: none"> ▪ The arm must be able to reach 0.7m in vertical height; coupled with the height of the chassis, this will allow the robot to identify victims 1m off the ground ▪ There should be 180° rotation of the shoulder joint so that arm is capable of lying flat. Other joints should have adequate rotation to allow the centre of mass of the robot to change with incline/terrain by moving the position of the arm ▪ Use absolute encoders in the arm to record joint rotation to increase accuracy in visual representation on operator HMI screen
Rigidity	<ul style="list-style-type: none"> ▪ The arm must provide adequate stability of the sensors in the head and precise movement of the end effector
Packaging	<ul style="list-style-type: none"> ▪ The joints along with the gearing must be compact and packaged efficiently
Thrust Spigot and Ball Bearing	<ul style="list-style-type: none"> ▪ A thrust spigot and ball bearing should be used to counteract the forces in the transmission during joint rotation
Mass	<ul style="list-style-type: none"> ▪ The mass of the mechanical arm above the shoulder joint should not exceed 3kg
Manufacture	<ul style="list-style-type: none"> ▪ Design joints in a modular fashion and facilitate the manufacture of parts using 3-axis milling machines ▪ Rapid prototype parts using Selective Laser Sintering and Fused Deposition Modelling technology
Assembly/Disassembly	<ul style="list-style-type: none"> ▪ To allow parts to be easily replaced and interchanged when necessary
Cost	<ul style="list-style-type: none"> ▪ The costs of development and manufacture should not exceed £3000 from the project budget

4.4.Mechanical Breakdown

Figure 10 and Table 9 outlines the breakdown of the 2012 Mechanical Arm.

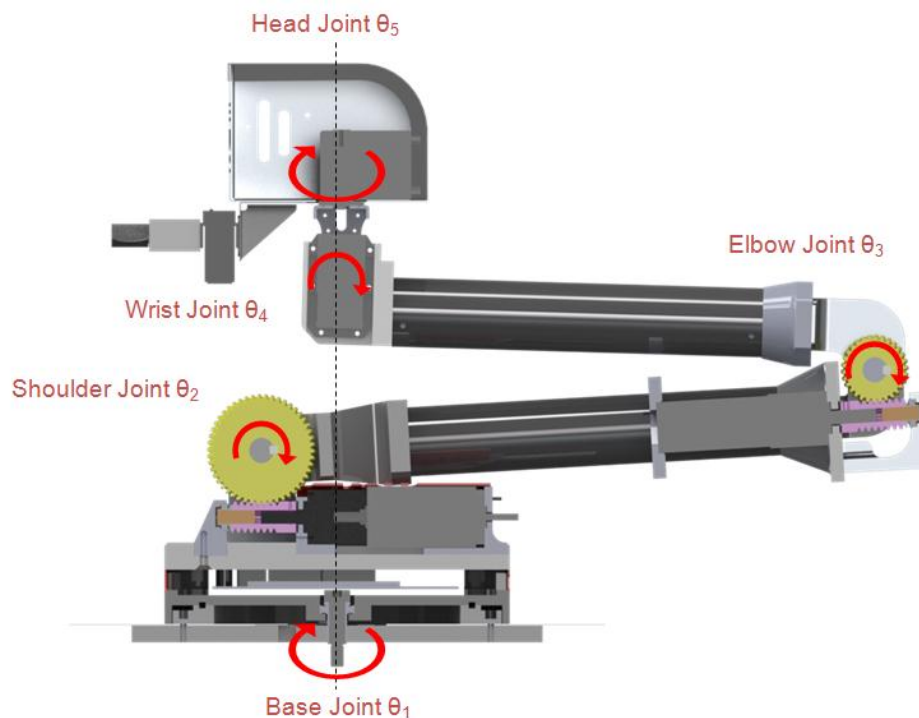


Figure 10: Five Revolute Joints of the Arm

JOINT		DESCRIPTION
1	Base Joint	Rotation in the z-axis. Powered by a Maxon A-max 26 motor with GP32C 246/1 planetary gearbox meshed with a spur gear and annulus ring on the top of the robot chassis. Provides 350 degree rotation.
2	Shoulder Joint	Rotation in the y-axis. Powered by a Maxon RE-36 motor with GP32C 23/1 planetary gearbox. Transmission consisting of a brass 50 tooth anti-backlash worm wheel gear meshed with a hardened steel worm gear. Provides 180 degree rotation.
3	Elbow Joint	Rotation in the y-axis. Powered by a Maxon RE-30 motor with GP32C 23/1 planetary gearbox. Transmission consisting of a brass 30 tooth worm wheel gear meshed with a hardened steel worm gear. Provides 180 degree rotation.
4	Wrist Joint	Rotation in the y-axis. Provided by a RX-64 Servomotor. Provides 140 degree rotation.
5	Head Joint	Rotation in the z-axis. Provided by a RX-64 Servomotor. Provides 350 degree rotation.

Table 9: Revolute Joint Descriptions

4.5.Design Intent

A thorough and detailed evaluation of the 2010/2011 mechanical arm was carried out and is fully detailed in Appendix A.1 at the end of the report. The following design changes are aimed at removing the problems observed in the arm and delivering the project objectives of making the mechanical arm functional and reliable.

4.5.1 Fully Supported Motor Shaft

Last year's mechanical arm suffered from bent motor shafts due to inadequate support provided by the thrust bearing, as outlined in Appendix A.1.1. The new motor shaft support mechanism is highlighted in Figure 11; a ball-bearing is encased in a support housing to fully support the worm gear and Maxon planetary gearbox shafts during operation. A thrust spigot is used to mechanically connect the worm gear to the ball bearing. Cantilever beam action is reformed to a beam supported at both ends to reduce deflection, improving the reliability of meshing and reduction in backlash which is critical when the joint is subjected to load and vibration.

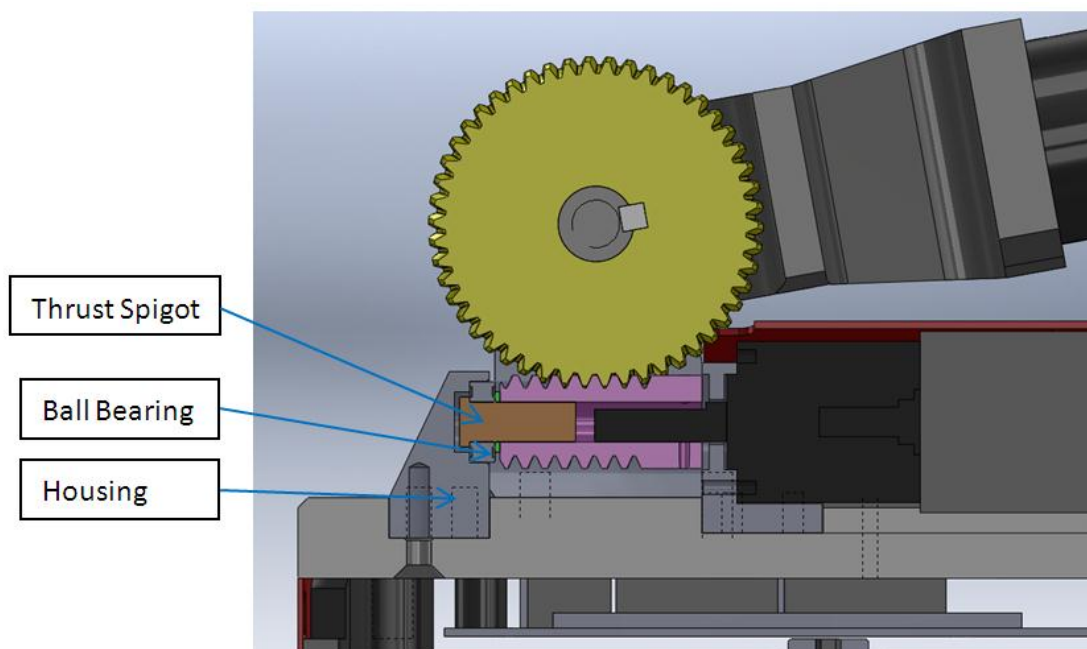


Figure 11: Thrust Spigot and Ball Bearing

4.5.2 Modular Design of Joints

A major issue with last year's mechanical arm was the over complex joints that were expensive and time consuming to manufacture, as outlined in Appendix A.1.4. The new joint structures were developed with significant consideration of the manufacturing processes. Parts assigned for machining processes have been designed to meet the specific geometry conditions for the use of 3-axis milling only and reduce the number of machine set-ups required. This has simplified the manufacture of components in terms of equipment and skilled resource needed. Modular design of joints has also allowed the centre distance (CTS) between the worm and worm wheel to be easily modified by using shims as shown in Figure 12. This mechanism therefore contributes to the objective of having a stable Mechanical Arm by ensuring accurate meshing of teeth. An additional benefit of using simple parts concerns the ease and speed of modification and replacement of small pieces rather than large blocks, essential for a bespoke design.

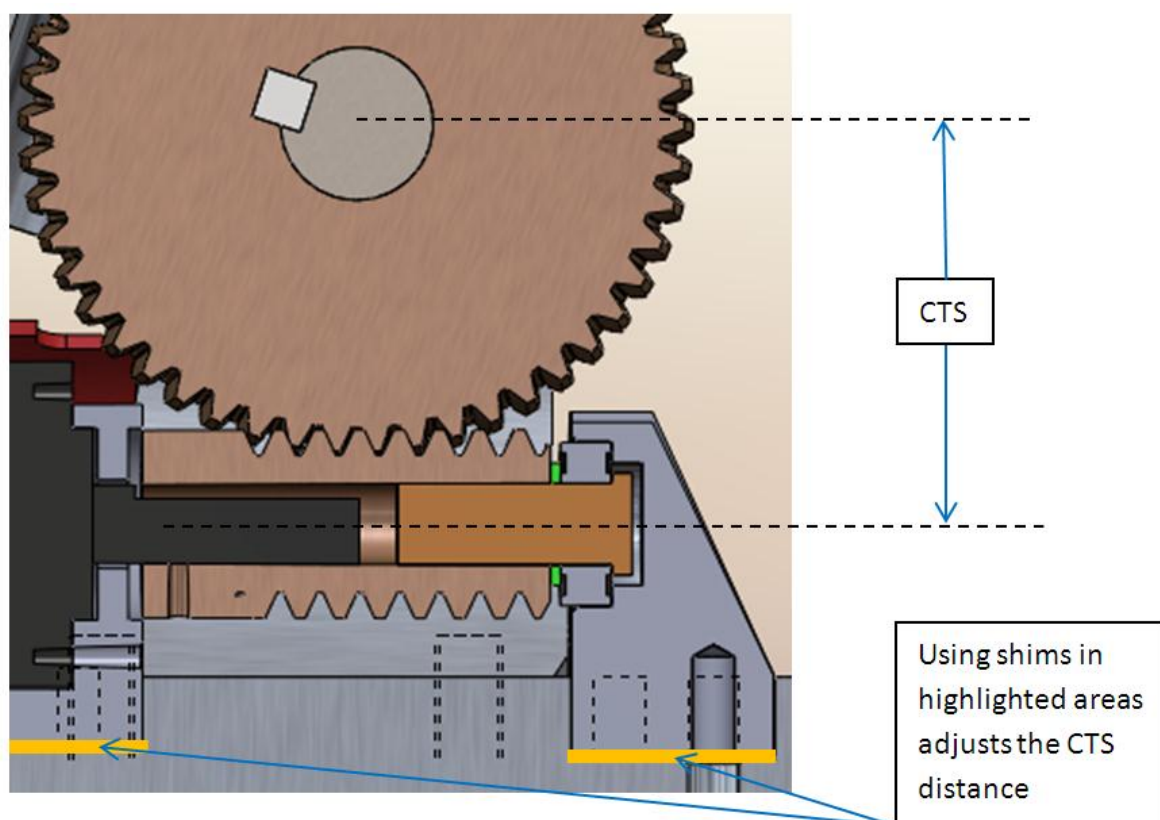


Figure 12: Centre Distance altered by adding and removing shims

4.5.3 Mass Re-distribution

A critical design objective, as stated in section 3.2.1.1, was to relocate mass nearer to the body of the robot to keep overall centre of mass as low as possible.

Moving mass closer to the base of the arm reduces the total moment of inertia around the shoulder joint axis (see section 4.4) and will reduce the likelihood of the robot toppling. The arms resistance to changes in motion is therefore lowered, reducing backlash susceptibility.

Amalgamation of the router into the base joint, as shown in Figure 13 below, is one mass re-distribution measure applied. Appendix A.1.3 details the previous router positioning in the Head and the recommended replacement to a safer location ⁽¹⁸⁾.

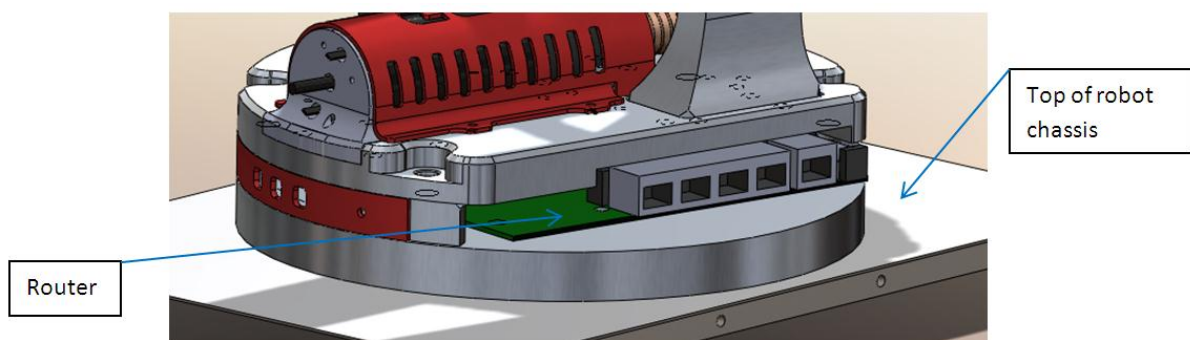


Figure 13: Router in the Base Joint

Components of the wrist and elbow joint include rapid prototyped parts from Selective Laser Sintering Technology. This has reduced total joint mass and reduced the stress on the motors in the arm. The power transmission system used in the wrist now comprises of an RX-64 servo motor rather than a Maxon motor and worm gear transmission (moving mass away from the end effector).

4.5.4 Shoulder Joint Loading

Appendix A.1.5 highlighted the problems with overloading of the shoulder motor and backlash observed in the shoulder joint. The motor powering the shoulder joint is under the highest load as it accounts for the movement of mass in the whole structure. Figure 14 highlights the re-configuration

of the gearing mechanism where the motor has been placed in a static position to drive the worm gear about a fixed axis. Convention states that in a worm and worm wheel configuration, the worm drives the worm wheel ⁽¹⁹⁾. The shoulder joint mechanics, designed to enable rotation of the worm and the worm wheel about their own rotational axis rather than fully constraining the worm wheel as used in previous designs where the worm had a moving rotational axis. Torque requirements can therefore be calculated conventionally, eliminating risk of motor failure. The motor is now in a lower position, moving mass nearer to the robot body and decreasing force needed to lift the arm.

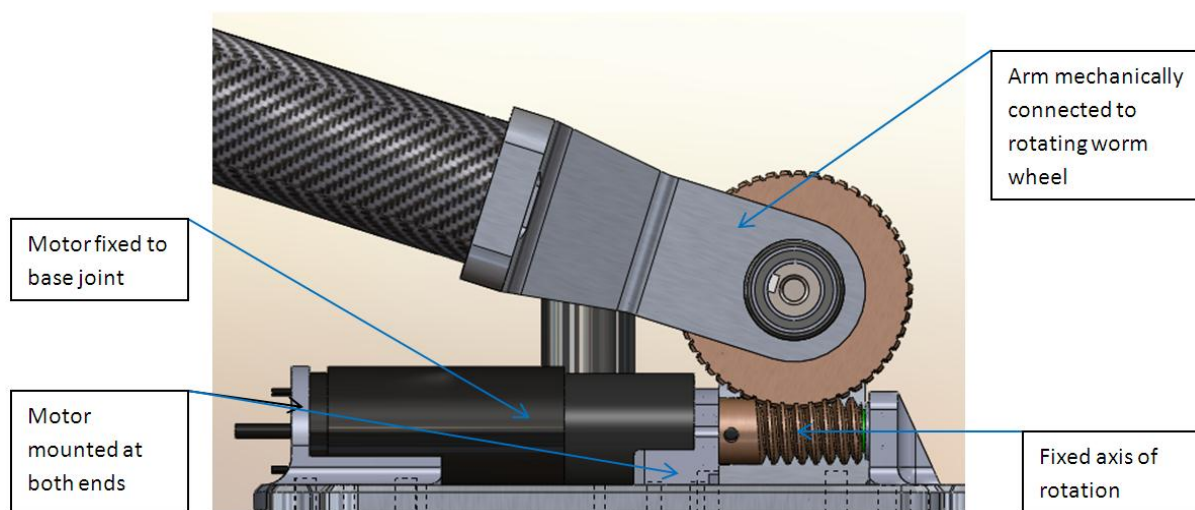


Figure 14: Shoulder Joint Motor Positioning and Accurate Meshing of Teeth

4.5.5 Concentric Mounting of Base Rotation

There was a lack of accuracy in the alignment of the base joint in last year's mechanical arm, as documented in Appendix A.1.6. Concentricity of the connection between the Mechanical Arm and the robot body simply increases the functionality and reliability of the system because the spur gear used for base rotation can be accurately and consistently meshed with the annulus ring. Figure 15 shows the precise alignment of connection using a shoulder bolt and sleeve to eradicate movement.

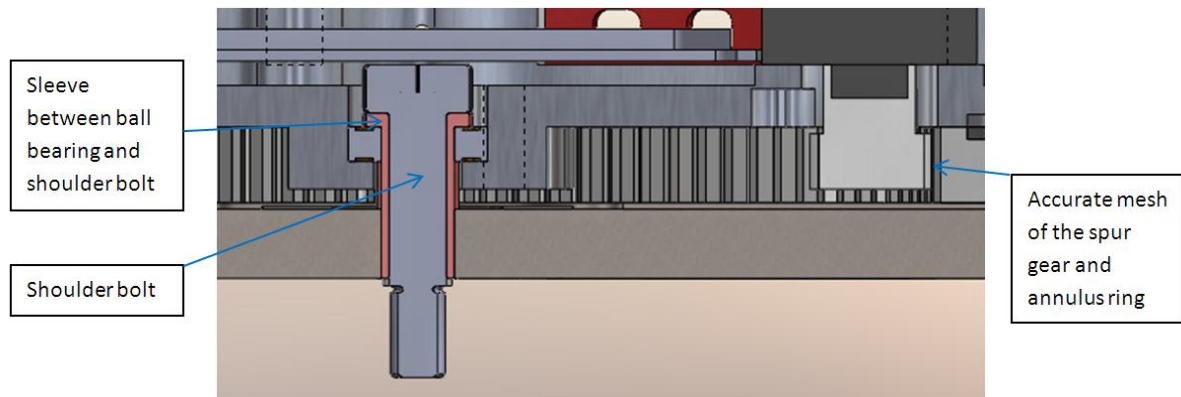


Figure 15: Cross-section of sleeve and Shoulder Bolt with Teeth Mesh

4.5.6 Potentiometers

Absolute position of the shaft angles, where joints use Maxon motors, needs to be measured for software collaboration and control. Encoders of the motors will not give absolute reference position, but it is important these are known to prevent random movements when power is turned on and off ⁽²⁰⁾. The encoders used for the application in the Mechanical Arm are outlined in section 8.4.1.3. They are fixed to the side of joints with a screw thread and placed within the keyway shaft using an interference fit as shown in Figure 16.

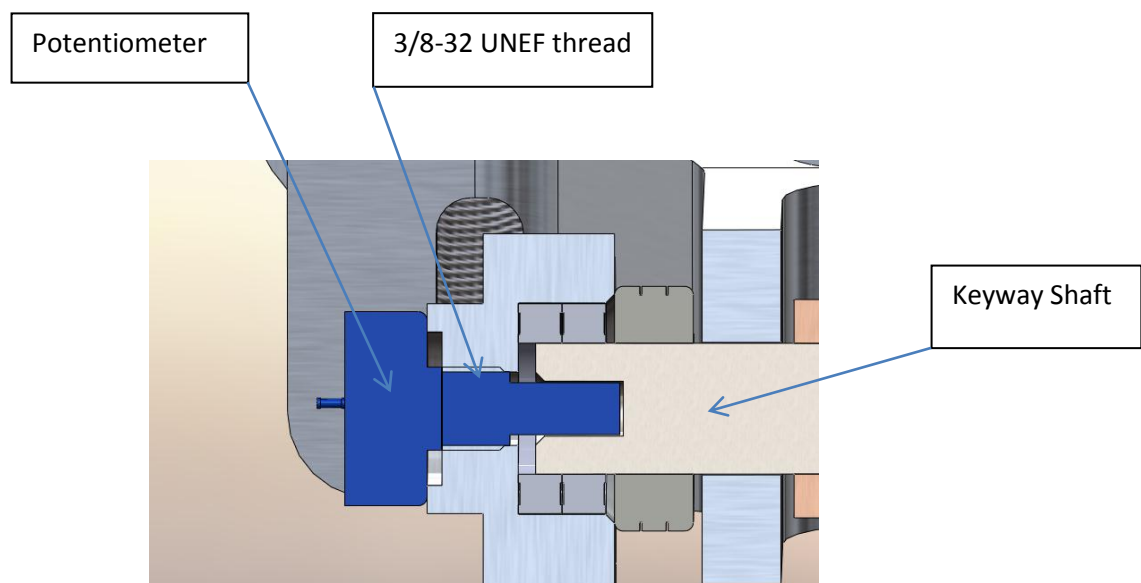


Figure 16: Mounting of Potentiometer

4.6.Design Calculations

Torque requirements of the mechanical arm were calculated in the design phase of development. The highest torque requirement to move the arm is when it is fully extended, as described in section 4.5.4; this is modelled in Figure 17 with corresponding values shown in Table 10. The calculation shown derives the necessary torque needed for the shoulder joint using a bending moment diagram.

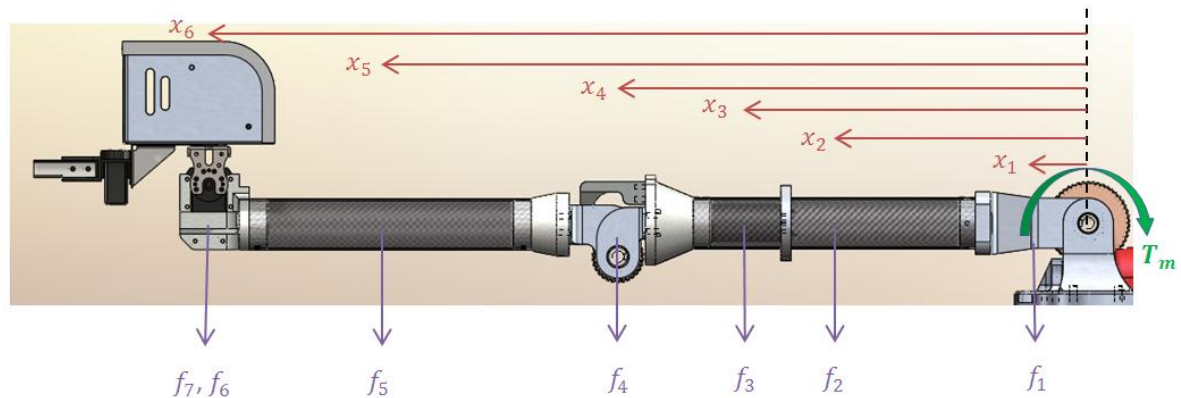


Figure 17: Torque Requirement Diagram

Part of mechanical arm	Label on Diagram	Mass (kg)	Label on Diagram	Distance from Shoulder joint (m)
Shoulder link joint	f_1	0.8	x_1	0.04
Lower arm carbon tubes and motor back plate	f_2	0.25	x_2	0.203
Elbow joint motor	f_3	0.47	x_3	0.308
Elbow joint	f_4	1.05	x_4	0.374
Upper arm carbon tubes	f_5	0.13	x_5	0.557
Wrist joint and Servo-motor	f_6	0.22	x_6	0.7
Head and end-effector payload	f_7	2.0	x_6	0.7

Table 10: Calculation Values

$$T_m = \sum_{i=1}^N (F_i \times x_i)$$

$$\begin{aligned}
T_m &= (F_1 \times x_1) + (F_2 \times x_2) + (F_3 \times x_3) + (F_4 \times x_4) + (F_5 \times x_5) + (F_6 \times x_6) + (F_7 \times x_6) \\
&= (0.8gN \times 0.04m) + (0.25gN \times 0.203m) + (0.47gN \times 0.308m) + (1.05gN \times 0.374m) \\
&\quad + (0.13gN \times 0.557m) + (0.22gN \times 0.7m) + (2gN \times 0.7m) \\
&= 0.314 + 0.498 + 1.42 + 3.852 + 0.710 + 1.51 + 13.734 \\
&= \mathbf{22.03 Nm}
\end{aligned}$$

The torque required from the shoulder joint motor has been calculated to be 22.03 Nm. Hence, there must be at least 22.03 Nm exerted by the motor in order to lift the arm from a horizontal position.

The Maxon RE-30 has a maximum continuous torque of 0.085Nm⁽²¹⁾ and the GP32C planetary gearbox associate has a reduction ratio of 23:1, which increases the nominal torque of the motor and gearbox to 0.085Nm x 23 = 1.955Nm.

The reduction ratio between the worm and worm wheel gears is calculated as:

$$\frac{\text{Number of teeth in worm wheel}}{\text{Number of starts in worm}} = \frac{50}{1} = 50$$

Therefore the reduction ratio of the gearbox and worm gear transmission combined is 50 x 23 = 1150:1, and the nominal torque of the combination is 0.085 x 1150 = 97.75Nm.

The efficiency of the worm and worm wheel gear transmission was calculated as 52% (calculation method is compiled in Appendix A.3).

Thus the effective torque available in the shoulder joint is 97.75 x 0.52 = 50.83 Nm

As the effective torque calculated is greater than the torque requirements in the fully extended position, it can be concluded that the configuration of the shoulder joint will be sufficient during the operation of the mechanical arm.

4.7. Joint and Link Design

4.7.1 Base Joint

The base joint consists of the support plate (from the previous WMR design) and consists of a lower and upper plate that houses the router. The Maxon A-Max 26 motor is mounted to the lower plate and meshes with the annulus ring on the support plate to provide base joint rotation. Table 11 describes the assembly sequence as viewed in Figure 18.

Order	Task
1	Fasten the A-Max 26 motor to the lower support plate by three M3 x 10mm cap head bolts
2	Insert ball-bearing into lower plate and fasten to support plate with M8 Shoulder bolt and sleeve, aligning spur gear with annulus ring. Tighten M8 nut on the underside of the support plate
3	Place router on top of the lower support plate, aligning the mounting holes on the PCB board with the holes in the plate. Fasten the router to the plate using four M2.5 x 10mm cap head screws. Clearance from the bottom components to the plate for achieved using nylon washers
4	Once shoulder joint components are fastened to upper plate, fasten upper plate to lower plate using four M8 x 25 mm bolts
5	Fasten side cover to lower plate using two M3 x 10 mm screws

Table 11: Base Joint Assembly Sequence

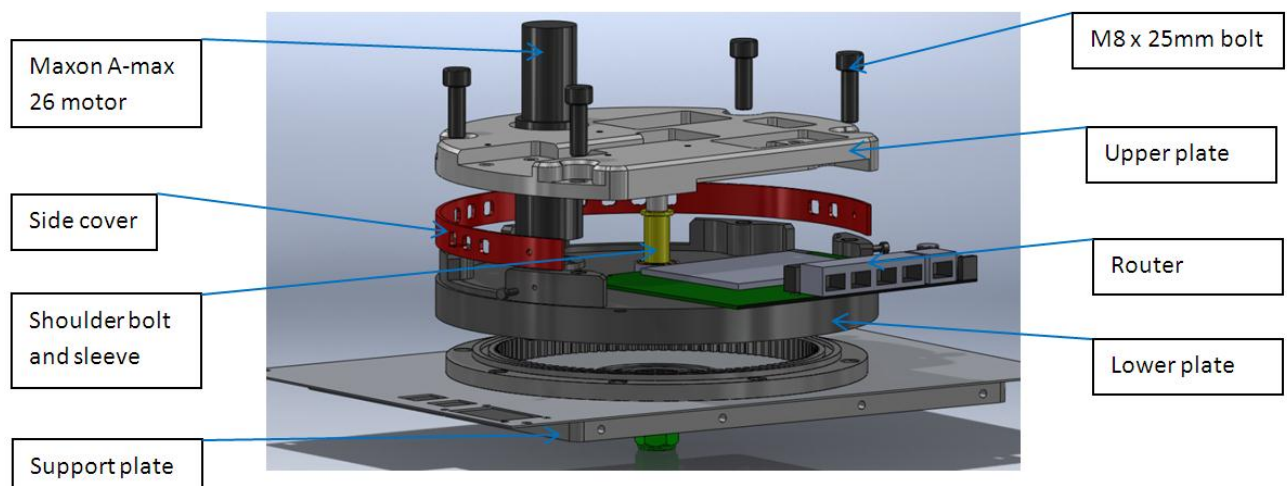


Figure 18: Exploded Diagram of the Base Joint

4.7.2 Shoulder Joint

The shoulder joint comprises of the driving and driven components secured to the upper base plate of the base joint.

Driving: Figure 19 and 20 show the mounting of the Maxon RE-36 motor at both ends with thrust spigot and ball bearing housing.

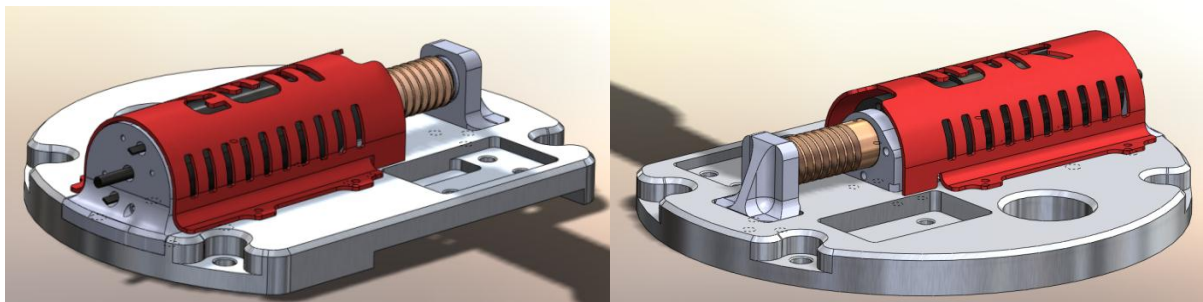


Figure 19: (shown left) Rear View of Motor

Figure 20: (shown right) Front View of Motor

Driven: Figure 21 consists of the uprights and ball-bearings along with thrust bearings and worm wheel. The shoulder link joint connects to the rigid members and rotates using the worm wheel, mechanically joined with a square keyway and shaft.

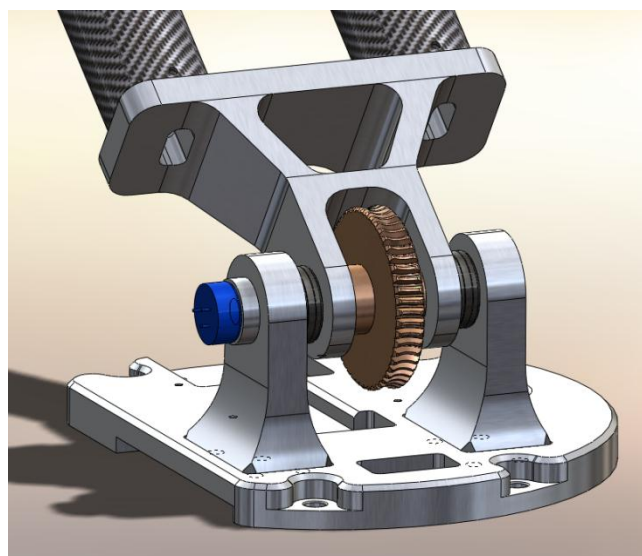


Figure 21: Driven Joint (Shoulder Joint)

The following Figure, 22, provides an exploded view of the shoulder joint, displaying how the driving and driven joints combine.

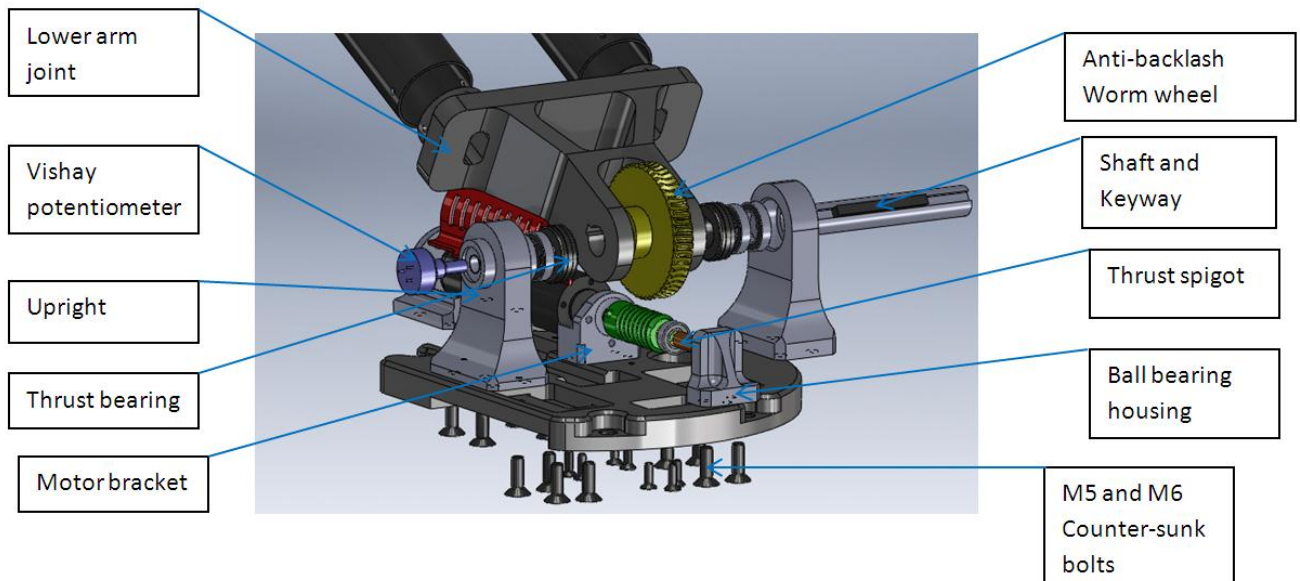


Figure 22: Exploded Diagram of Shoulder Joint

Table 12 describes the assembly sequence of the shoulder joint as viewed in Figure 22.

Order	Task
1	Fasten the RE-30 motor to the front and rear support brackets by four M3 x 10mm and two M2.5 x 8mm cap head bolts
2	Attach the worm gear to the motor and fit on washer, thrust spigot and ball bearing. Fit ball bearing into housing
3	Place front and rear motor brackets and ball bearing housing into pockets of the top base plate. Fasten from below using M5 counter-sunk bolts
4	Insert ball bearings into uprights and fit shaft and keyway through thrust bearings, lower arm joint and anti-backlash worm wheel
5	Screw Vishay potentiometer to upright and fit through shaft
6	Place both uprights into pockets of the top base plate. Fasten from below using M6 counter-sunk bolts

Table 12: Assembly Sequence of Shoulder Joint

4.7.3 Elbow Joint

The elbow joint is situated between the lower and upper arm members. The driving portion of the joint consists of parts that mount the Maxon RE-30 motor and house the thrust spigot and ball

bearing, providing full support. The driven portion of the joint consists of the worm wheel and uprights mechanically connected via square keyway and shaft. Figure 23 explains the joint structure with labelled parts.

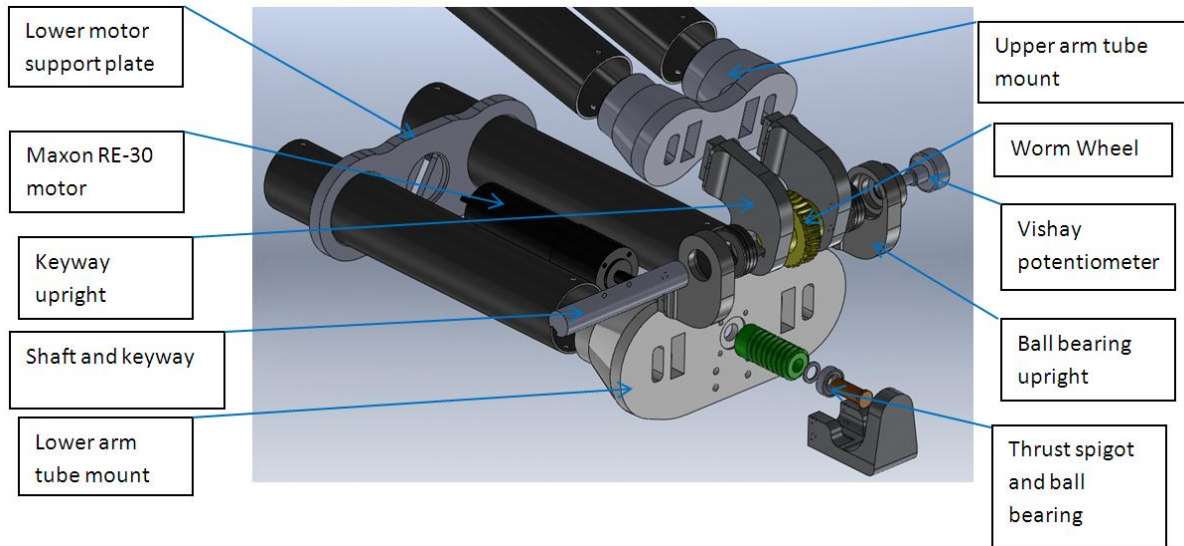


Figure 23: Exploded Diagram of the Elbow Joint

Table 13 describes the assembly sequence corresponding to Figure 23.

Order	Task
1	Fasten the RE-30 motor to the rear motor bracket and fasten motor to the lower arm tube mount using four M3 x 10mm bolts
2	Attach the worm gear to the motor shaft and fit on washer, thrust spigot and ball bearing. Fit ball bearing into housing. Attach ball bearing housing the lower arm tube mount using four M4 x 15mm bolts
3	Fit shaft and keyway through worm wheel and keyway uprights. Push fit thrust bearings and ball bearing uprights on both ends.
4	Fasten ball bearing uprights to lower arm tube mount through counter sunk holes on the underside of the tube mount. Use four M4 x 30mm bolts
5	Fasten keyway uprights to upper arm tube mount through counter sunk holes on the underside of the tube mount. Use four M4 x 30mm bolts
6	Screw Vishay potentiometer to ball bearing upright and fit through shaft

Table 13: Assembly Sequence for the Elbow Joint

4.7.4 Wrist Joint

The wrist joint houses a RX-64 Servomotor, used as a mass saving measure as opposed to a Maxon motor with worm gear transmission. This joint is Rapid Prototyped from PA2200 which allows excellent design freedom in gaining the required geometry and reduces mass at a point furthest from the base. The servomotor is mounted to the wrist joint through six mounting holes on each side that line up with the mounting positions on the servomotor housing. This is shown in Figure 24.

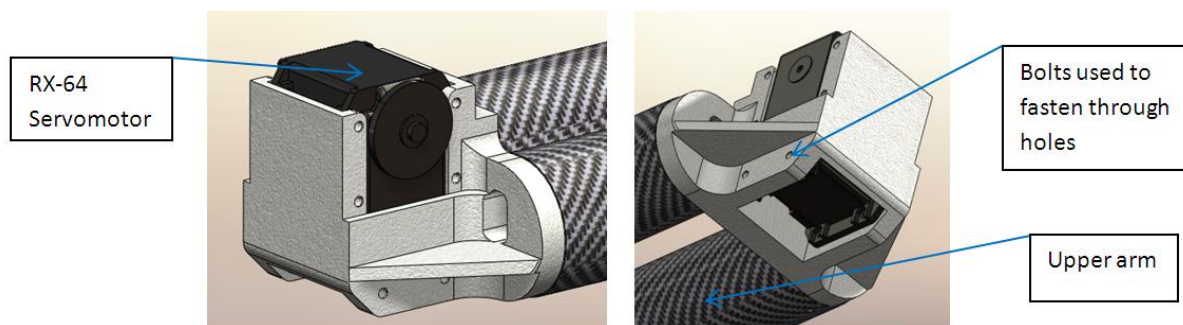


Figure 24: Wrist Joint (Housing RX-64 servo-motor)

4.7.5 Head Joint

The head joint simply comprises of a bent steel sheet bracket which connects the RX-64 servomotor in the wrist joint, with the RX-64 motor placed in the head, as shown in Figure 25. This joint provides the final degree of freedom for the mechanical arm

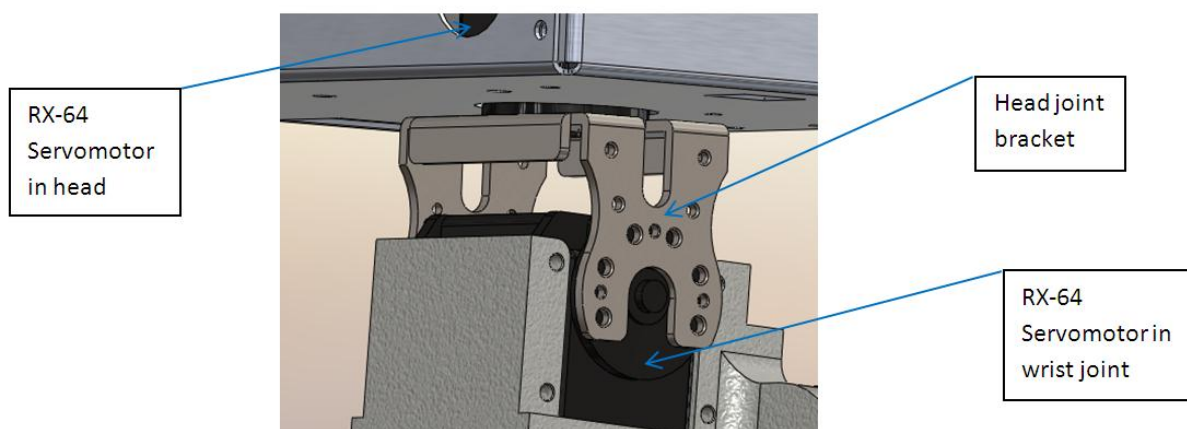


Figure 25: Head Joint

4.7.6 Rigid Links

The rigid links between the shoulder to elbow and elbow to wrist joints comprise of 1.4mm thick dual carbon fibre tubes, each of 41mm outer diameter. Carbon fibre provides an unrivalled level of strength to weight ratio, which is an important attribute aligned to meeting the project objectives set. A dual design specifically aids torsional strength, does not compromise range of motion available when using thrust spigot housings (as shown in Figure 26) and enables clear access to motors (as opposed to situating the motors within the link). These advantages are visually displayed in the figure below:

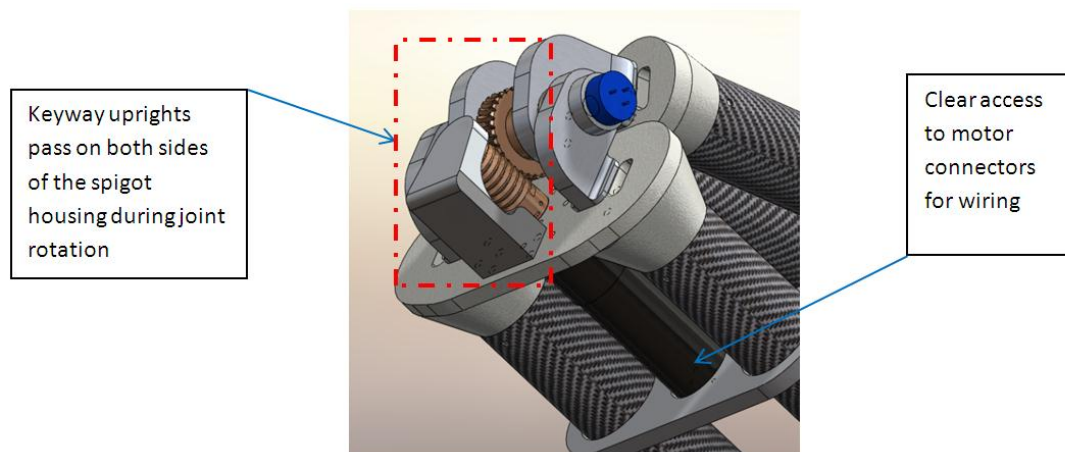


Figure 26: Advantages of Dual Tube Design

4.8. Post Design Analysis

Structural analysis was carried out using Finite Element Analysis (FEA) packages within both Solidworks and Abaqus. After looking at the results of the tests, changes were made to geometry and material thickness to satisfy the overall project aims of making the mechanical arm functional and reliable.

4.8.1 Shoulder joint analysis

The shoulder joint was evaluated due to its importance in the mechanical structure of the arm. As the shoulder joint is subjected to the majority of the mass, it was critical that the part would not break under the expected forces during robot motion.

This analysis provides a maximum Von Mises stress of 0.06225MPa with a maximum deflection of 4×10^{-7} m when subjected to a stress of 60Nm of torque on the keyway, as shown in Figure 27 and 28.

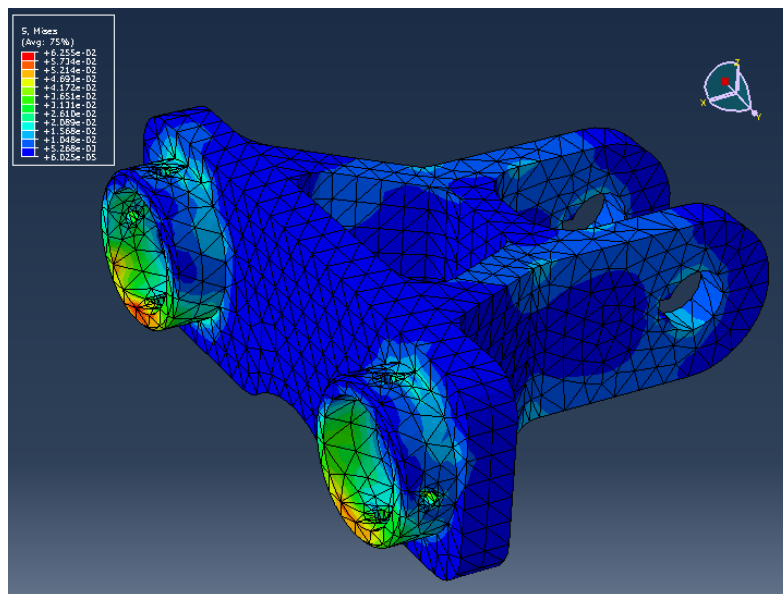


Figure 27: Shoulder Link Analysis (Abaqus)

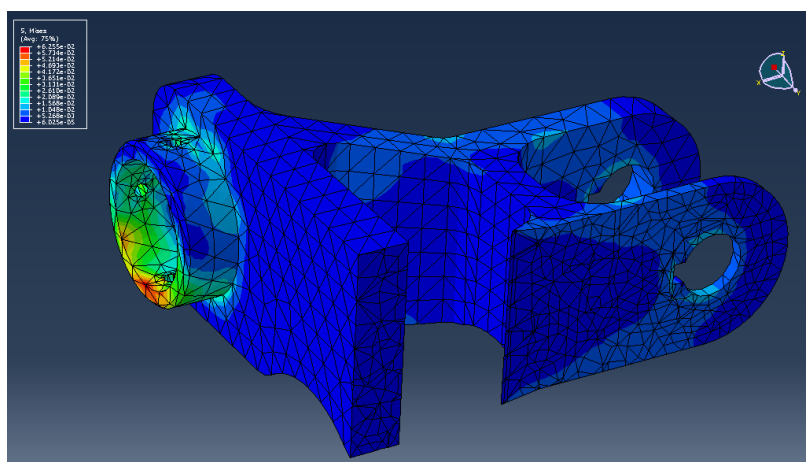


Figure 28: Section View through FEA Analysis of the Shoulder Joint

Low Stress values are shown in the area of the keyway, with the peak stresses appearing where the underside of the carbon tubes push upwards on the lip of their hollow boss cylinders on the shoulder joint.

4.8.2 Elbow joint analysis

Two are the critical areas of the elbow joint were analysed for their structural integrity; the ball bearing housing and keyway uprights. The analysis of the ball bearing housing has highlighted a maximum Von Mises stress of 0.0162 MPa with a maximum deflection of 0.4mm when subjected to an 1800N force vertically on the bearing surface, as shown in Figure 29.

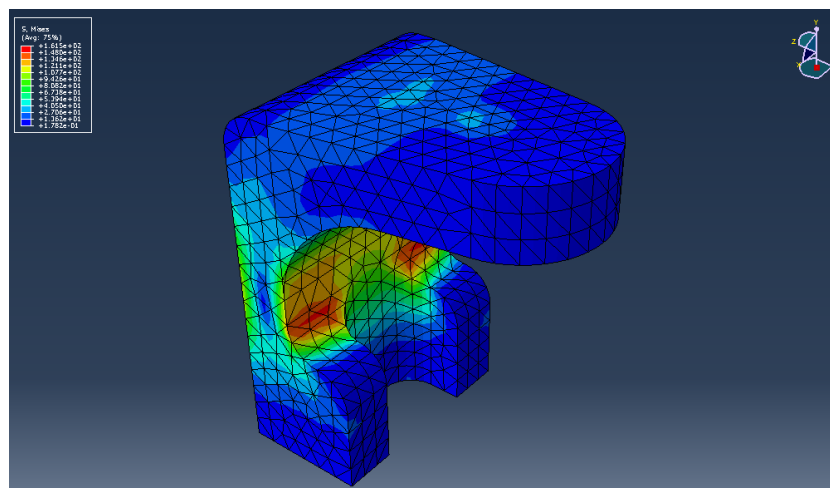


Figure 29: FEA Analysis of Ball Bearing Housing

This section view, shown in Figure 30, illustrates the key points of stress in the ball bearing and shows that the maximum stress points occur in the sharp bends and at the contact point of the ball bearing.

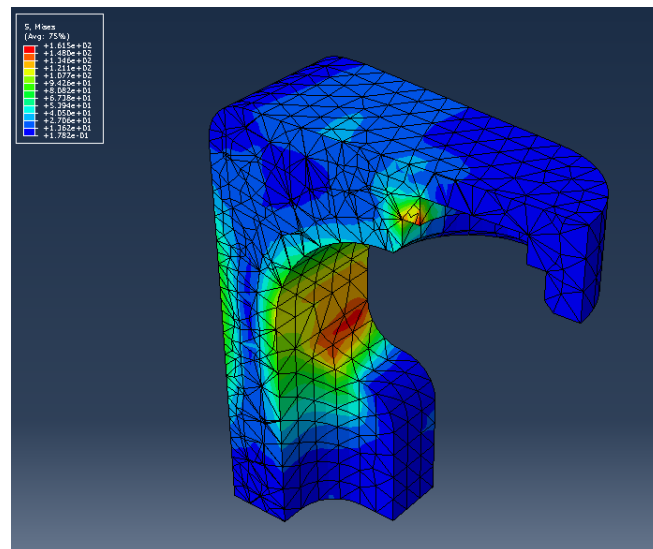


Figure 30: Section View through the FEA Analysis of the Ball Bearing Housing

This analysis of the keyway uprights provides a maximum Von Mises stress of 0.164 MPa with a maximum deflection of 8.1×10^{-8} m when subjected to a 30Nm torque at the keyway, as shown in Figure 31.

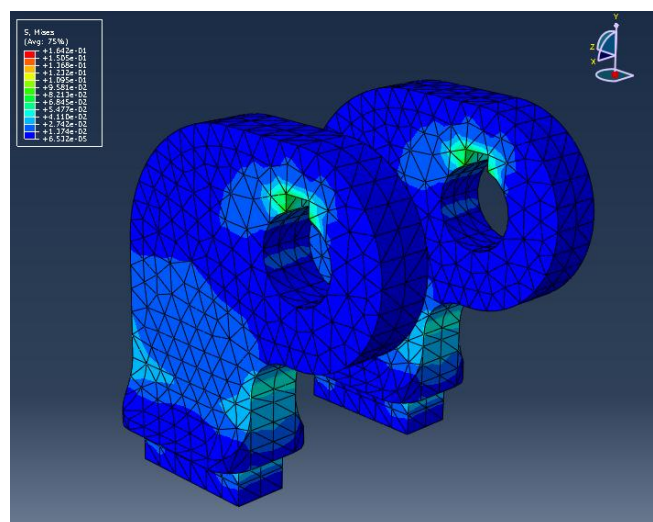


Figure 31: FEA Analysis of the Keyway Uprights

The section view below, Figure 32, illustrates that the key points of stress on the part are in the interface between the external thread of the M4 bolts and the internal thread of the tapped hole.

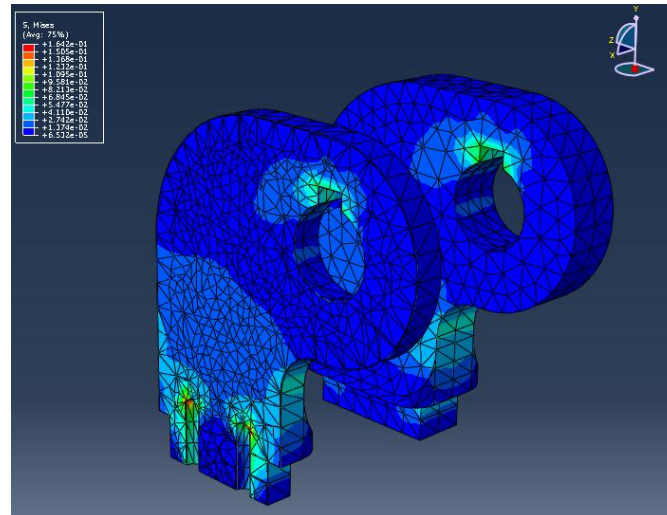


Figure 32: Section View of Elbow Joint Upright

The structural analysis carried out indicates that the critical parts of the arm are capable of supporting the specified loads with acceptable levels of deformation. It can be concluded that the arm is fit for purpose, and will be able to operate under the conditions it is likely to be subject to.

4.9. Manufacture

4.9.1 Design for Manufacture

Manufacturing processes and material selection have been considered and identified during the initial stages of the design process. The geometrical makeup of parts are directly related to the capability of manufacturing processes and deliberately tailored to enhance ease and speed of manufacture. This has reduced costs and the use of resource, which is of particular importance any engineering application. Design has also accounted for assembly and disassembly, for which mechanical fastening has been considered for all connections. It should however, be noted that a designing processes are not consistent with all manufacturing techniques. For example, when considering Rapid Prototyping instead of Machining for some mechanical arm parts, a much greater design freedom is exposed. Yet, in both cases the design process must take into account of the specific material being used.

4.9.2 Machining

Machined parts were designed for 3-axis machining from Aluminium 60-82 T6 and 70-75 T6. Features such as internal radii of pockets were consistent throughout the design to reduce tool changes and floor radii were kept square to eliminate the need for ball nosed cutters and specialised tooling. These features along with intuitive design have minimised set-ups required to machine billets of material. Technical drawings for each machined part are provided in Appendix A.7. Figure 33 is an example of a component which required only two set-ups and three tool changes. Figure 34 shows the machine used to make this part.



Figure 33: Base Plate - Two Set-ups and Three Tool Changes



Specification:

Bridgeport Series II Interact 4:

CNC milling machine

X Axis travel: 760mm

Y Axis travel: 370mm

Z Axis travel: 335mm

Spindle Speed: 4000rpm

Figure 34: Bridgeport Series II Interact 4 - CNC Milling Machine⁽²²⁾

4.9.3 Rapid Prototyping

Some parts of the design have been Rapid Prototyped, which has the considerable benefit of foregoing some conditions used in designing for machining. Parts used in the Mechanical Arm assembly have been made from PA2200 and in contrast to machining can be developed from one machine set-up only, directly from CAD data. Geometry can be more advanced and a range of profiles will not impact time to manufacture. Normally, rapid prototyped parts from CAD data have a tolerance of 100 microns (0.1mm). However due to a serious calibration error (most likely caused by the uncontrolled ambient temperature and conditions where the machine has been set-up) the parts produced were inaccurate. Figure 35 shows the scaling error.

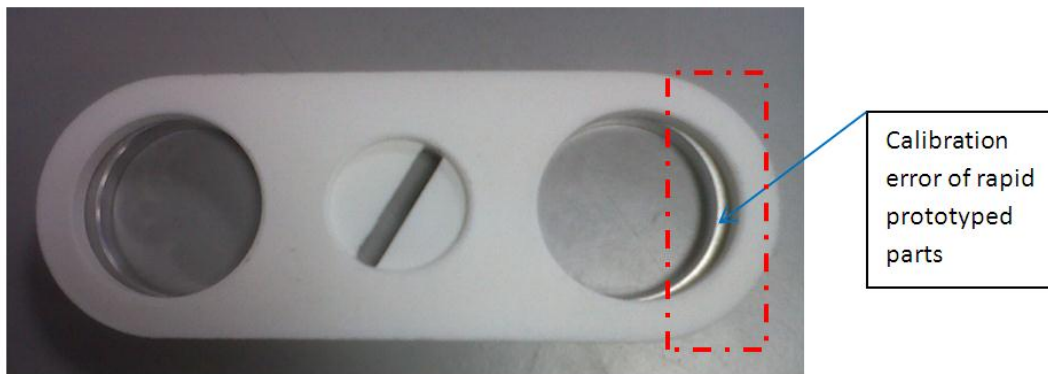


Figure 35: Support Motor Plate - Difference in Machined Part vs. Rapid Prototyped Equivalent

Rapid prototyped parts were considered for the whole mechanical arm design, but inaccuracies prompted the decision to machine critical parts for dimensional precision.

4.10. Testing

4.10.1 Packaging of the Base Joint

It was important to check the assembly of the base joint due to the tight packaging of the various parts. Figure 36 below displays the router inside the base joint. Nylon washers are used to provide clearance between the lower and upper plates.

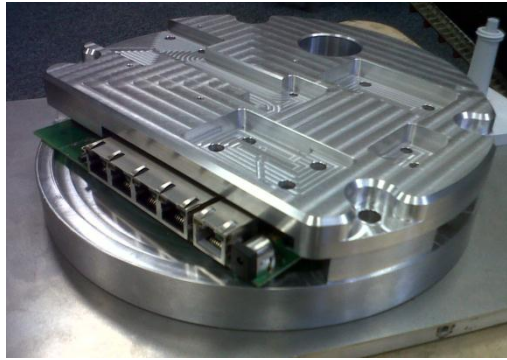


Figure 36: Router in the Machined Base

4.10.2 Elbow Joint

Figure 37 and 38 show the assembled elbow joint.



Figure 37: (shown left) Arm Structure

Figure 38: (shown right) Complete Elbow Joint Assembly

The elbow joint was assembled into its final configuration and the motor was powered using the table top power supply within the laboratory. Ballasts was used instead of the base joint/chassis. The backlash was observed as minimal, with the only backlash observed to be due to the natural backlash created by the distance 'between mating teeth measured along the circumference of the pitch circle' ⁽²³⁾.

4.10.3 Shoulder Joint

The shoulder joint was assembled to the upper base plate of the base joint and the motor was powered using the table-top power supply, pictured in Figure 39. The amount of backlash observed

in the shoulder joint was minimal, assessed in Figure 40. The arm assembly successfully raised a mass of 2kg from all tested starting positions.

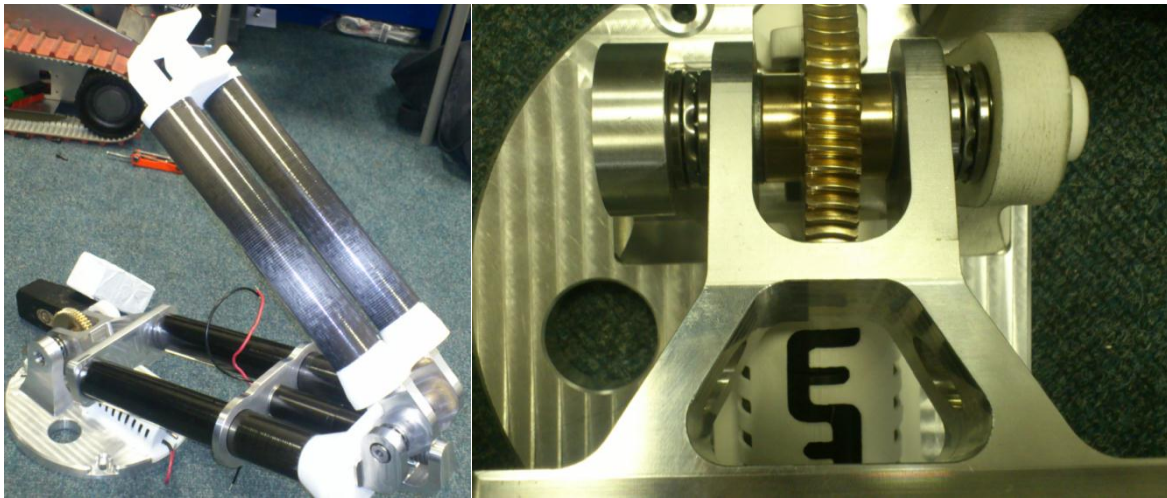


Figure 39: (shown left) Base Joint Construction

Figure 40: (shown right) Shoulder Joint Gearing Construction

5 Head

5.1 Objectives

To meet the purpose of being functional and reliable the Head needs to:

- Maintain structure and house sensors indefinitely
 1. Maintain integrity and not break in its environment
 2. Secured sensors so they do not move position
 3. Preserve electrical connections
- The head needs to be lightweight so the arm is able to lift it

5.2 Requirements

To fulfil the objectives stated, it is necessary to reduce the mass of the base plate and hood cover by reducing overall size and selecting appropriate materials. Where possible, the moments introduced

by sensor weights should be minimised. The design and material needs to be strong enough to withstand possible impacts, with fastening mechanisms that also meet the necessary standard. Sensors and electrical components should be securely mounted to the head assembly to prohibit movement and the likelihood of damage.

5.3 Formal Specification

SPECIFICATION: HEAD	
Size	<ul style="list-style-type: none"> Reduce current head size to approx. dimensions of L=20cm, H=6-8cm and W=12cm (contain all sensors) Efficient design to remove router from head
Weight	<ul style="list-style-type: none"> Reduce head weight from 2kg to 1-1.5kg
Part Placement	<ul style="list-style-type: none"> Secure parts to prevent damage Secure wiring Position webcam centrally to see gripper, enabling effective pick and place action
Rotation	<ul style="list-style-type: none"> 180° in conjunction with top joint of robot
Material	<ul style="list-style-type: none"> Sheet Aluminium of approx. 0.5-2mm thickness Stable if there is an impact from debris Hood to be lightweight and durable
Sensors	<ul style="list-style-type: none"> Integrate several sensors to one device (security webcam) Correctly size holes for component on head front
Access	<ul style="list-style-type: none"> Hinge on head for easy access to sensors Secure with quick access method, screws/clips
Gripper	<ul style="list-style-type: none"> Use existing mechanism Adapt claws with rubber sleeves to add flexibility

5.4 Design Intent

5.4.1 Integration of Sensors

Strategic planning of sensor positioning was conducted in order to reduce total size and utilise the space available. To maximise this and the reliability of sensor performance in a search and rescue mission, a new webcam was purchased to consolidate the LED, microphone, amplifier and webcam into a single unit (as shown in Figure 41).



Figure 41: Axis M1054 Security Webcam ⁽²⁴⁾

5.4.2 Mounting

The orientation of the servo-motor in the head joint was rotated 90° to accommodate the sensors in a compact setting. Brackets made out of Aluminium sheet securely fix the sensors to the outer shell with mechanical fastening mechanisms for ease of application and strength. This prevents the sensors from moving during operation. The electronic circuit boards used for the sensors in the head have been mechanically secured, reducing the amount of space required.

5.4.3 Material

5.4.3.1 Head Base Manufacture

The head base structure is made from Aluminium sheet of 1mm thickness, compared to the previous design constructed from stainless steel sheet of 1.0mm thick. This has reduced mass of the base part by 47.5%. The profile has been created using a laser cutter from a flat sheet, achieving net shape as shown in Figure 42. The sheet has been bent into its final shape as shown in Figure 43.

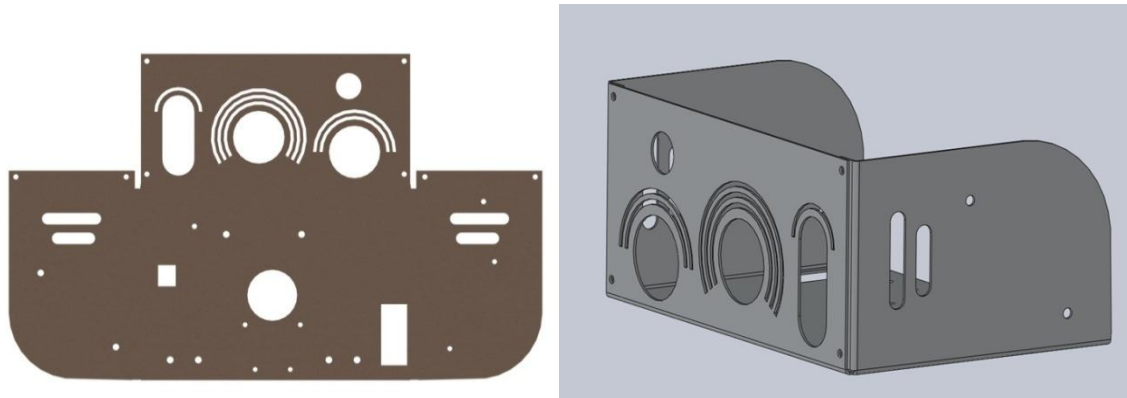


Figure 42: (shown left) Net Shape of Head

Figure 43: (shown right) CAD Image of Head Base Plate

5.4.3.2 Hood Manufacture

The hood cover has been developed by SLS Rapid Prototype facilities in PA2200 (Polyamide) ⁽²⁵⁾. This facility and material enables the part to be quickly produced with accuracy, required strength and relatively low cost. Figure 44 displays the CAD image of the hood cover which is attached to the aluminium structure with a simple hinge system, allowing sufficient access to the array of sensors stored in the head.

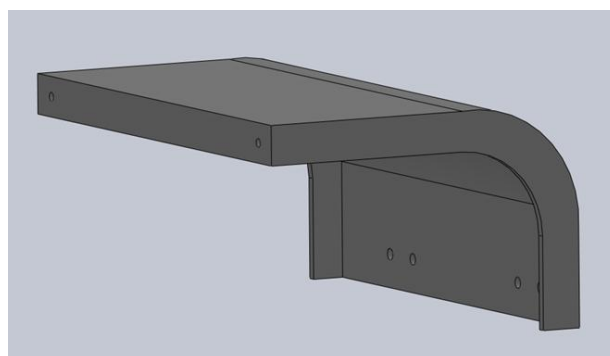


Figure 44: Head Hood Cover

6 Flippers

6.1 Objectives

To meet the purpose of being functional and reliable the Flippers need to:

- Lift the robot to move over obstacles
 1. Climb ramps and stairs, manoeuvre over step fields
 2. Rotate through 360°
- Minimise uncontrolled movement in the shaft
 1. Detail accurate position to the controller
 2. Enable accurate positioning by controller
- Withstand force exerted on the shaft and housing

6.2 Requirements

To fulfil the objectives stated it is necessary to identify the root cause of slack in the chain and devise solutions to this problem. There should be little movement in the Flipper shaft so that absolute encoders can be implemented to detail the exact position of the flippers to the operator. Deformation of the motor housing should be eradicated through design and material changes, with the force ideally being reduced or dispersed through the chassis.

6.3 Formal Specification

SPECIFICATION: FLIPPERS	
Slack Reduction	<ul style="list-style-type: none"> Investigate cause for the slack in the chain Replace the chain and sprocket to gears Design an adjustable housing
Motor Housing	<ul style="list-style-type: none"> Strengthen the housing Dimensions to secure the motor (35 mm diameter) Remove the spacing inside the housing to retain more of the structural integrity Using carbon steel
Absolute Encoder	<ul style="list-style-type: none"> Implement absolute encoder Ensure enough space is available in the chassis Ensure appropriate mounting
Space Requirement	<ul style="list-style-type: none"> Assess design changes based on existing space in the body The Flipper system should not interfere with other components
Force	<ul style="list-style-type: none"> Estimate the force exerted onto the shaft Deduce the possible causes of distorted shaft Design a bearing system to reduce force acting on the shaft Use thrust bearings to transfer a large portion of the force through the chassis

Table 14: Flipper formal specification

6.4 Process Flowchart

Figure 45 below displays the logical procedure undertaken to meet the objectives set. New problems were identified throughout the Flipper configuration process with designs and thoughts constantly changing as a result. To achieve one of the most critical objectives, to detail accurate position to the controller, an interim solution of simply re-pinning the flipper shafts and replacing the motor housing to reduce 'slack' was implemented as a final decision.

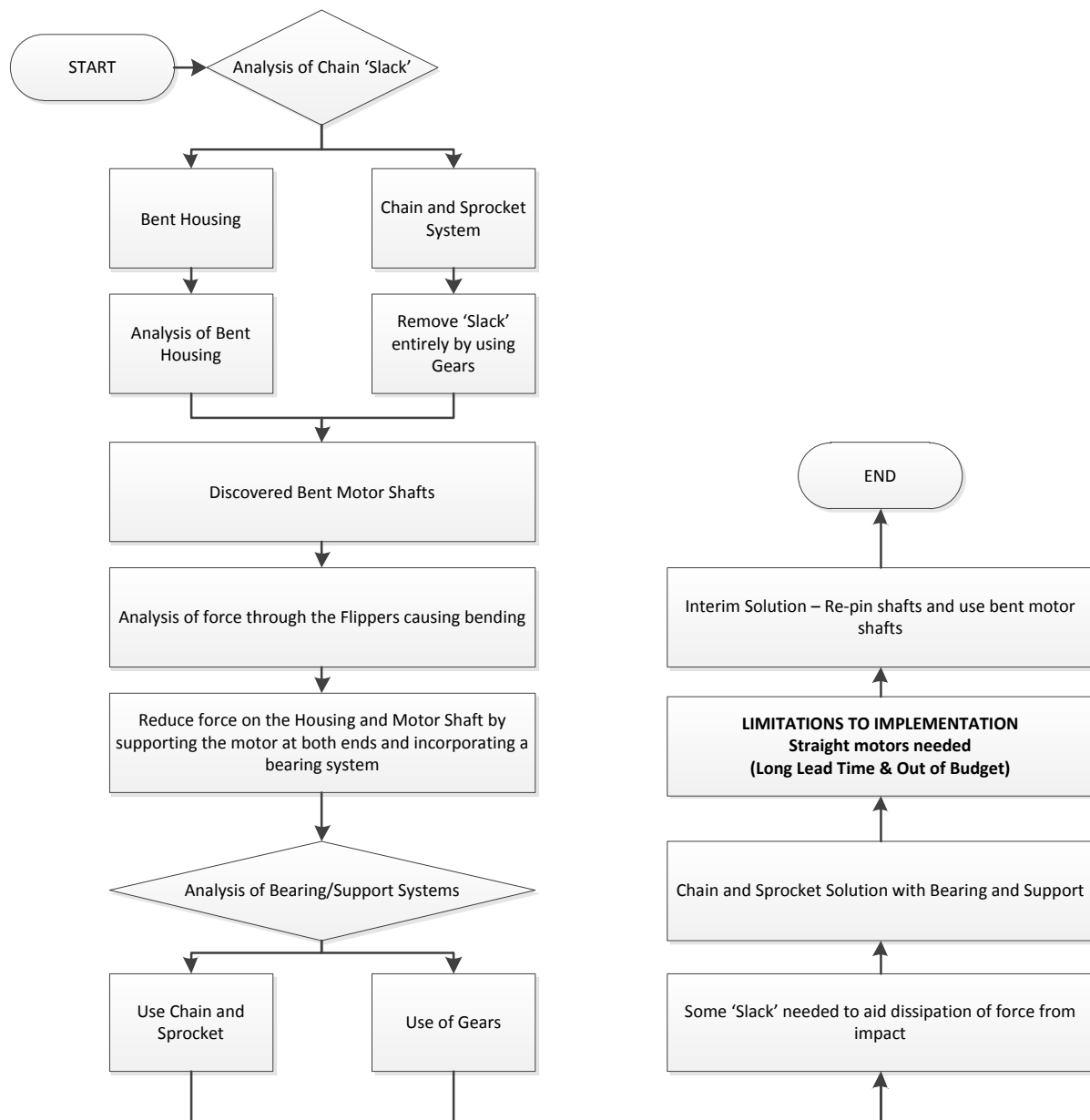


Figure 45: Process Flowchart of Flipper Design Process

One of the main hindering factors to an alternative solution, which would meet the objective of withstanding force exerted on the shaft and housing, was the discovery of bent motor shafts. The extent of deformation in both the motor shaft and housing is shown in Appendix C.1. The cause of the bending was a consequence of cyclic loading. Cyclic loading in this instance can be divided into two categories:

1. The Force acting on the motor shaft due to the weight of the robot, calculated as 2.7 kN, as shown in Appendix C.2
2. The Force experienced due to an impact from a step field, calculated as 21 kN, as shown in Appendix C.3

The most successful system to reduce the degree of Force acting on the shaft would be to implement a bearing system connected to the chassis, transferring the Force through the body rather than the shaft itself. By supporting the shaft fully at both ends this replaces the cantilever beam scenario currently in use. Appendix C.4 shows the supporting analysis used to predict the level of deflection reduction and proves the integrity of the design.

Straight motor shafts are an obvious prerequisite to incorporating a bearing system into the chassis. Integration with bent motor shafts would only jeopardise the functionality and reliability of the Flipper mechanism, bringing validity to the overall engineering process, as shown in Figure 45, and the implementation decision.

7 Software and Systems

7.1 Objectives

- Inverse Kinematics Implementation: The interface is to be modified to allow direct control of head position using a 6-axis gamepad controller.
- SLAM software is to be written to make use of external sensors to build a digital representation of the robot's surroundings, and the robot's position within.
- The robot and client software are to be modified to find and decode QR codes in the robot's main camera feed.
- The interface visual robot representation is to be improved, adding representation of robot title and centre of gravity, as well as improving flipper and arm position representation.

7.2 Requirements

In order to enable inverse kinematics, software must be developed containing the necessary equations and logic to accept a goal end-effector position, calculate potential joint angle combinations and select the most practical combination.

SLAM can be achieved using data from a LiDAR, Kinect-style RGB-D camera, or simple RGB camera⁽²⁶⁾. 3D LiDAR scans will require the tilt, roll and pitch of the LiDAR unit to be sensed, as described in section 7.4.1.1.1. Software must be written to combine these values with LiDAR distance readings (likely by trigonometry) and produce 3D Cartesian coordinates representing each laser pulse's obstacle intersection. Given their wide angle of sensing, both RGB and RGB-D cameras would require no more actuation than simple robot rotation. The collected data must then be utilised in software to build a 2D or 3D model of the robot's surroundings, including the robot's current position. Methods vary wildly depending on hardware and are discussed in section 7.4.1.

As stated above, the ability to read QR codes requires very little work other than software; the hardware and systems required are already in place. Software must be written to identify QR codes within a still bitmap image (supplied by the IP camera), process the image for optimised QR decoding, decode the code, and store and relay the results to the robot operator.

The centre of gravity (CoG) of each limb and the central body needs to be calculated and the average represented visually in either 2D or 3D on the interface. This will require accurate tilt information, likely provided by an xSens unit or accelerometer, as well as all limbs equipped with absolute encoders. Software must be written to accept these inputs, and using knowledge of the robot geometry, calculate an aggregated centre of gravity. This must be represented on the operator interface.

7.3 Formal Specification

SPECIFICATION: Software and Systems	
Inverse Kinematics	<ul style="list-style-type: none"> Can result in any joint combination that the arm is physically capable of Robot-damaging joint angles should be impossible Interface warns if requested position is unattainable Capable of maintaining a horizontal end-effector for various sensor usage while mobile
SLAM	<ul style="list-style-type: none"> Capable of returning some real-time representation of environment for the operator interface Capable of returning a real-time representation of the robot's position Capable of building an accurate arena representation (either in real-time or post-run) for judging post-run
Centre of Gravity Calculation	<ul style="list-style-type: none"> Capable of collecting data regarding chassis tilt and limb angles from xSens MTi and absolute encoders (attached to motor control boards) Capable of combining said data with robot geometry to calculate an aggregated centre of gravity
Visual Representation	<ul style="list-style-type: none"> Capable of displaying the aggregated centre of gravity Capable of accurate representing current flipper and arm positions
Improvements	
Reliability	<ul style="list-style-type: none"> Software should include error-handling so as to prevent failure in any situation the robot is likely to encounter Reasons for inaction on operator commands reported so as to avoid confusion
Speed	<ul style="list-style-type: none"> Software should be sufficiently simple/efficient to perform all functions as the robot navigates an arena at full speed

Table 15: Software and Systems specification

7.4 Design Intent

7.4.1 Mapping

7.4.1.1 LiDAR Scanning and SLAM

Previous teams have made use of Hokuyo's URG-04LX LiDAR ⁽²⁷⁾ (**L**ight **D**etection **A**nd **R**anging) scanner, mounted on a two-servo gimble intended to keep the scanner horizontal regardless of terrain ⁽¹⁷⁾. Details of the LiDAR module and its operation can be found on the manufacturer's website ⁽²⁷⁾. Previous robot iterations have made use of the module for 2-dimensional SLAM

(Simultaneous Localisation and Mapping)⁽¹⁷⁾, although last year's team did not implement SLAM⁽¹⁸⁾, and the scanner was effectively unused.

Previous SLAM development had taken place in partnership with the Computer Science department, with the main goal of furnishing the automated robot's navigation systems with 2-dimensional environment data with which to navigate. The Robocup 2012 rules specify 3D mapping as a scoring criteria; as such, a robot capable of only 2D mapping would lose points. In 2011, even 2D SLAM was not implemented, and as such no bird's-eye map could be displayed on the operator interface.

The use of a gimble is also a waste of resources and weight; the robot arm possesses sufficient degrees of freedom to maintain a horizontal LiDAR. It is possible that the gimble was necessary due to a lack of functional inverse kinematics software, which would allow the arm to perform the same function if the LiDAR were head-mounted. Conversing with members of previous teams revealed that the gimble had not performed well, due to significant lag in servo movement preventing chassis tilt compensation.

The first goal was to re-implement 2D SLAM, in order to produce a real-time bird's-eye map for display as part of the operator interface. Since a large part of the Robocup challenge is the navigation of maze-like arenas, this is likely to improve navigation times and allow more victims to be found. The second goal was to re-locate the LiDAR module to the head, allowing the removal of unnecessary gimble servos, and reducing level-correction lag. The third goal was to implement 3-dimensional mapping of arenas.

7.4.1.1.1 Sensory Input

3D LiDAR mapping requires reliable information as to the roll, pitch and yaw of the LiDAR module. These values, when combined with the radial offset of each distance measured by the module, allow the calculation of Cartesian coordinates for each laser beam surface intersection. The xSens MTi module, described in previous technical reports⁽¹⁸⁾ and the xSens website⁽²⁸⁾, is designed to return real-time values for each of the above using a combination of gyroscopes, accelerometers and

magnetometers. By mechanically fixing both the LiDAR and MTi modules to the robot head, these values can be made to represent the LiDAR roll, pitch and yaw. As such, whatever the orientation of the head/LiDAR, a set of Cartesian coordinates (relative to the LiDAR) can be returned.

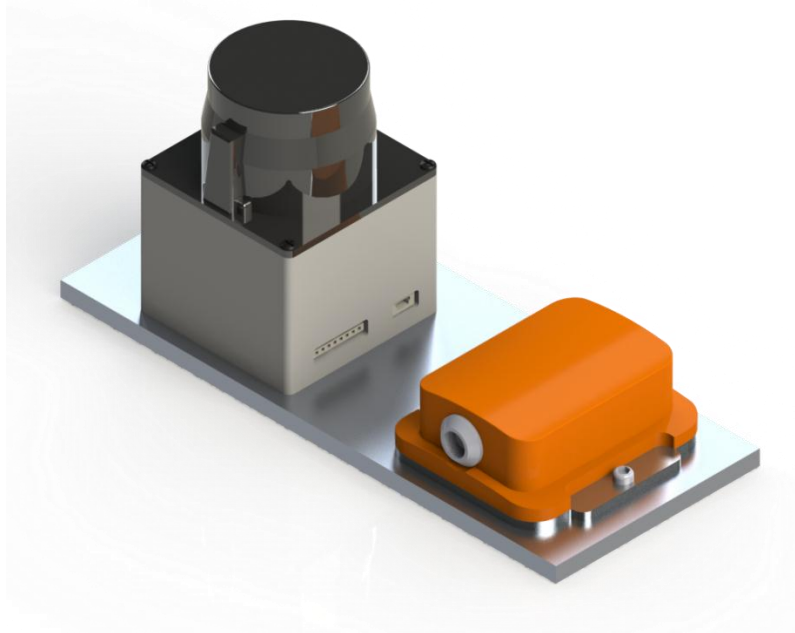


Figure 46: The Hokuyo URG-04LX and xSens MTi mounted for positional agreement

In order to create a 3D Cartesian point-cloud of physical objects surrounding the robot, the LiDAR must be rotated (principally in pitch or roll) about the origin of its laser pulses, so as to maintain a constant Cartesian origin. With the implementation of inverse kinematics, this is easily achieved, and could be triggered from the operator interface with a simple button-press.

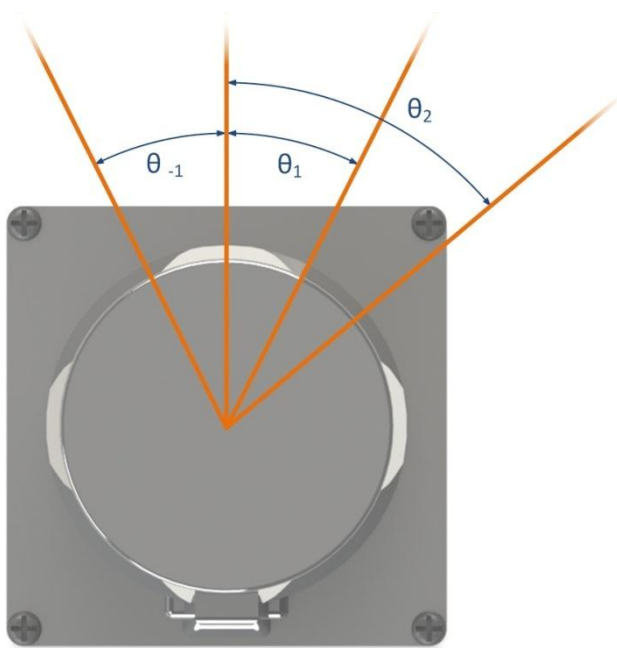


Figure 47: LiDAR orientation definitions

If the LiDAR module's pitch, roll and yaw are represented by α , β and γ respectively (see Figure 47), and the rotational offset of an individual laser pulse is represented by θ (see Figure 48), then the pulse's angles from horizontal and magnetic north, ζ and σ respectively, can be given by:

$$\sigma = \alpha + \theta \sin \beta$$

$$\zeta = \gamma + \theta \sin \beta$$



Then the Cartesian coordinates given by said pulse (of length L) can be given by:

$$x = L \cos \sigma$$

$$y = L \sin \sigma$$

$$z = L \sin \zeta$$

To clarify, the pulse angle of a particular LiDAR pulse is given by:

$$\theta_n = n\lambda$$

Figure 48: LiDAR pulse angles

Where λ is the step angle: the angle between each pulse. In the case of the Hokuyo URG-04LX:

$$\lambda = \frac{360^\circ}{1024} = 0.3516^\circ$$

All realistically-implementable SLAM algorithms are based on the comparison of each LiDAR scan's Cartesian results with the last. This comparison allows the robot to mathematically estimate any change in its position that occurred between the two frames, as shown in Figure 49. Keeping a

record of previous points (a “point cloud”) allows a map of the arena to be built, as well as knowledge of the robot’s current position within the arena.

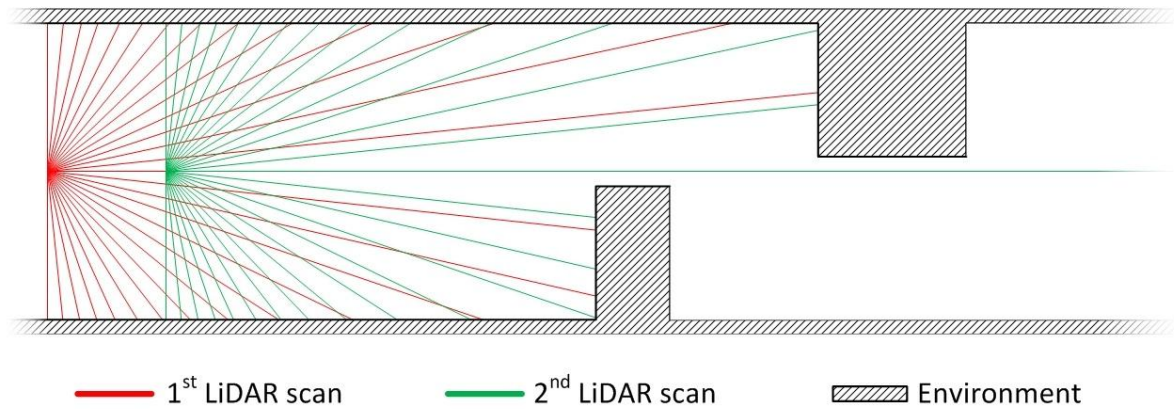


Figure 49: Simultaneous Localisation and Mapping (SLAM) using a LiDAR module

This mathematic comparison of LiDAR data is not trivial in 2 dimensions – in 3, it becomes prohibitively complex.

7.4.1.2 Data Processing/SLAM Algorithms

Since previous teams failed to produce a 3D mapping algorithm, even when supported by a team of computer science undergraduates, the decision was made to implement an algorithm developed elsewhere. A number of systems were considered, using relevant author papers and example results summarised in Table 16.

Algorithm Name	Advantages	Disadvantages
DP-SLAM ⁽²⁹⁾ ⁽³⁰⁾	<ul style="list-style-type: none"> • High accuracy, to the point that large maps require no loop-closing (see Figure 50) • Takes raw LiDAR data and odometry 	<ul style="list-style-type: none"> • 2D only • Linux-based C, would require file interface to transfer data to/from Java • Designed for off-line processing, on-line may not be possible • Large memory (4+GB) needed for large maps
HOG-Man ⁽³¹⁾	<ul style="list-style-type: none"> • Designed for on-line operation • Capable of 2D and 3D • Sped up by considering only coarse map corrections during run-time 	<ul style="list-style-type: none"> • Not written for raw LiDAR/point-cloud data – is a SLAM “back-end” • Requires data pre-processing to produce vertex and edge data

		<ul style="list-style-type: none"> Linux-based C, would require file interface to transfer data to/from Java
RGBDSLAM ⁽³²⁾	<ul style="list-style-type: none"> Produces 3D textured models of objects/small environments using only xBox Kinect image data Utilises the above HOG-Man algorithm for map building Designed/tested for/on Ubuntu 	<ul style="list-style-type: none"> Makes no use of LiDAR data Linux-based C, would require file interface to transfer data to/from Java Not suitable for Tele-operated chassis due to Kinect mounting complexity
RobotVision ⁽³³⁾	<ul style="list-style-type: none"> Requires single, ordinary (non-distance sensing) camera Designed for run-time operation 	<ul style="list-style-type: none"> Makes no use of LiDAR data by default, can be implemented More prone to drift than LiDAR techniques, resulting in inaccurate final maps Linux-based C, would require file interface to transfer data to/from Java
6DSLAM	<ul style="list-style-type: none"> Capable of constructing large 3D point-clouds from individual 3D scans 	<ul style="list-style-type: none"> Requires robot to pause to produce 3D scans, often enough for them to overlap Not capable of run-time operation Requires pre-processing of LiDAR data into 3D scans Linux-based C, would require file interface to transfer data to/from Java
tinySLAM ⁽³⁴⁾	<ul style="list-style-type: none"> Very small (200 lines of code!) simple SLAM algorithm Intended for real-time SLAM Tested with Hokuyo 04-LX Designed for “black box” use but can be modified Code simplicity may allow re-writing in Java for easy integration Possible improvement with xSens data implementation 	<ul style="list-style-type: none"> Limited to 2D mapping Linux-based C, would require file interface to transfer data to Java. Produced maps somewhat “messy”, see Figure 51. Does not utilise xSens data
TreeMap	<ul style="list-style-type: none"> Extreme efficient with in-built error checking and optimisation 	<ul style="list-style-type: none"> Like HOG-Man, more of a SLAM “back-end”, requiring pre-processed data Requires data already separated into 3D features Linux-based C, would require file interface to transfer data to Java

Table 16: SLAM Algorithms considered for use and their advantages and disadvantages

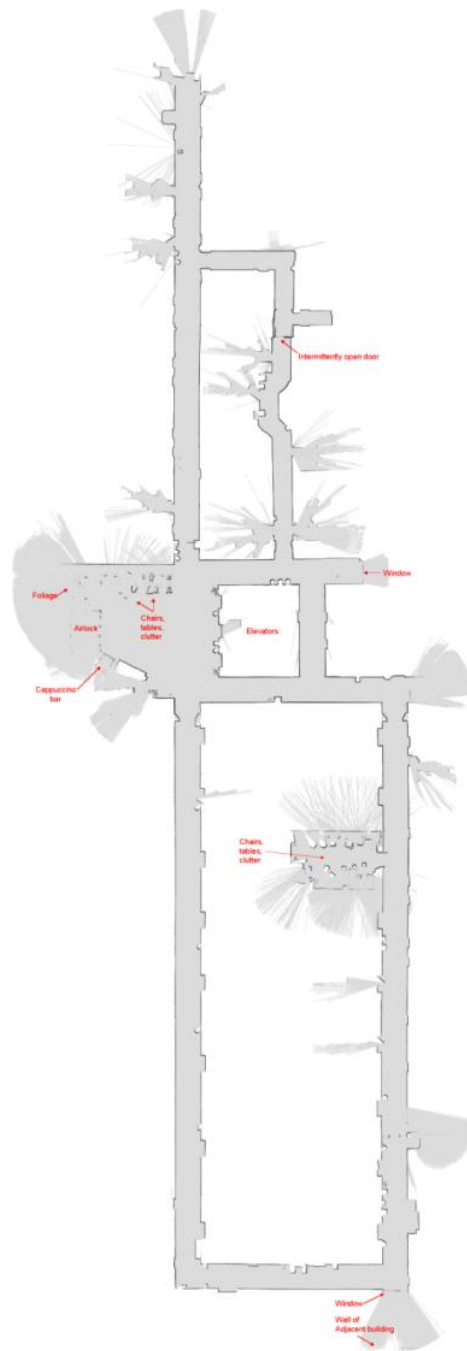


Figure 50: Large 2D map produced by Duke University's DP-SLAM

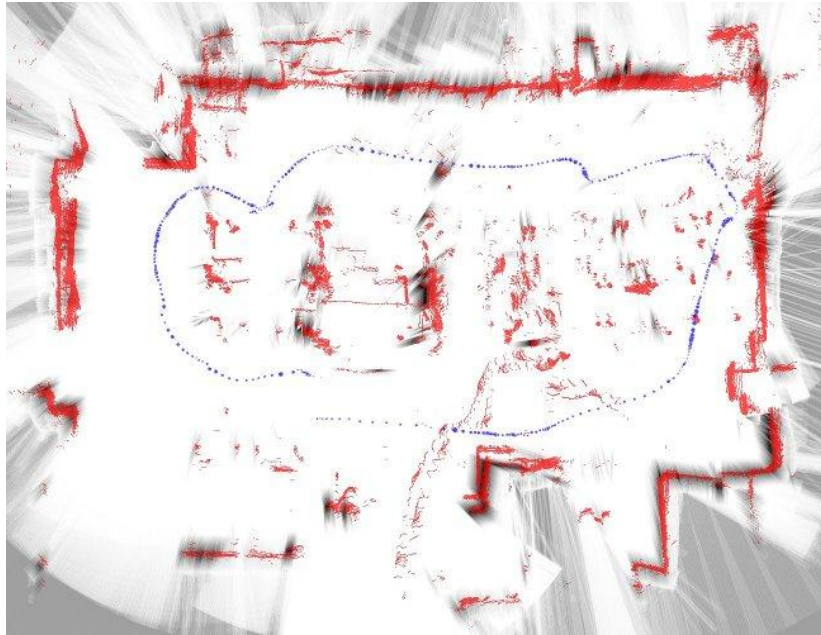


Figure 51: Map produced by tinySLAM

Algorithm Name	Disqualifying factor
2D I-SLSJF ⁽³⁵⁾ ⁽³⁶⁾	<ul style="list-style-type: none"> MATLAB-based code, inaccurate (blurry) results
GMapping ⁽³⁷⁾ ⁽³⁸⁾	<ul style="list-style-type: none"> Requires CARMEN, a C-based robot navigation toolkit designed for specific robot chassis (iRobot, ActivMedia, Nomadic Technologies etc.)
GridSLAM ⁽³⁹⁾	<ul style="list-style-type: none"> Also requires CARMEN
Robomap Studio	<ul style="list-style-type: none"> MATLAB-based Evolutionary code, young field of study, mostly academic value at current

Table 17: Rejected SLAM algorithms along with the reason for rejection

Likely due to its complexity, no readily-implementable 3D SLAM algorithm was found. It was decided that due to its simplicity and potential for modification, tinySLAM would be employed for real-time 2D SLAM during competition runs. The algorithm would be supplied with 2D LiDAR data extracted from 3D data using narrow a (~100mm) Z-axis filter, and process it to provide a top-down view of obstacles, as well as the robot's position. In an attempt to earn 3D mapping points, the robot will still be capable of pausing and performing/recording a 3D LiDAR scan. This scan's position will be informed by the still-running 2D slam algorithm, with height being calculated from arm joint angles.

It should then be possible to perform a post-run 3D arena construction, encompassing only those points of interest in 3D dimensions.

7.4.1.3 *RGBD/Kinect SLAM*

SLAM algorithm research unearthed an algorithm programmed in C, specifically to construct a 3D map of environments and objects using only the visual and distance data from a Microsoft Kinect: RGBDSLAM. Since the code is complex, conversion to Java is unrealistic; the utilisation of a Java Native Interface class to communicate with the software would be necessary. To assess the reward for such investment of effort, the software was run stand-alone on the autonomous robot, and the outcomes examined.

7.4.2 *Inverse Kinematics*

Rather than approach the problem of inverse kinematics with traditional matrices transformation methods, it was decided to make use of the arm's unique architecture to simplify mathematics. For example, given a specified goal end-effector position, the rotational base joint may take only two positions: pointed directly at the point, or directly away from the point. Before calculating possible joint angles, the magnitude of the distance between base joint and goal position is checked, such that calculation is halted and the operator informed if the arm cannot reach the distance.

The problem is further simplified by treating the two final joints as point rotations; that is to say the two final limbs have length zero. The error introduced by this will be easily corrected by operator human anticipation. We are now left with a single-joint, two-limb problem to solve, which has only two possible solutions.

Therefore, in total, we have four solutions. Each solution produces some rotation, and simple mathematics allows the calculation of wrist joint angles required to achieve goal orientation. Each solution is checked to ensure possible joint angles; if no possible combination exists, the operator is informed and no movement is undertaken. If more than one solution is possible, the best is chosen

on a weighted least-effort basis; the movement of larger joints is considered “more costly”, such that smaller, lower powered joint movements are preferred.

7.4.3 QR Code Reading

In a change to competition rules, the German Robocup Rescue competition will also be judged on the robot’s ability to find and decode printed 2-dimensional “QR codes” on arena walls and (rarely) ceilings. An example code can be seen in Figure 52. Failure to implement such functionality would result in lost points at the competition.



Figure 52: An example QR code, containing WMR's homepage URL

Likely due to the recent surge in QR code popularity, especially for

use in smartphone applications, a Java API called ZXing (pronounced “Zebra Crossing”) already exists and is capable of finding and decoding 1 or 2-dimensional barcodes, including QR codes, in a bitmap ⁽⁴⁰⁾. Since the IP camera used returns video in the MJPEG (Motion JPEG) format, a URL of the latest frame, which is simply a JPEG, is readily available. Implementing live QR decoding was simply a case of downloading said latest frame as a bitmap, converting it to a binary (black and white) image, and supply said binary image to the ZXing API methods. These methods then return value indicating whether the image contains a barcode, and (if applicable) where it is within the image and what it contains.

The ZXing API’s ability to specify the area of the image in which a QR code lies is particularly useful. Each pixel in the video camera’s feed can be considered a vector from the camera’s CCD outwards; therefore, the pixels that ZXing returns as of interest can be converted to vectors within the 3D point-cloud. The intersection of these vectors with existing groups of points will allow the addition of QR code location data to the final arena point-cloud, hopefully scoring points. There is the possibility of a similar system being implemented with regard to victim location and information.

7.4.4 Centre of Mass

The centre of gravity of each member is represented by a unit vector P , given by {1.1}, where i, j and k represent unit vectors in the x, y and z directions respectively.

For simplicity the CoG position is evaluated along the x and z axes independently as seen in equations {1.1} and {1.2}.

$$P = \begin{bmatrix} a_x \\ b_y \\ c_z \end{bmatrix} = a_x i + b_y j + c_z k \quad \{1.1\}$$

The transformation matrix for pure rotation about the y axis is given by equation {1.2} ⁽²⁰⁾, where θ is the angle rotation of the member from the z axis from the origin of the respective coordinate system.

$$Rot(y, \theta) = \begin{bmatrix} \cos \theta & 0 & \sin \theta \\ 0 & 1 & 0 \\ -\sin \theta & 0 & \cos \theta \end{bmatrix} \quad \{1.2\}$$

Taking a right handed reference frame with the origin at the centre of the axis of rotation and the z axis orientation being in line with the neutral position of the joint, we can use the above rotation matrix to discern the new position of the arm when it is rotated through an angle θ about the y axis.

Once movements of the arm and head are evaluated to find the effective CoG of the arm at its new position the entire arm assembly is rotated about the z axis using equation {1.3} to find the real CoG position.

$$Rot(z, \theta) = \begin{bmatrix} \cos \theta & -\sin \theta & 0 \\ \sin \theta & \cos \theta & 0 \\ 0 & 0 & 1 \end{bmatrix} \quad \{1.3\}$$

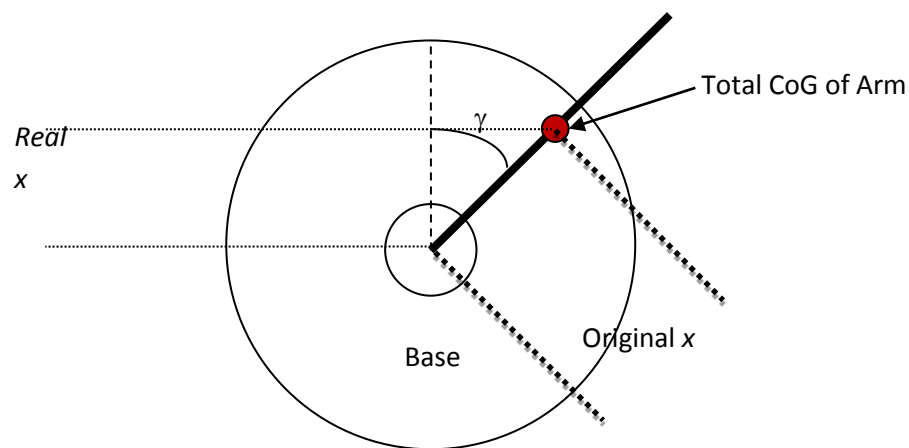


Figure 53: Final rotational transformation

The centre of gravity program calculates the position of the centre of gravity of the entire robot many times per second by evaluating joint movements and the relative masses of components.

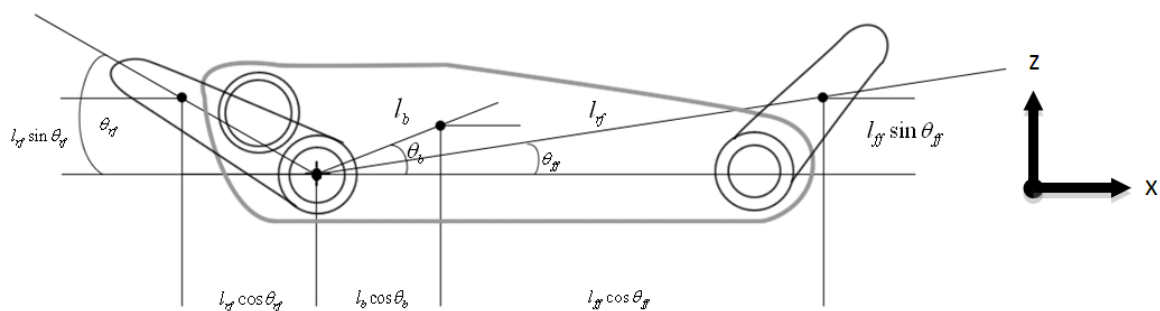


Figure 54: Robot centre of gravity geometry

Position of CoG (x,z) is given by:

$$x = \frac{m_b l_b \cos \theta_b + m_{rf} l_{rf} \cos \theta_{rf} + m_{ff} l_{ff} \cos \theta_{ff}}{m_b + m_{rf} + m_{ff}}$$

$$z = \frac{m_b l_b \sin \theta_b + m_{rf} l_{rf} \sin \theta_{rf} + m_{ff} l_{ff} \sin \theta_{ff}}{m_b + m_{rf} + m_{ff}}$$

Java code implementing the above calculations can be found in Appendix D.2.

7.5 Testing

7.5.1 Mapping

7.5.1.1 LiDAR 3D functionality

After much tweaking of the trigonometric equations, the 3D LiDAR software now produces good 3D point-clouds when the xSens-LiDAR module is rotated about a point. A good example is shown in Figure 55. Different colours indicate different scans.

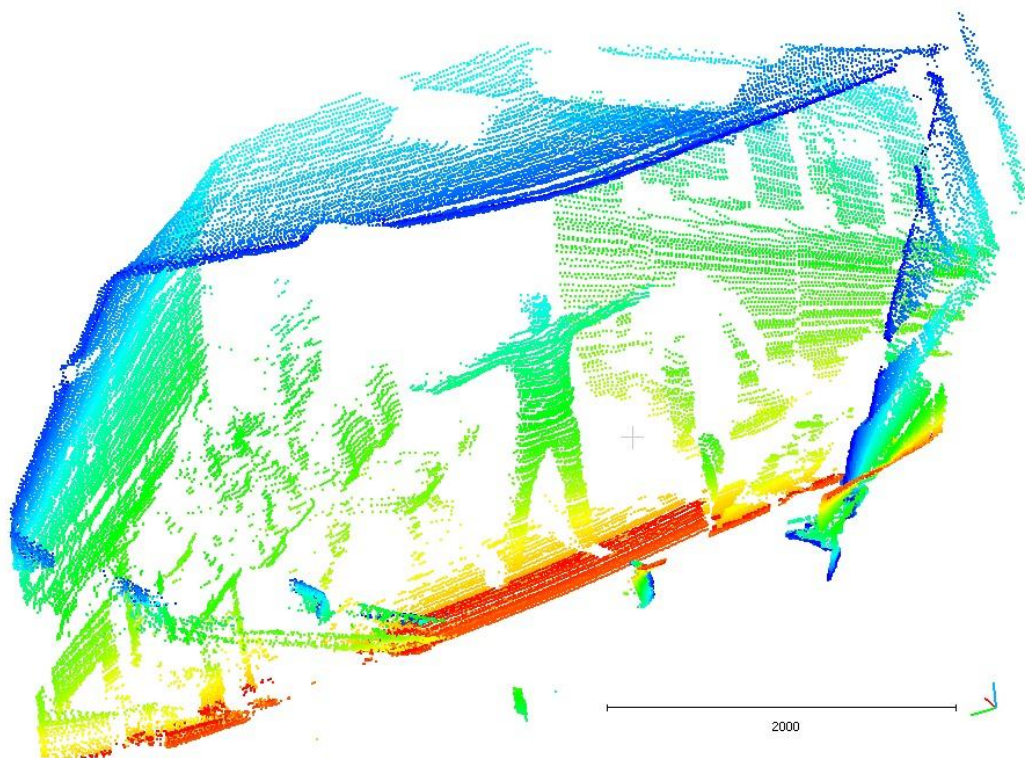


Figure 55: A 3D point cloud of the project leader, created by new LiDAR software

7.5.1.2 RGBDSLAM

The software was effective, producing a textured 3D map of either environments or objects (see Figure 56). However, it was highly processor-intensive, struggling to create maps combining more than 10 images, even while running no other software, making it unfeasible for implementation on

the current robot platforms. Significant computational hardware upgrades may allow its implementation.

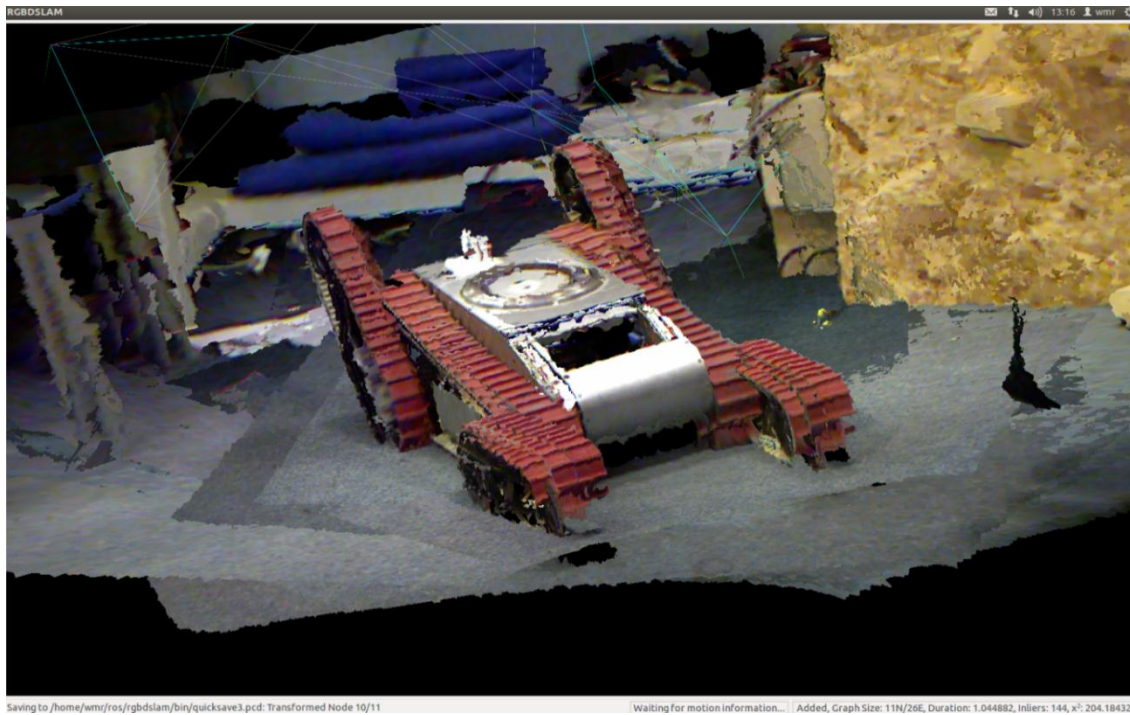


Figure 56: The textured point-cloud resulting from a Kinect (RGBD camera) scan of the teleoperated chassis

7.5.2 Inverse Kinematics

At the time of writing, the new arm is not in a state capable of inverse kinematics testing; once it is, code integration will be a simple case of tweaking values, such as maximum and minimum safe joint angles, and joint offset angles.

7.5.3 QR Code Reading

The QR functionality has been implemented successfully; video feeds are continuously monitored for QR codes, and they are automatically decoded and the results displayed on the interface when present. The results are also stored, along with the robot's position at the time. Vector and point-cloud position calculation is yet to be implemented.

7.5.4 Centre of Mass

While the centre of mass software will return realistic coordinates when supplied with example data, lack of finalised hardware has prevented full-scale testing.

8 Electronics

8.1 Objectives

To meet the purpose of being functional and reliable the Electronics need to:

- Maintain connectivity to all essential parts
 1. Mechanical components
 2. Computer system
 3. Sensors
- Allow for assembly and disassembly of the Electronic network
- Incorporate encoders in the Flippers with absolute encoding
- Output absolute position data from the Mechanical Arm encoders
- Identify when battery charge is low to prevent over-discharging

8.2 Requirements

To fulfil the objectives quantified, the electronic network must be re-wired with all connections successfully being integrated in the Stack using industry standard connectors. An effective method of sensing absolute Flipper position needs to be chosen and further, output meaningful results. This principle is also required for recognising the position of the joints in the Mechanical Arm. Encoders for this purpose should be fully encased to prevent damage from the environment. To maintain the operative nature of the batteries, a warning system which informs the controller of low charge should be used.

8.3 Formal Specification

SPECIFICATION: ELECTRONICS	
Stack	<ul style="list-style-type: none"> ▪ Add two more AX3500 motor control boards to replace old AX500's. ▪ Focus on connecting the robot to the stack, not connecting the stack to the robot
Flipper Encoders	<ul style="list-style-type: none"> ▪ Need to be absolute ▪ Need to fit with the existing systems and limited space available
Harwin Connectors	<ul style="list-style-type: none"> ▪ Harwin connectors need to be replaced with correct models and without the application of glue ▪ Replacing the spade connectors for Harwin connectors in the arm will allow for continuity in the robots design
Battery Sensor	<ul style="list-style-type: none"> ▪ Adding a battery sensor for each battery to allow for accurate reading of the battery voltage ▪ Prevents over-discharging of batteries which is a costly mistake
Wiring	<ul style="list-style-type: none"> ▪ Wiring should be easy to follow throughout ▪ Coloured wiring to identify similar positioning (e.g. red at top of head, which follows to the power board) ▪ Produce wiring diagram to illustrate the wiring of the robot to people unfamiliar with the design
Arm Encoders	<ul style="list-style-type: none"> ▪ Immune to dirt affecting reliability ▪ Lightweight

Table 18: Electronics Specification

8.4 Design Intent

8.4.1 Absolute Encoders

Absolute encoders give positional feedback of the flippers and have advantages over incremental encoders. Every position of an absolute encoder is unique and absolute encoders do not lose position when power is removed ⁽⁴¹⁾.

8.4.1.1 Hall Effect Encoders (Flippers)

Hall Effect Encoders, shown in figure 57 and further described in Appendix E.1, were chosen based their relative ease of placement and mounting. Ideally, an encoder would have been placed directly

on the Flipper shaft but this would have required an alternative chassis design to form the required space and protection.

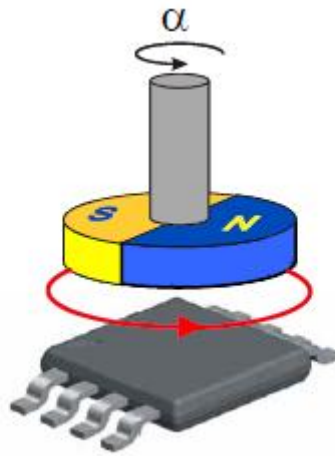


Figure 57: Melexis MLX90316 (42)

8.4.1.2 PCB

The Encoder is a surface mount package and as such needs to be mounted for use. A PCB shown in figure 58 has been designed to be mounted at the end of the Flipper shaft, utilising the space between the sprocket and the exterior wall.



Figure 58: Encoder PCB

8.4.1.3 Encoders (Mechanical Arm)

As described in section 4.5.6, the encoders have been fitted to the shafts of the joints in the Mechanical Arm. Specifically the Vishay 357 as shown in Figure 59 has been used. This is of a resistive configuration and is a closed pot configuration to prevent damage from external factors. The model is a single turn version which greatly aids sensitivity, ideal for this application where motion being controlled and is often small.



Figure 59: Vishay Model 357 (43)

8.4.2 Battery Sensor

Lithium Polymer batteries are sensitive to over-discharging, causing permanent non-function and potentially combustion. To prevent over-discharge a simple warning indicator system has been fitted to the battery housing. The solution consists of connections to each individual cell within the battery and provides the most accurate feedback. The signal for low voltage is set to 3.3V, where once reached a buzzer will sound. This is a particularly useful because the lowest cell is considered, even if other cells have higher voltages, therefore preserving the battery to the best ability. Figure 60 displays the LiPO battery sensor.



Figure 60: Battery with attached LiPo warning circuit

8.4.3 Stack Configuration

The stack has been reconfigured by the replacement of two AX500 motor controller boards with two AX3500 motor controller boards. The AX3500 boards are capable of handling powerful motors used in the arm, as well as having suitable encoder inputs to provide feedback for accurate positioning. Figure 61 is a simple representation of the Stack arrangement.

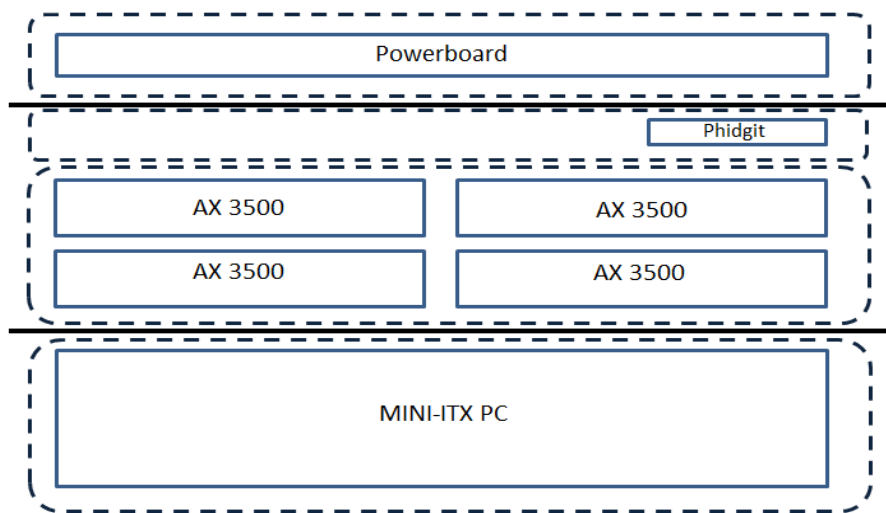


Figure 61: Stack Configuration

8.4.4 Wiring

Connections to the Stack are now organised such that it is a removable entity; all connections from the robots components are made directly to the Stack using the connection devices shown in Figure 62.



Figure 62: Harwin Connectors (44)

Connectors have been used in all areas of the electrical network to increase the reliability and ease of access to all of connections and components.

8.4.4.1 Wiring Diagram

Figures 63 and 64 display how the electrical network of the robot is now connected together. This up to date version ensures connections are made in the correct place, preventing damage to the system.

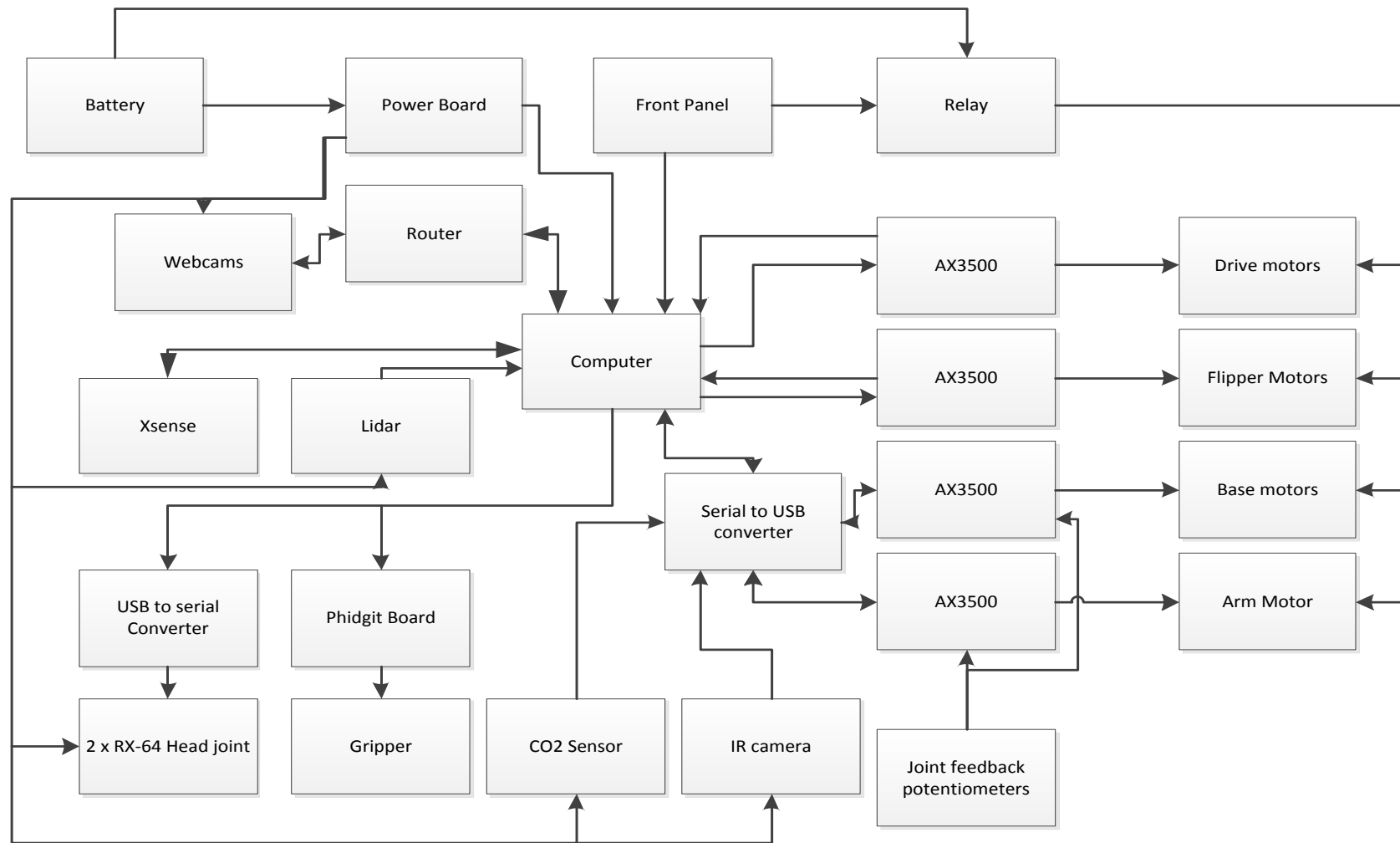


Figure 63: Stack Arrangement by Component

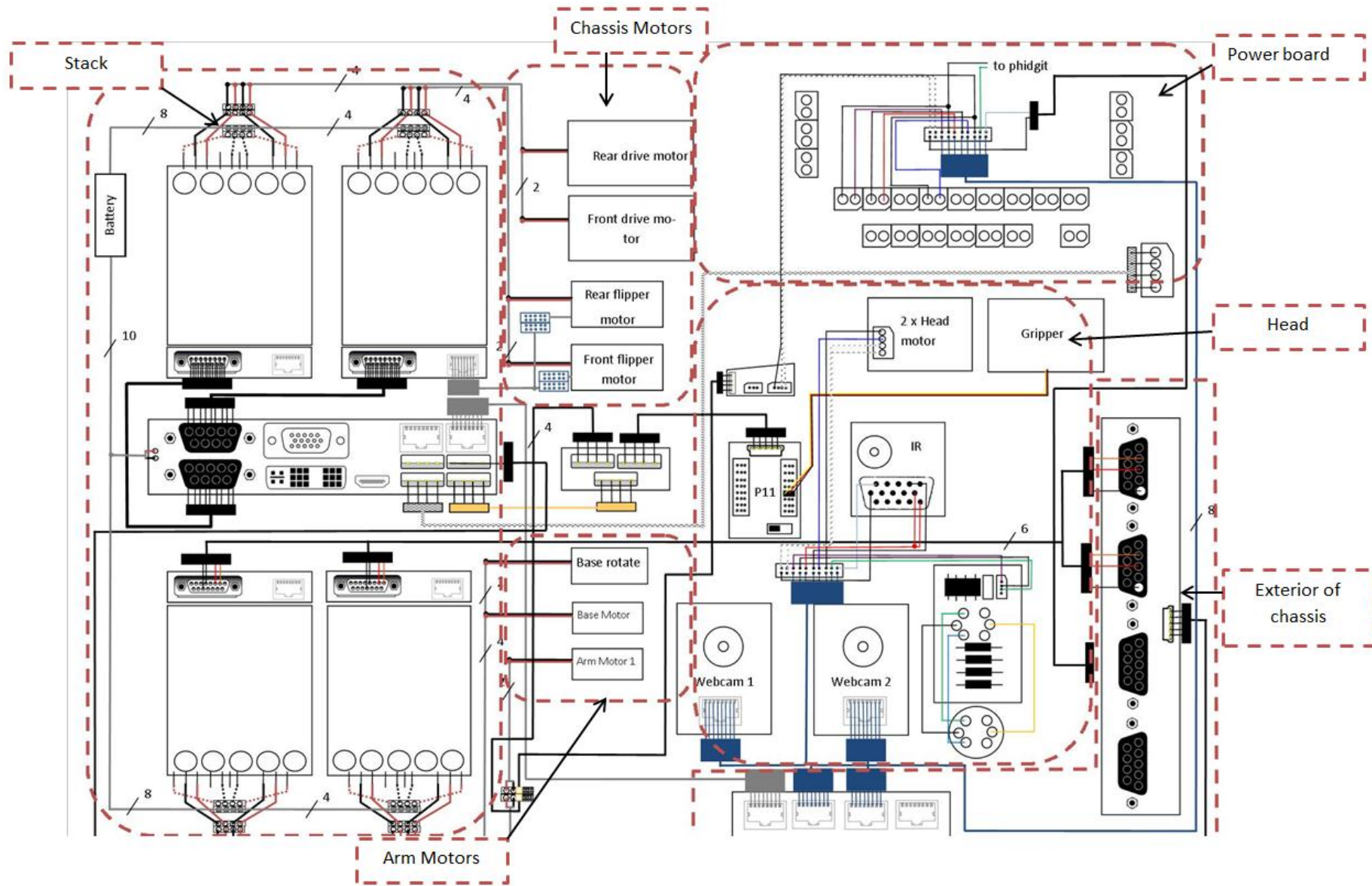


Figure 64: Wiring Diagram

9 Critical Review

9.1 Chassis Design

By utilising the existing chassis, we retain all of the positive attributes associated with it: strength, mobility and relatively low mass. Development of associated systems has also been aided by the immediate availability of a pre-existing chassis.

However, such a continuation could be regarded as a lack of progress; the aforementioned attributes have not been improved upon. The chassis still has a very poor resistance to particulates and moisture. Opportunities such as motor cantilever elimination and chassis size reduction have also been neglected.

9.2 Flipper Design

Similarly to chassis decisions, the maintenance of existing flipper configurations has allowed the retaining of high levels of mobility. By disassembly and close examination, backlash in the flipper shaft has been reduced to negligible. Although problems with flipper chain slack were deemed insurmountable in the time-frame available, a feasible solution has been readied for next year's team. The rear flippers' inability to raise the robot's weight has also been resolved, increasing manoeuvrability.

Had the key issues causing flipper chain slack been identified earlier, however, a more realistic time-frame may have been available to move the relevant shafts and eliminate excessive slack. Chain slack still results in significant backlash. No solution has been implemented to prevent repeat damage to motor shafts.

9.3 Mechanical Arm Design

The arm design and manufacture have both been highly successful: backlash has been reduced to negligible; the total arm assembly weight has been reduced by 1.1kg from 2.4kg to 1.3kg, a

reduction of just over 45%. The modular and ease of manufacture design results in the requirement of common workshop tooling, and the easy replacement of damaged parts.

However, rapid prototyping parts brought several drawbacks; FEA analysis of such materials is near impossible, and their highly brittle nature makes estimating yield strength difficult. Only costly destructive testing will reveal their physical limits. The arm assembly is also fairly complex, making the task of removing and replacing parts time-consuming.

9.4 Head Design

The laser-cut bent-aluminium basis results in both cheap, fast manufacture and low weight. When the head is inevitably required to accommodate new hardware, the design can quickly be adapted and re-manufactured.

However, the bent-aluminium design has resulted in low force and impact tolerances relative to the rest of the robot, as well as an increased risk of vibration fatigue. FEA has been employed to mitigate these risks. The rapid-prototyping of the head 'hood' has resulted in significant warping.

9.5 Software and Systems

3D LiDAR scanning and QR code reading have been implemented. IR camera functionality has been restored. Code is theoretically ready to perform inverse kinematics and 2D SLAM, but untested. RGBD scanning has been shown to be functional.

The inverse kinematics and 2D SLAM code written is not guaranteed to work; testing must be carried out after the arm is complete. 3D SLAM is as-yet unimplemented, despite the demonstrated 3D LiDAR scanning and RGBD scanning. RGBD scanning in its current form is too processor-intensive to be of any practical use. There has been little progress on autonomous/black-out zone operation.

9.6 Electronics

Higher-rated motorboards (AX3500s) have been installed in an effort to avoid future over-current and allow more motors to be utilised. A Better motorboard can provide more current to motors while receiving positional information. New flipper encoders should give us accurate flipper positioning from the moment the robot is turned on.

The powerboard design may be flawed, making it uncertain that populating a new board will fix the issues. The electronics can still be wired up in reverse polarity causing damage due to the lack of diode protection.

10 Conclusions

Improvements have been made to aid the Functionality and Reliability of the robot structure as whole entity and not purely individual robotic elements. The whole systems performance based on these criteria will be tested in the RoboCup Rescue League Competition. The integrated system can truly be compared to the previous WMR robot of 2010/11, with quantitative and qualitative feedback from the event. This will either support our theoretical design approach or highlight areas where important considerations were overlooked or failed in some form.

Actual conclusions that can be drawn are explained below.

- The Mechanical Arm's manufacturing process was simple and enabled all parts to be acquired within a two week period
- Mass of the Mechanical Arm was reduced by 45%, with a 1kg mass relocation from the end effector position to the base joint
- Simple parts have allowed for quick manufacturing changes, as found with the Elbow Joint Spigot Housing, which was manufactured from billet in 1 day after a necessary design change

- Backlash in the Shoulder Joint has been reduced to a level where the only 'play' in the joint is caused by the distance between the tooth thickness and space width in any gearing transmission
- Rapid Prototyped parts are not exempt from dimensional error
- Design intent cannot always be implemented due to resource and conflicts with other engineering problems, as identified in deriving solutions for reduced chain 'Slack' in the Flippers
- Different methods of mapping technology have been tested in a stationary situation but not yet incorporated in a SLAM system
- Theoretical analysis is only a small part of the design process and the importance of hardware testing succeeds any form of modelling

Although re-engineering has a lower risk of failure in terms of design improvements, devising and implementing an entirely new concept can provide greater benefits. Recommendations for future development based on this principle include innovation of a new Chassis, the use of a larger amount of rapid prototype parts and incorporation of a 'Raspberry Pi' computer system to create a lighter and smaller rescue robot.

11 References

1. **Birk, Andreas and Matsuno, Fumitoshi.** Editorial: Safety, Security, and Rescue Robotics Special Issue. *Journal of Field Robotics*. 2011, Vol. 28, 6.
2. **Sandin, Paul E.** *Robot Mechanisms and Mechanical Devices (Illustrated)*. New York : McGraw Hill , 2003.
3. **Toto, Serkan.** Bari Bari: New exploration and rescue robot. *TechCrunch*. [Online] 18 December 2009. [Cited: 11 March 2012.] <http://techcrunch.com/2009/12/18/bari-bari-new-exploration-and-rescue-robot-video/>.
4. **Trends in Japan.** Rescue Robots: Machines Play Vital Roles in Disaster Relief. *Trends in Japan*. [Online] 2010. [Cited: 11 March 2012.] http://web-japan.org/trends/09_sci-tech/sci100909.html.
5. **Burion, Steve.** *Human Detection for Robotic Urban Search and Rescue*. s.l. : Swiss Federal Institute of Technology, 2004.
6. **RoboCup.** Robot League: Rules. *RoboCup* . [Online] 18 January 2012. [Cited: 11 March 2012.] http://wiki.robocup.org/wiki/Robot_League.
7. *Competing in the RoboCup Rescue Robot League.* **Michael , Tandy, Winkvist, Stefan and Young, Ken.** Sheffield : University of Warwick, 2010.
8. *A Method for Fast Encoder-Free Mapping in Unstructured Environments.* **Milstein, Adam , et al., et al.** 6, Sydney : Wiley Periodicals , 2011, Vol. 28.
9. **Kleiner, Alexander and Dornhege, Christian .** *Real-time localization and elevation mapping within urban search and rescue scenarios*. s.l. : Wiley Periodicals, 2007.
10. *Design and Control of a Second-Generation Hyper-Redundant Mechanism.* **Brown, H, et al., et al.** California : s.n., 2007.
11. *Design and Control of a Mobile Hyper-Redundant Urban Search and Rescue Robot.* **Wolf, A, et al., et al.** 2005.
12. **Unknown.** *Fundamentals of Robotics*. s.l. : The Goodheart-Willcox Co.
13. *Pneumatic Artificial Muscles: actuators for robotics and automation.* **Daerden, Frank and Lefeber, Dirk.** Brussels : s.n., 2000.
14. **Dravid, Raja.** *Pneumatic Robot. ai lab: Department of Informatics, University of Zurich.* [Online] [Cited: 13 March 2012 .] http://www.expo21xx.com/automation21xx/17887_st3_university/default.htm.

15. **Sytrama: Automation for the Plastics Industry.** Robot Models . *Sytrama: Automation for the Plastics Industry*. [Online] [Cited: 13 March 2012 .] http://www.sytrama-usa.com/sytrama_products-61G-71G-81G.html.
16. **Quanser.** Unmanned Vehicle Systems Research at Quanser. *Quanser*. [Online] 16 June 2011. [Cited: 13 March 2012 .] <http://quanser.blogspot.com/2011/06/unmanned-vehicle-systems-research-at.html>.
17. **Warwick Mobile Robotics.** *Technical Report*. University of Warwick : School of Engineering, 2010.
18. —. *Technical Report*. University of Warwick : School of Engineering, 2011.
19. Types of Wormgearing, p294. [book auth.] Robert Mott. *Machine Elements in Mechanical Design*. s.l. : Prentice-Hall, 1999.
20. **Niku, Saeed B.** *Introduction to Robotics*. Hoboken : John Wiley & Sons, 2011.
21. **Maxon.** *Maxon Motors*. 2011.
22. **FindAMachine.com.** Bridgeport Series 2 Interact 4. *FindAMachine*. [Online] [Cited: 13 March 2012.] http://www.findamachine.com/milling_machine/BRIDGEPORT/SERIES_2_INTERACT_4.
23. Spur Gears, p691. [book auth.] Robert Norton. *Machine Design and Integrated Approach, 2nd Ed.* s.l. : Prentice-Hall, 2000.
24. **Axis.** Axis M1054. *Axis Communications*. [Online] [Cited: 12 March 2012.] http://www.axis.com/files/image_gallery/ph_m1054_right_0910.jpg.
25. **EOS Manufacturing Solutions.** Materials for Plastic Systems: PA2200/2201. *EOS Manufacturing Solutions*. [Online] [Cited: 12 March 2012.] <http://www.eos.info/en/products/materials/materials-for-plastic-systems/pa-22002201.html>.
26. **Grisetti, Giorgio, Frese, Udo and Stachniss, Cyrill.** Projects. *OpenSLAM.org*. [Online] [Cited: 3 March 2012.] <http://www.openslam.org>.
27. **Hokuyo Automatic Co. Ltd.** URG Series Download Page. [Online] [Cited: 4 March 2012.] <http://www.hokuyo-aut.jp/02sensor/07scanner/download/index.html>.
28. **xSens Technologies B.V.** MTi. *xSens.com*. [Online] [Cited: 4 March 2012.] <http://www.xsens.com/en/general/mti>.

29. **Eliazar, Austin and Parr, Ronald.** *DP-SLAML Fast, Robust Simultaneous Localisation and Mapping without Predetermined Landmarks*. s.l. : IJCAU, 2003.
<http://www.cs.duke.edu/~parr/ijcai03.ps.gz>.
30. —. *SP-SLAM 2.0*. <http://www.cs.duke.edu/~parr/dpslam2.pdf>.
31. **Grisetti, Giorgio, et al., et al.** *Hierarchical Optimization on Manifolds for Online 2D and 3D Mapping*. s.l. : IEEE International Conference on Robotics and Automation, 2010.
<http://www.informatik.uni-freiburg.de/~stachnis/pdf/grisetti10icra.pdf>.
32. **Engelhard, Nikolas, et al., et al.** *Real-time 3D visual SLAM with a hand-held RGB-D camera*. Vasteras, Sweden : RGB-D Workshop on 3D Perception in Robotics at the European Robotics Forum, 2011. http://cvpr.in.tum.de/_media/spezial/bib/engelhard11euron.pdf.
33. **Strasdat, Hauke, Montiel, J. M. M. and Davison, Andrew J.** *Scale Drift-Aware Large Scale Monocular SLAM*. s.l. : Robotics: Science and Systems, 2010.
http://www.doc.ic.ac.uk/~ajd/Publications/strasdat_etal_rss2010.pdf.
34. **Steux, Bruno and El Hamzaoui, Oussama.** *tinySLAM: a SLAM Algorithm in less than 200 lines of code*. s.l. : International Conference on Control, Automation, Robotics and Vision, 2010. <http://www.openslam.org/tinyslam.html>.
35. **Huang, Shoudong, Wang, Zhan and Dissanayake, Gamini.** *Sparse local submap joining filter for building large-scale maps*. s.l. : IEEE Transactions on Robotics, 2008.
http://services.eng.uts.edu.au/~sdhuang/SLSJF_IEEE_TRO_final_2008_May_27.pdf.
36. **Huang, Shoudong, et al., et al.** *Iterated SLSJFL A sparse local submap joining algorithm with improved consistency*. Canberra : Australasian Conference on Robotics and Automation, 2008. <http://www.araa.asn.au/acra/acra2008/papers/pap102s1.pdf>.
37. **Grisetti, Giorgio, Stachniss, Cyrill and Burgard, Wolfram.** *Improved Grid-based SLAM with Rao-Blackwellized Particle Filters*. s.l. : IEEE Transactions on Robotics, 2006.
<http://www.informatik.uni-freiburg.de/~stachnis/pdf/grisetti06tro.pdf>.
38. —. *Improviing Grid-Based SLAM with Rao-Blackwellized Particle Filters by Adaptive Proposals and Selective Resampling*. s.l. : IEEE International Conference on Robotics and Automation, 2005. <http://www.informatik.uni-freiburg.de/~stachnis/pdf/grisetti05icra.pdf>.
39. **Haehnel, D., et al., et al.** *A highly efficient FastSLAM algorithm for generating cyclic maps of large-scale environments from raw laser range measurements*. s.l. : Conference on Intelligent Robots and Systems, 2003. <http://www.informatik.uni-freiburg.de/~haehnel/old/papers/haehnel.iros03.pdf>.

40. **30+ Contributors.** ZXing ("Zebra Crossing"). *Google Project Hosting*. [Online] [Cited: 4 March 2012.] <http://code.google.com/p/zxing/>.
41. **K.N.Toosi University of Technology.** Basics - Absolute Encoders. *Electrical Engineering Teachers Domain* . [Online] [Cited: 14 March 2012.] <http://saba.kntu.ac.ir/eecd/ecourses/instrumentation/absolute%20encoders%20principle%20of%20operation.pdf>.
42. *Melexis MLX90316.* **Melexis.** 2011.
43. *Vishay Model 357.* **www.vishay.com.** 2011.
44. **www.interconnectionworld.com.** www.interconnectionworld.com. [Online] [Cited: 2012 03 15.] <http://www.interconnectionworld.com/index/display/article-display.articles.connector-specifier.connector-applications.military-aerospace.2012.february.commercial-aircraft.QP129867.dcmp=rss.page=1.html>.
45. Mead info. [Online] [Cited: 09 03 2012.] Ref: <http://www.meadinfo.org/2008/11/gear-efficiency-spur-helical-bevel-worm.html>.
46. Worm Gears. *Roytech.* [Online] [Cited: 01 03 2012.] Ref: http://www.roytech.co.uk/Useful_Tables/Drive/Worm_Gears.html.
47. Roytech. *Worm gears.* [Online] http://www.roytech.co.uk/Useful_Tables/Drive/Worm_Gears.html.
48. **Stokes, Alec.** *Gear handbook design and calculations.* s.l. : Butterworth - Heinemann, 1992.
49. *VISHAY MODEL 357.* **VISHAY.** 11/03/11, 7/8" (22.2 mm) Conductive Plastic Potentiometer, Bushing Mount Type.
50. **Niku, Saeed Benjamin.** *Introduction to Robotics: Analysis, Control, Applications.* s.l. : Wiley, 2011.

Appendices

A Mechanical Arm

A.1 Analysis of 2010/2011 arm

A.1.1 The source of backlash

In order to reduce the amount of backlash observed in the arm joints, it is essential to identify where the backlash occurs and why it is occurring. Whilst all gear systems include a natural level of backlash due to the “distance between mating teeth measured along the circumference of the pitch circle” [23]. The main source of backlash in the mechanical arm was caused by the poor gear alignment and inaccurate mesh of teeth between the worm and worm wheel gears in the joints. Bent motor shafts caused by the forces of the mechanical arm acting on the motor shaft that act as a cantilever load.

The scenario is shown in the figure below:

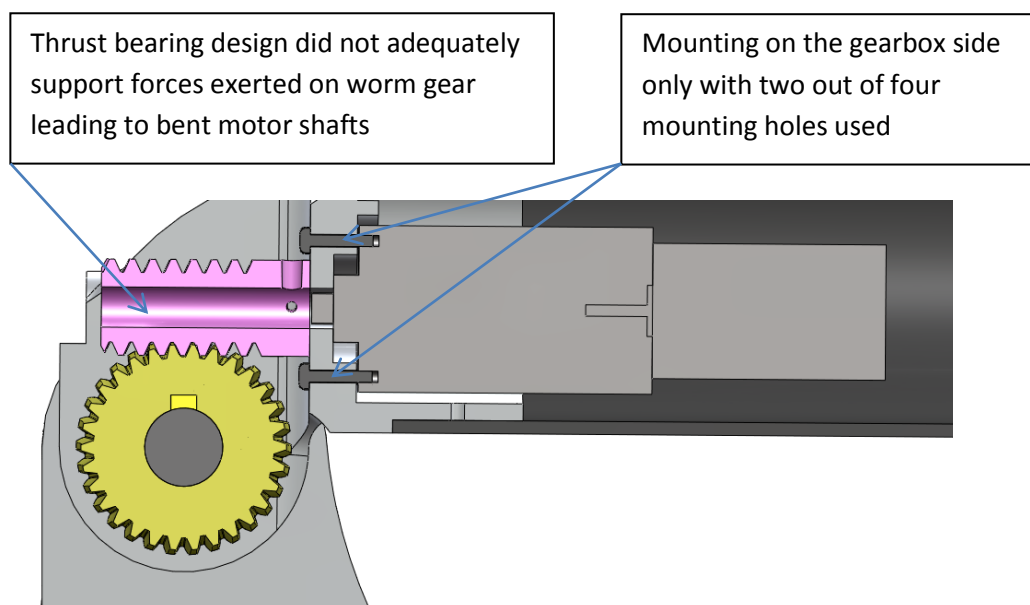


Figure 65: The cantilever loading on an unsupported motor shaft

The Maxon motors in the arm were only mounted on the gearbox side (using two out of the four mounting holes) which did not adequately support the motors during the motion of the arm.

A.1.2 Thrust Bearings

The team implemented a thrust bearing and housing in an attempt to support the forces exerted on the worm gear during stationary and dynamic movement. Unfortunately significant damage was quickly sustained to the housings as shown below and the thrust bearings were unable to support the load. This inadequate support led to the bending of the motor shafts.

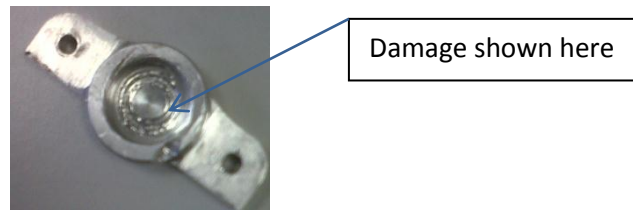


Figure 66: The damaged thrust bearing housings

A.1.3 Weight distribution

The mechanical arm suffered from being top-heavy. This was the reason for the robot toppling-over during an incline of the 2011 Robocup competition and damaging the sensors in the head, disabling the robot (18). The centre of gravity of the robot was also compromised by the high moment of inertia of the mechanical arm.

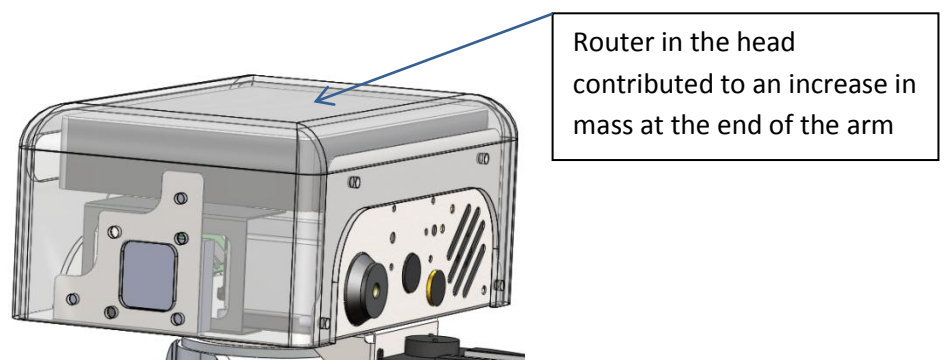


Figure 67: The router in the head

A.1.4 Complex arm joints

In last year's mechanical arm each joint had to be machined from 5-axis CNC milling machines. On top of this each joint took over a week to be manufactured due to the specialist tooling and set-up jigs required. Several iterations of each joint had to be made when problems were identified with the design.

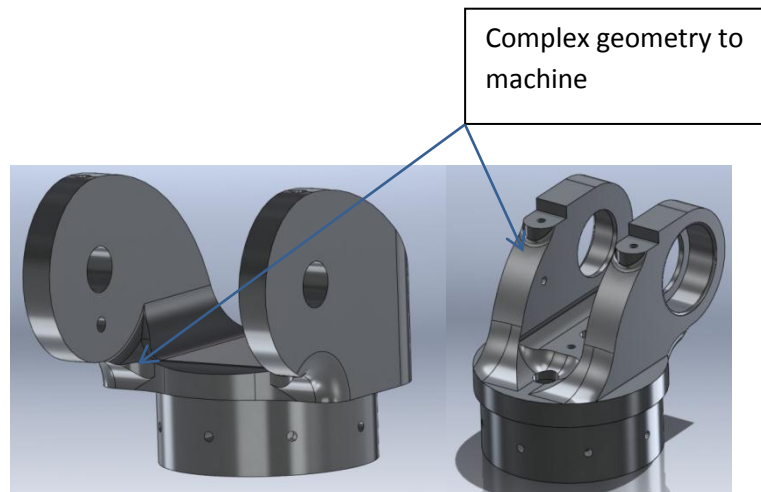


Figure 68: The complex geometry from the arm joints

A.1.5 Burn-out of the shoulder joint motor

The shoulder joint motor from last year's mechanical arm was mounted in the lower arm as shown in the figure below. The setup of the shoulder joint was unusual due to the fact that the worm gear attached to the Maxon motor was driving against a stationary and fully constrained worm wheel. Rotational movement in the shoulder joint was provided by the worm gear screwing against the stationary worm wheel to move the arm. The force required for this motion was higher than the capabilities of the Maxon motor and led to the burn-out and replacement of the shoulder joint motor.

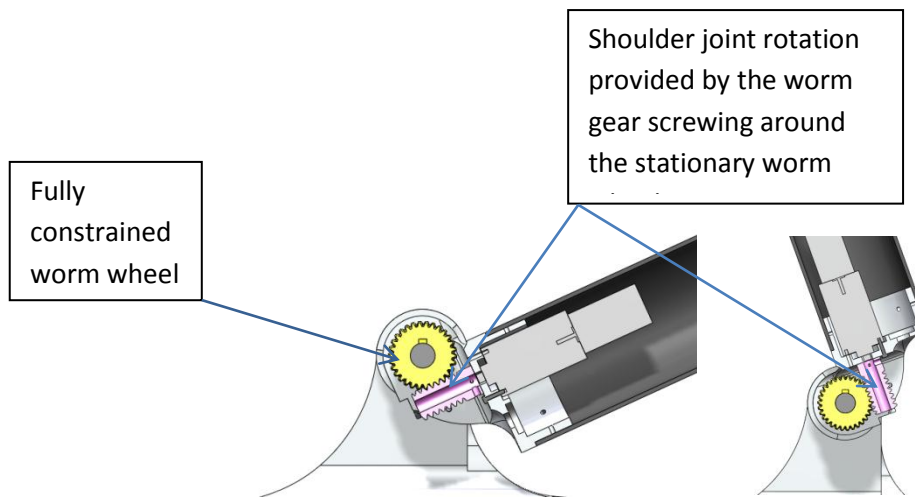


Figure 69: Shoulder joint motor position

A.1.6 Lack of concentricity in the base joint

The lower base plate was mechanically connected to the base support plate by an M10 bolt and nut as shown below. The clearance between the outer thread of the bolt and hole diameter led to inaccuracies in the location of the base joint and affected the mesh between the spur gear and annulus ring.

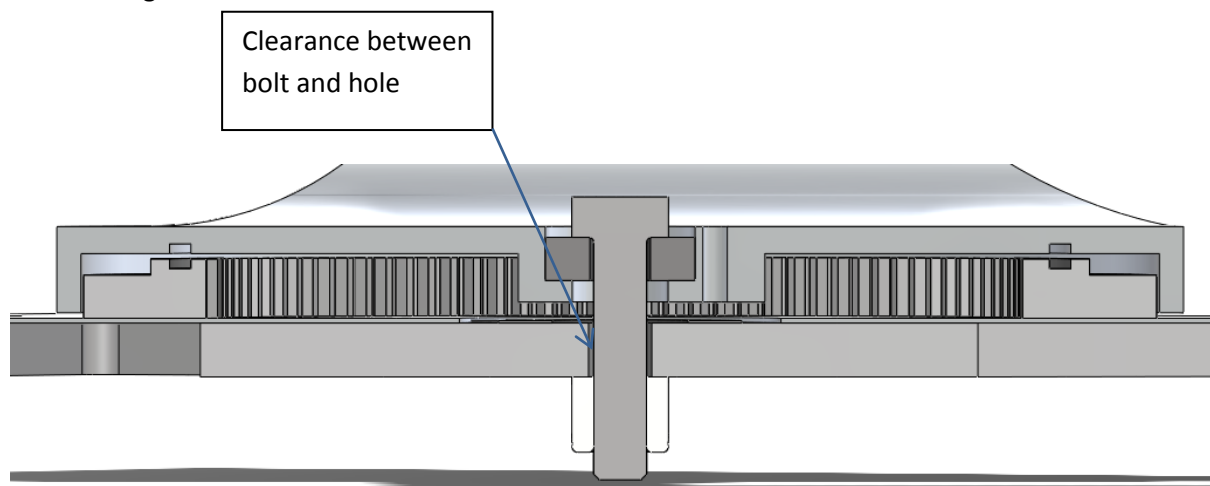


Figure 70: Section through the base joint

A.2 Motor shaft straightening jig

In order to utilise the thrust spigot and ball bearing support, it was essential that the bent Maxon motor shafts were straightened. The figure below highlights the fact that the bearing support system would fail with a lack of concentricity between the end of the shaft and the ball bearing.

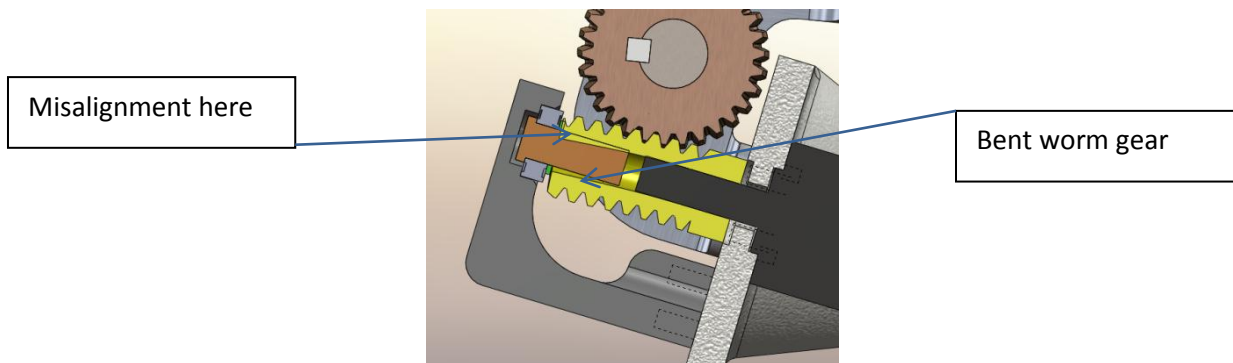


Figure 71: Cross section of a bent worm gear

Due to financial and lead time constraints it was not possible to purchase new motor shafts or send the current bent shafts to Maxon for repair. The only alternative was to use a jig to straighten the shafts in-house. The following figure displays the jig that was designed and manufactured from 32mm diameter steel bar.

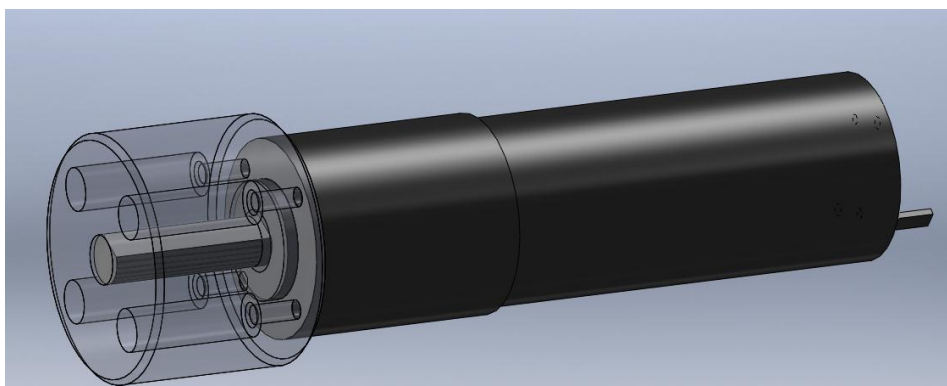


Figure 72: The motor shaft straightening jig

A.3 Efficiency calculations

The efficiency of a worm gear transmission is the output power divided the input power. Losses within the system are due to significant frictional losses due to sliding action between the worm and worm wheel (19).The efficiency of a worm gear transmission can be calculated from the equation below (45):

$$\eta = \frac{1 - \left(\frac{p\mu}{2\pi r}\right)}{1 + \left(\frac{2\pi r\mu}{p}\right)}$$

Where μ = coefficient of friction for worm gears

p = pitch of the worm thread

r = mean radius of the worm

The pitch of the worm thread was measured as 3.84mm and the mean radius was 8mm. In order to work out the coefficient of friction for the worm gear, the sliding velocity had to be calculated (46)

Sliding velocity (m/s) $V_s = 0.00005236 \times d_1 \times n_1 \times \sec\zeta$

Where d_1 = diameter of the worm gear

n_1 = rotational speed of the worm gear (revs/min)

$$\sec\zeta = \frac{1}{\cos\zeta} = \frac{1}{\cos \times \text{lead angle}}$$

Substituting in the values in the sliding velocity equation:

$$V_s = 0.00005236 \times 16 \times 251 \times 1.03 = 0.21\text{m/s}$$

Using the following table (47)

Friction coefficients - For Case Hardened Steel Worm / Phos Bros Wheel

Sliding Speed	Friction Coefficient	Sliding Speed	Friction Coefficient
m/s	μ	m/s	μ
0	0,145	1,5	0,038
0,001	0,12	2	0,033
0,01	0,11	5	0,023
0,05	0,09	8	0,02
0,1	0,08	10	0,018
0,2	0,07	15	0,017
0,5	0,055	20	0,016
1	0,044	30	0,016

From the table, a sliding speed of 0.21m/s equates to a friction coefficient of 0.07. Substituting the friction coefficient along with pitch and mean radius of the worm:

$$\eta = \frac{1 - 0.00534}{1 + 0.916} = 0.52 = \mathbf{52\%}$$

A.4 Speed calculations

The Maxon RE-30 motor has nominal speed of 8050rpm. The planetary gearbox and worm drive provide a total reduction ratio of 552:1. This provides the worm wheel with a rotational speed of 7 rpm. This will allow the shoulder joint to rotate 360° in 8.6 seconds.

The Maxon Amax motor has a nominal speed of 8820rpm. The planetary gearbox provides a speed reduction of 246:1. Coupled with a 80:12 reduction provided by the internal spur gear and annulus ring, the speed reduction is 1640:1. Therefore the output speed can be calculated as 5.4rpm which allows the base joint to rotate 360 ° in 11 seconds.

A.5 Tangential loading calculations

The forces acting on a worm and worm wheel gear interaction is made of three perpendicular components: Tangential, radial and axial components act on each member. If the worm and worm wheel are mounted on perpendicular axes, the tangential component on the worm wheel equals the axial component on the worm gear.

The tangential loading on the worm gear can be calculated as:

$$F_{worm\ tangential} = \frac{2T}{d} = \frac{2 \times 1.74Nm}{0.016m} = 217.78N$$

Assuming the motor is running on maximum torque.

This year's joint design utilises a thrust spigot and ball bearing in order to deal with the deflection of the worm gear. The bearings are rated to over 1000N of force which is enough to deal with the subjected loading.

A.6 Worm gears and backlash

Worm Gears

A wormset or worm gearing consists of a shaft with a spiral thread that engages with and drives a toothed worm wheel (23). The worm is similar to a screw in operation and the worm wheel is similar to a section of a nut. They are typically comprised of a steel worm and brass wheel. The wheel is made out of brass as it is designed to be sacrificial as it is easier to replace than the worm itself. The wheel has slightly angled and curved teeth. The worm rotates against the wheel and the screw face pushes on the teeth of the worm wheel causing it to rotate.

Worm gears are used when a large speed reduction ratio is required between non parallel and non-intersecting shafts, usually at right angles to one another. They provide a normal reduction ratio in the range of 5:1 to 75:1. The efficiency of a worm gear ranges from 95% for the lowest gear ratios to 20% for the highest ratios.

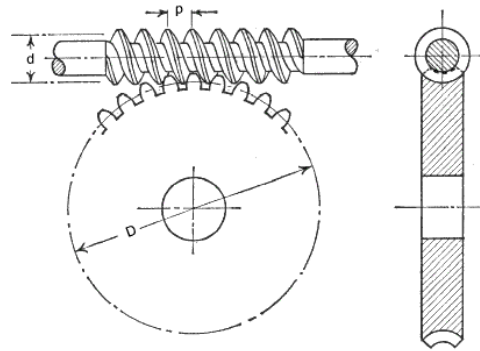


Figure 73: Diagram of worm and worm wheel gear transmission

Advantages and Disadvantages

The main advantage of using worm gearing is the high reduction ratio possible within a compact layout. This gives the possibility of greatly increasing torque or reducing speed, both of which are essential in the robot arm mechanism. Maxon motors have relatively low nominal torque levels with high rpm which makes them very suitable for worm gear transmission. To achieve the same reduction ratio with other gear sets such as helical and spur gears, compound layouts would be required with multiple reductions and larger amounts of space. Another advantage is the inability to reverse the direction of power due to the friction between the worm and wheel i.e allow the worm wheel to drive the worm. This removes the need to add a backstop to the design (48).

The main disadvantage of using worm gears is that lubrication which is required to reduce sliding friction and wear. The movement between the worm and wheel gear faces is entirely sliding and there is no rolling component to the interaction.

Gear Backlash

Backlash is the "distance between mating teeth measured along the circumference of the pitch circle". Backlash is included during normal manufacture to allow for the expansion of the worm

wheel during high temperatures. This backlash can be controlled by adjusting the gear wheel tooth thickness and centre distances.

Anti-Backlash Gears

Whilst there are different anti backlash gear design techniques, the most common is the spring loaded scissor gear. The assembly consists of mainly four parts: two gears and two compression springs. One gear acts as the standard gear connected to the transmission shaft whilst the other is inserted over the extended hub of the other gear and can freely rotate.

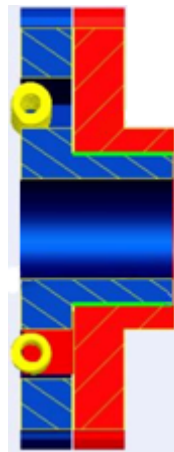
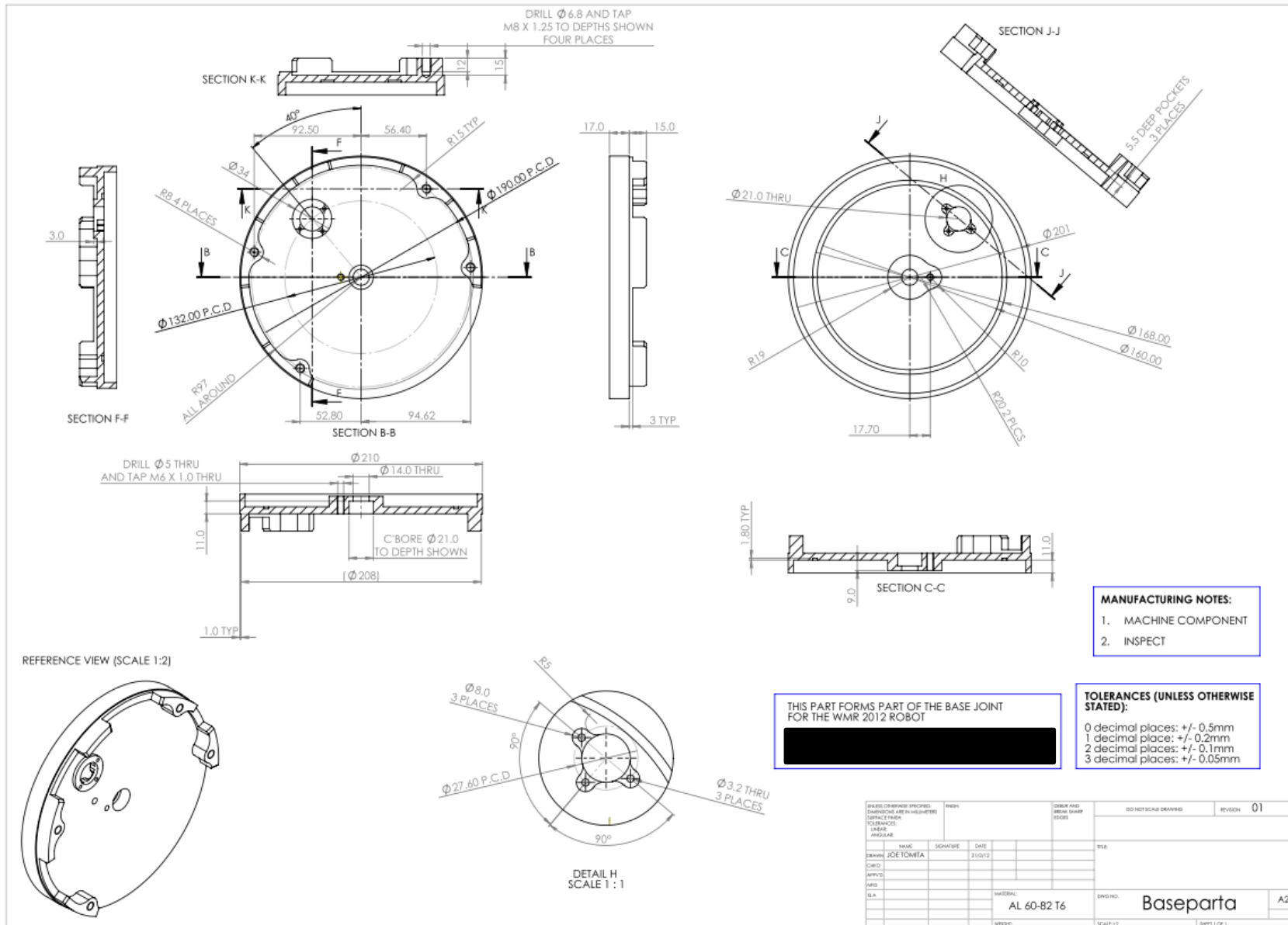
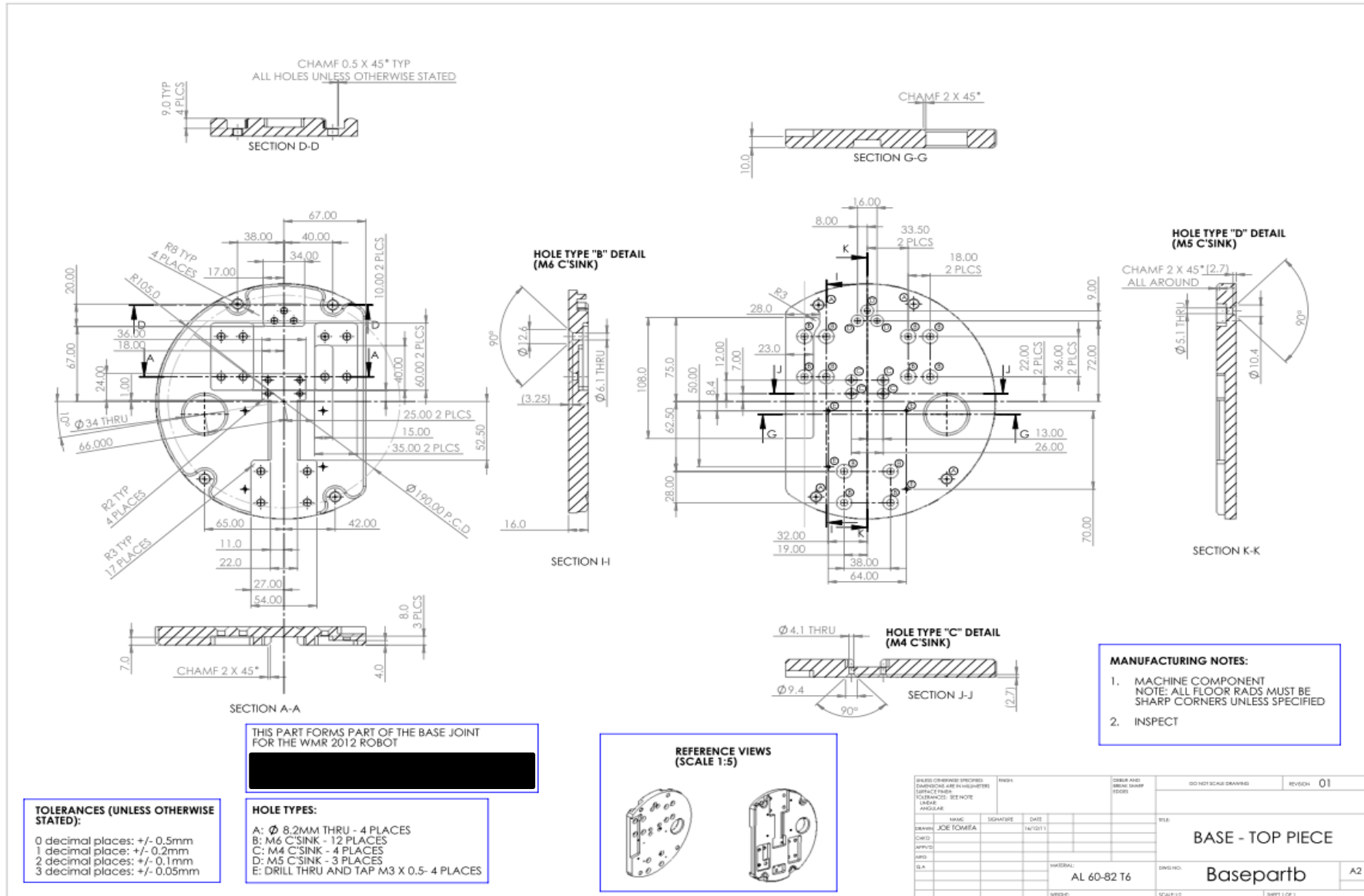


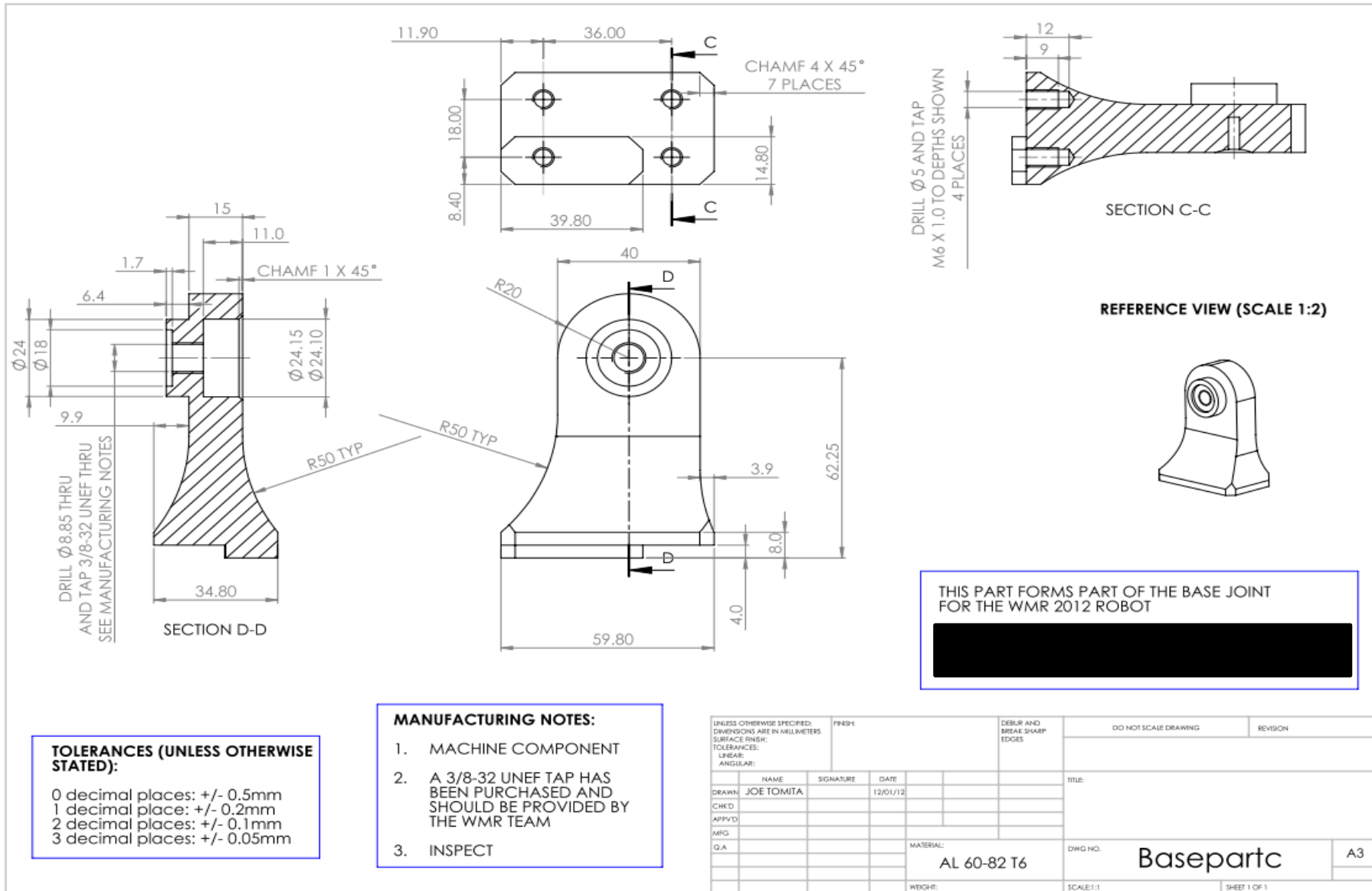
Figure 74: Anti-backlash gear design

The tabs of one gear place into the slot of the other. The compression springs are inserted in each slot and the backlash is absorbed by the gear assembly. During the operation of the gears, the spring pushes the free gear to remove backlash created.

A.7 Technical Drawings





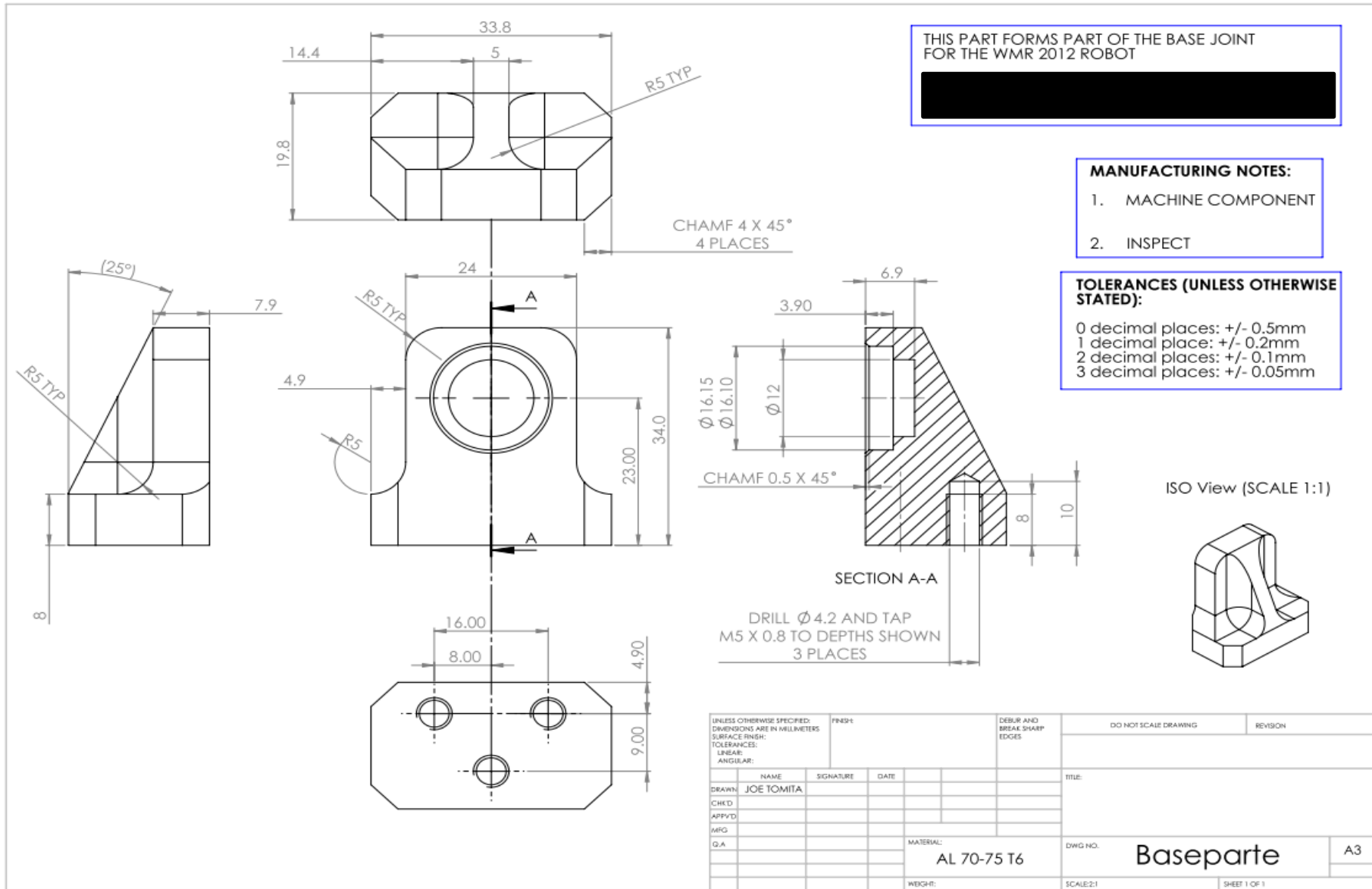


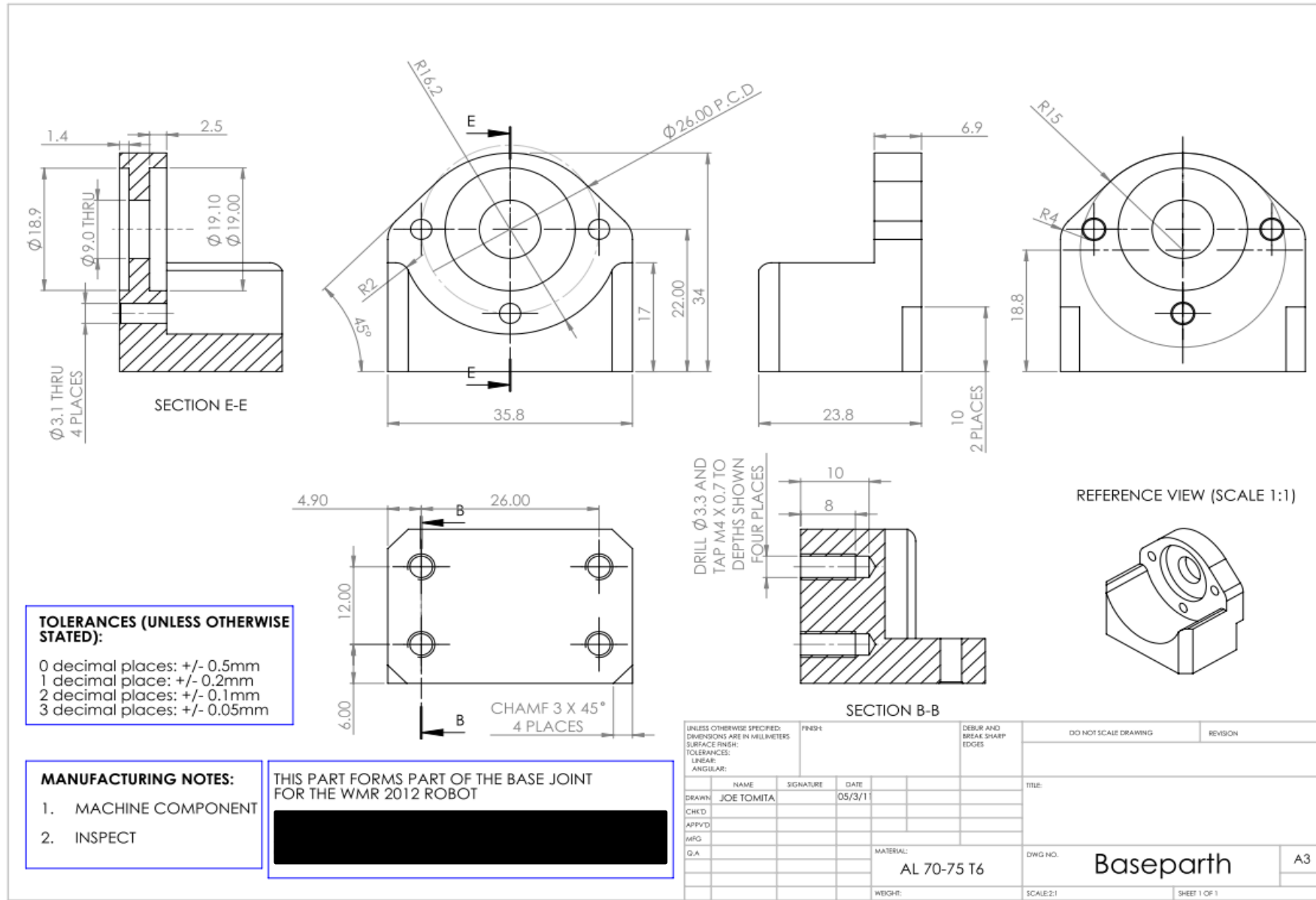
TOLERANCES (UNLESS OTHERWISE STATED):

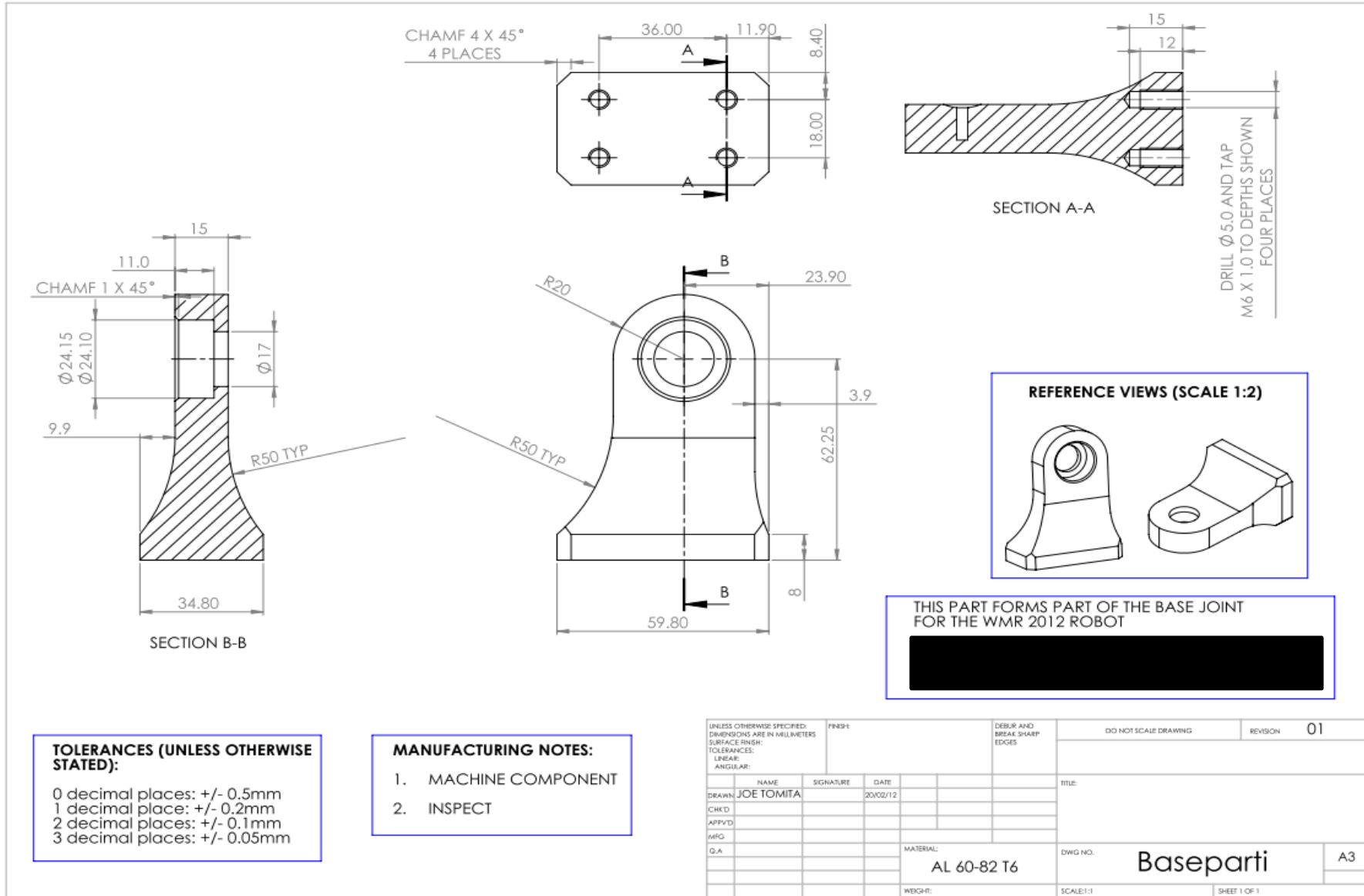
0 decimal places: +/- 0.5mm
 1 decimal place: +/- 0.2mm
 2 decimal places: +/- 0.1mm
 3 decimal places: +/- 0.05mm

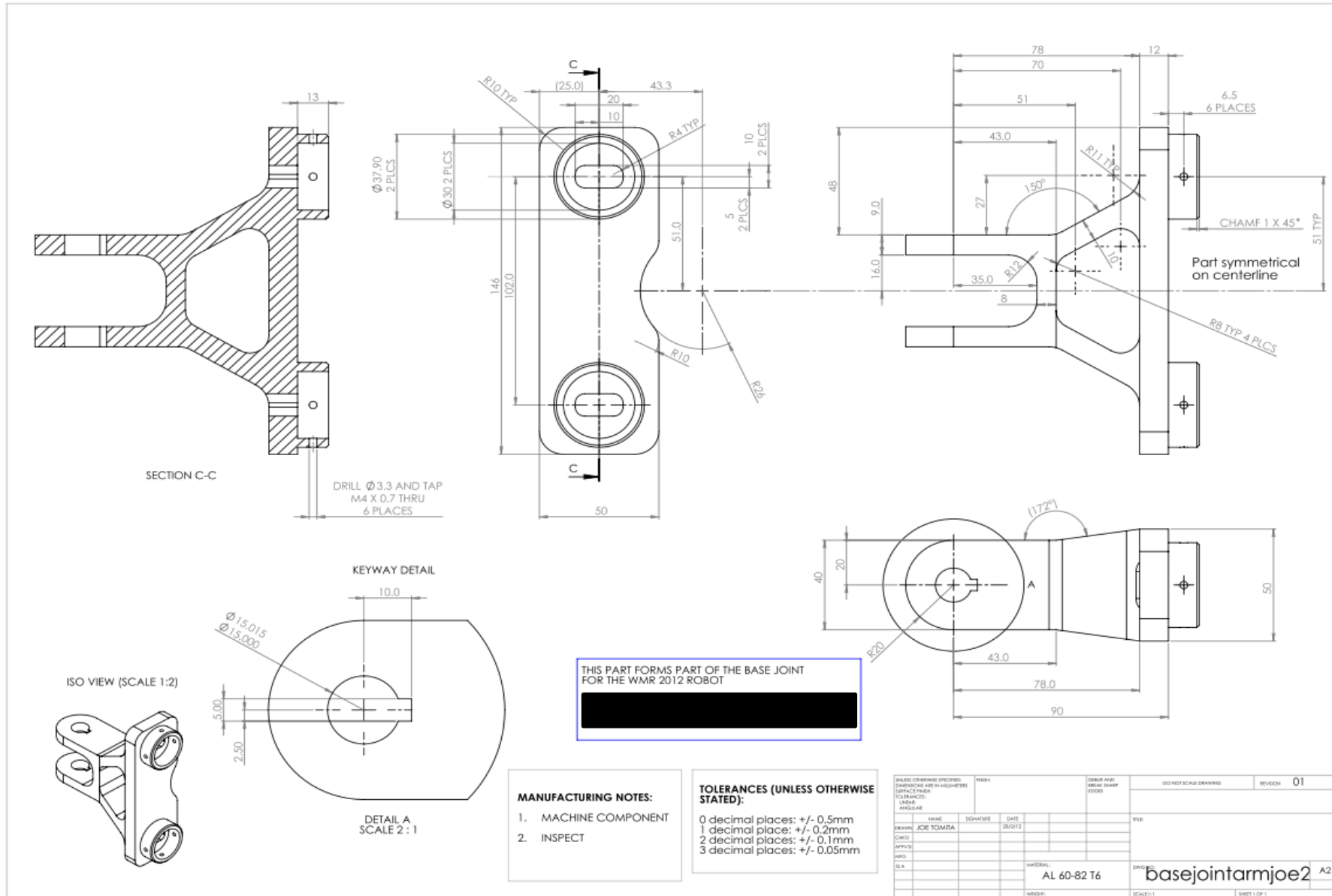
- MANUFACTURING NOTES:**
- MACHINE COMPONENT
 - A 3/8-32 UNEF TAP HAS BEEN PURCHASED AND SHOULD BE PROVIDED BY THE WMR TEAM
 - INSPECT

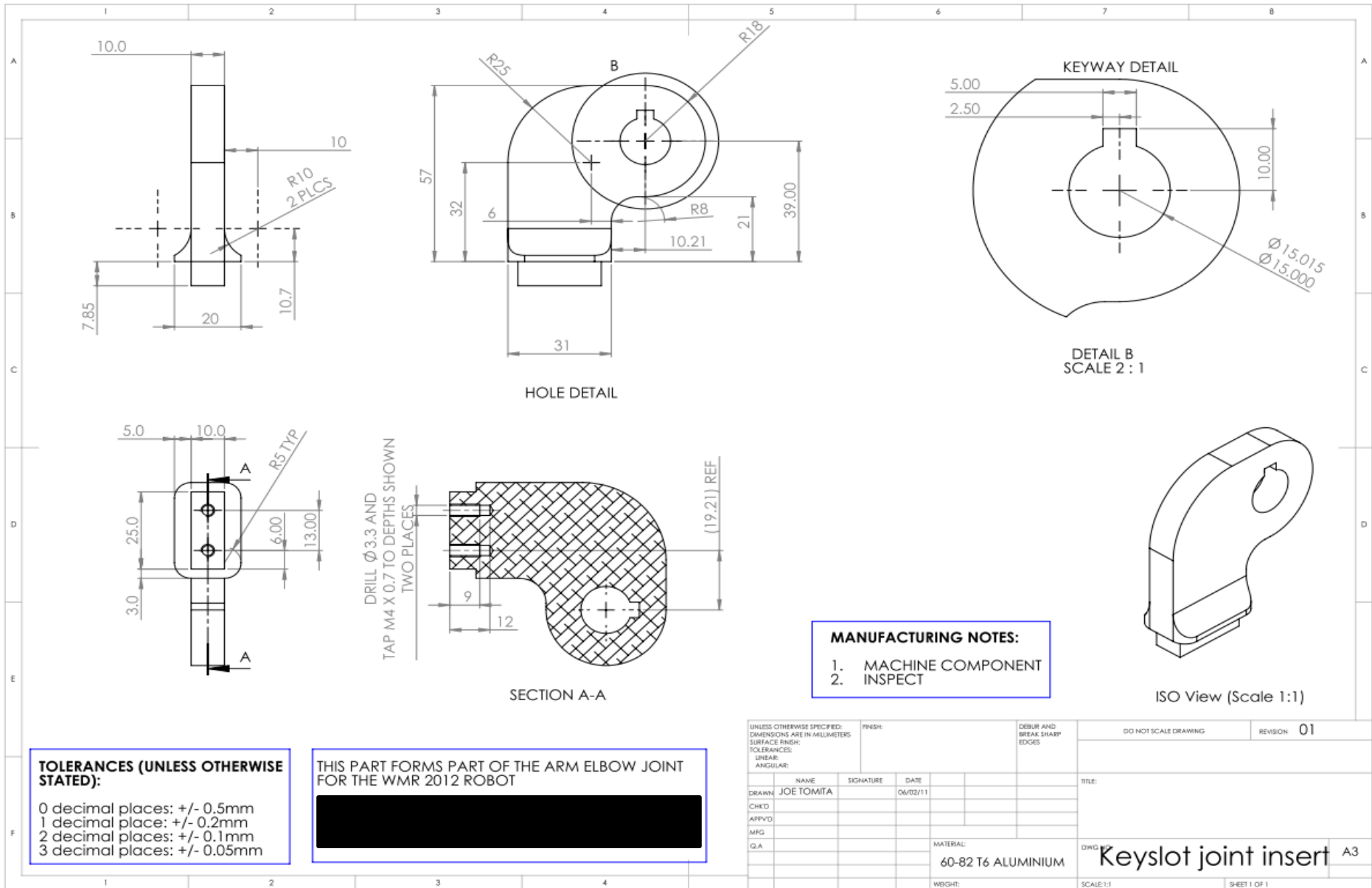
UNLESS OTHERWISE SPECIFIED: DIMENSIONS ARE IN MILLIMETERS		FR32:	DEBUR AND BREAK SHARP EDGES		DO NOT SCALE DRAWING	REVISION
SURFACE FINISH:						
TOLERANCES:						
LINEAR:						
ANGULAR:						
DRAWN:	NAME	SIGNATURE	DATE		TITLE:	
CHK'D:	JOE TOMITA		12/01/12			
APP'VD:						
MFG:						
G.A:						
MATERIAL:				DWG. NO.	Basepartc	
AL 60-82 T6					A3	
WEIGH:				SCALE:1:1	SHEET 1 OF 1	

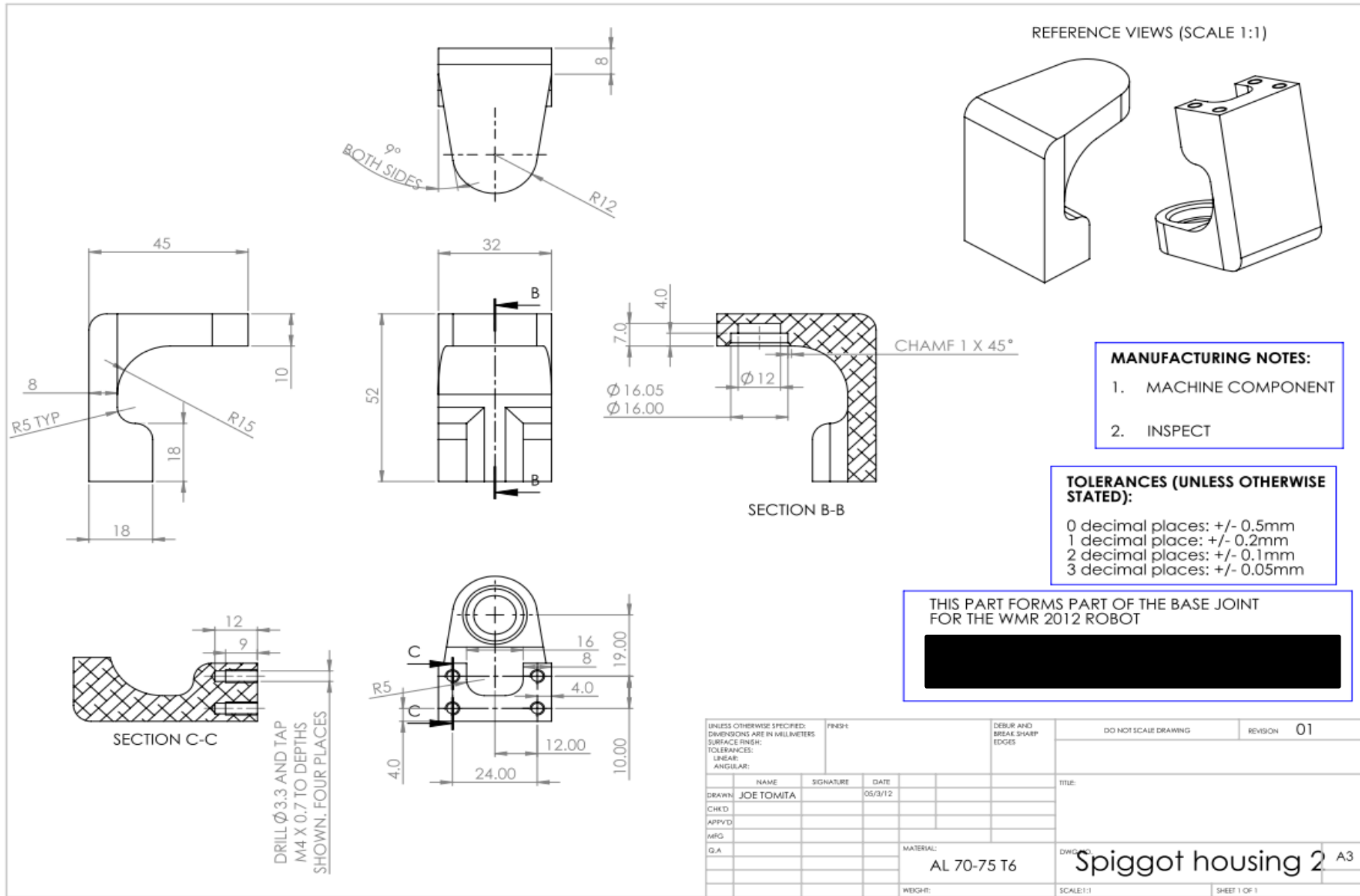


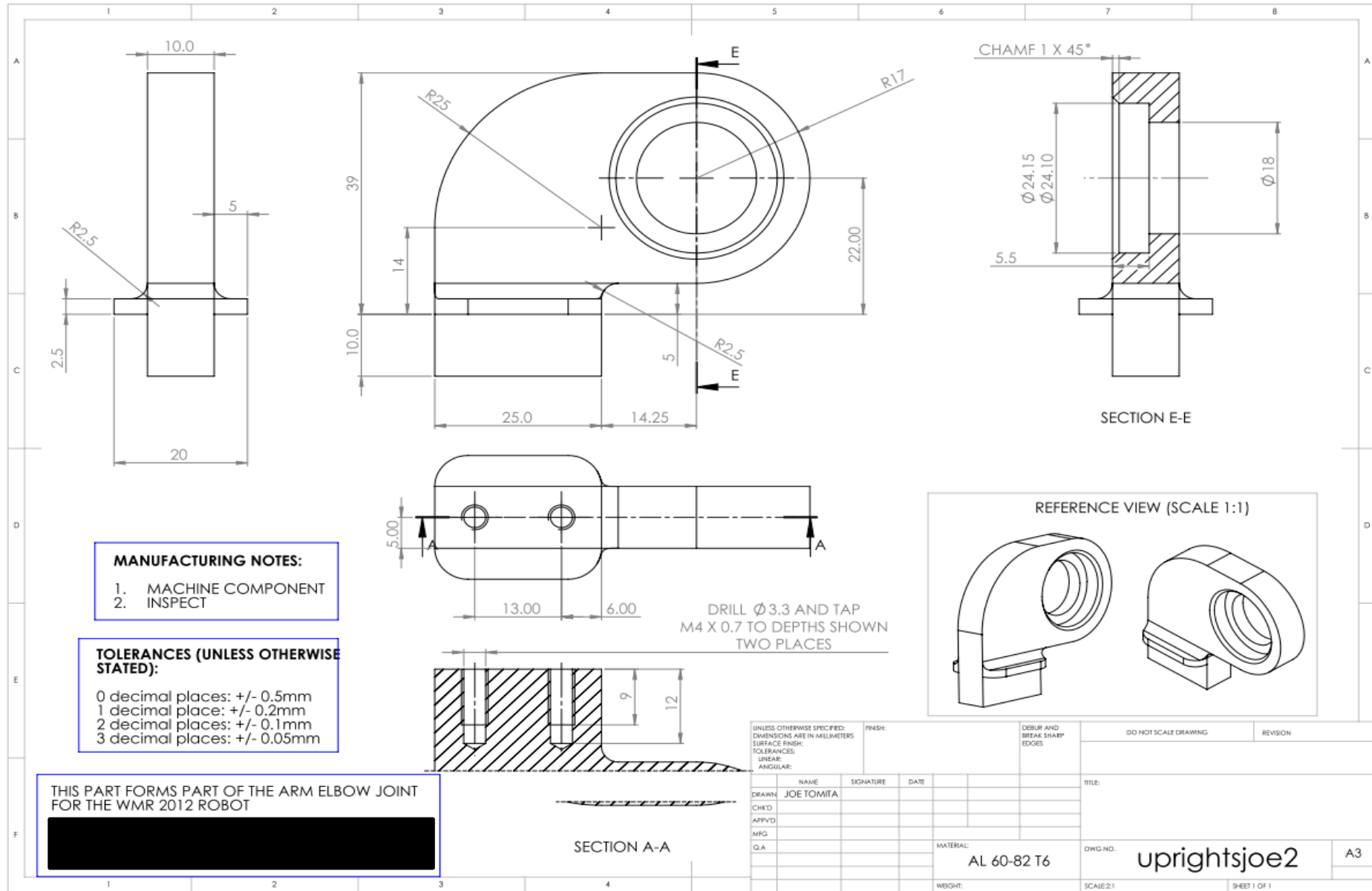


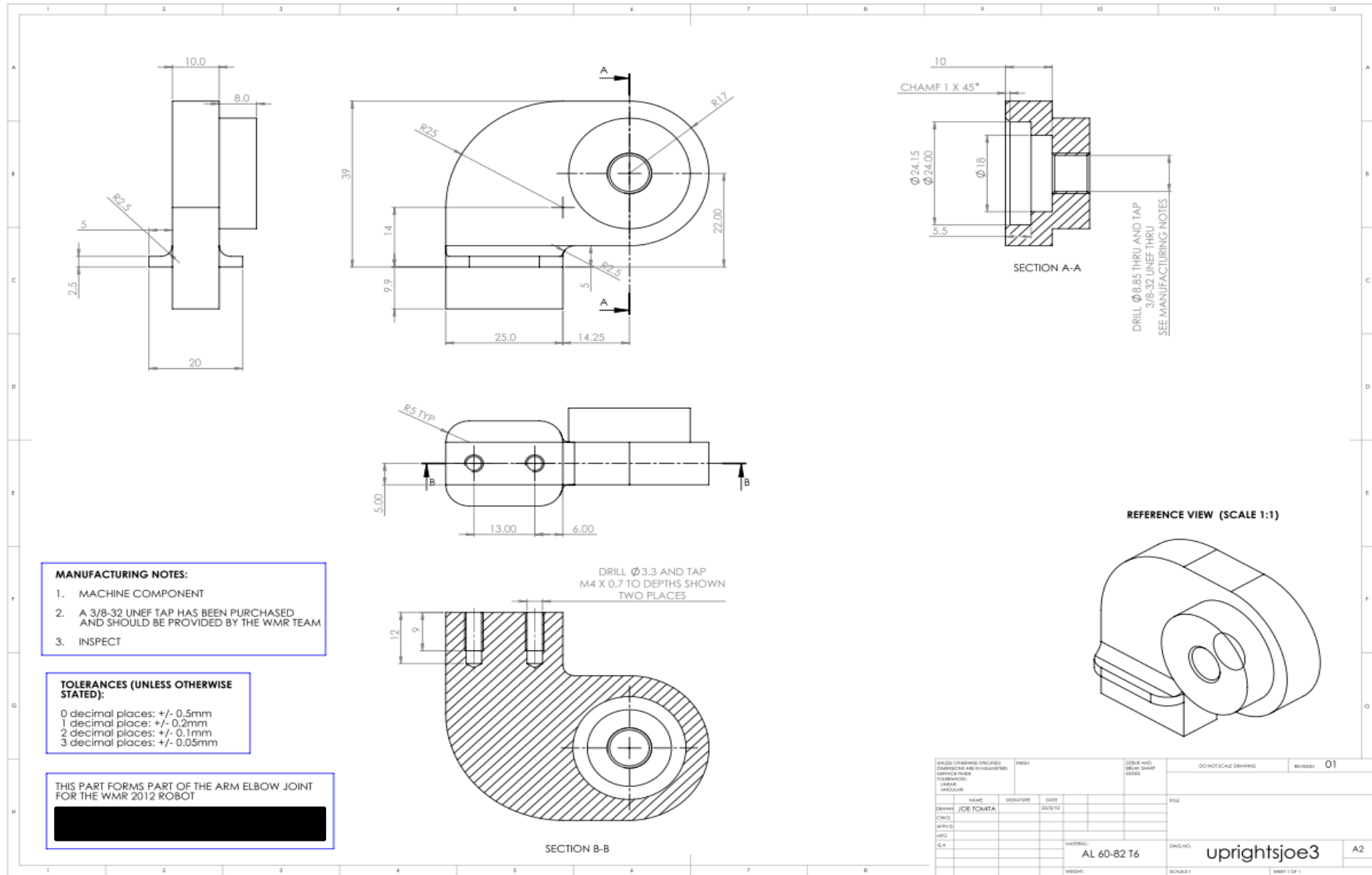


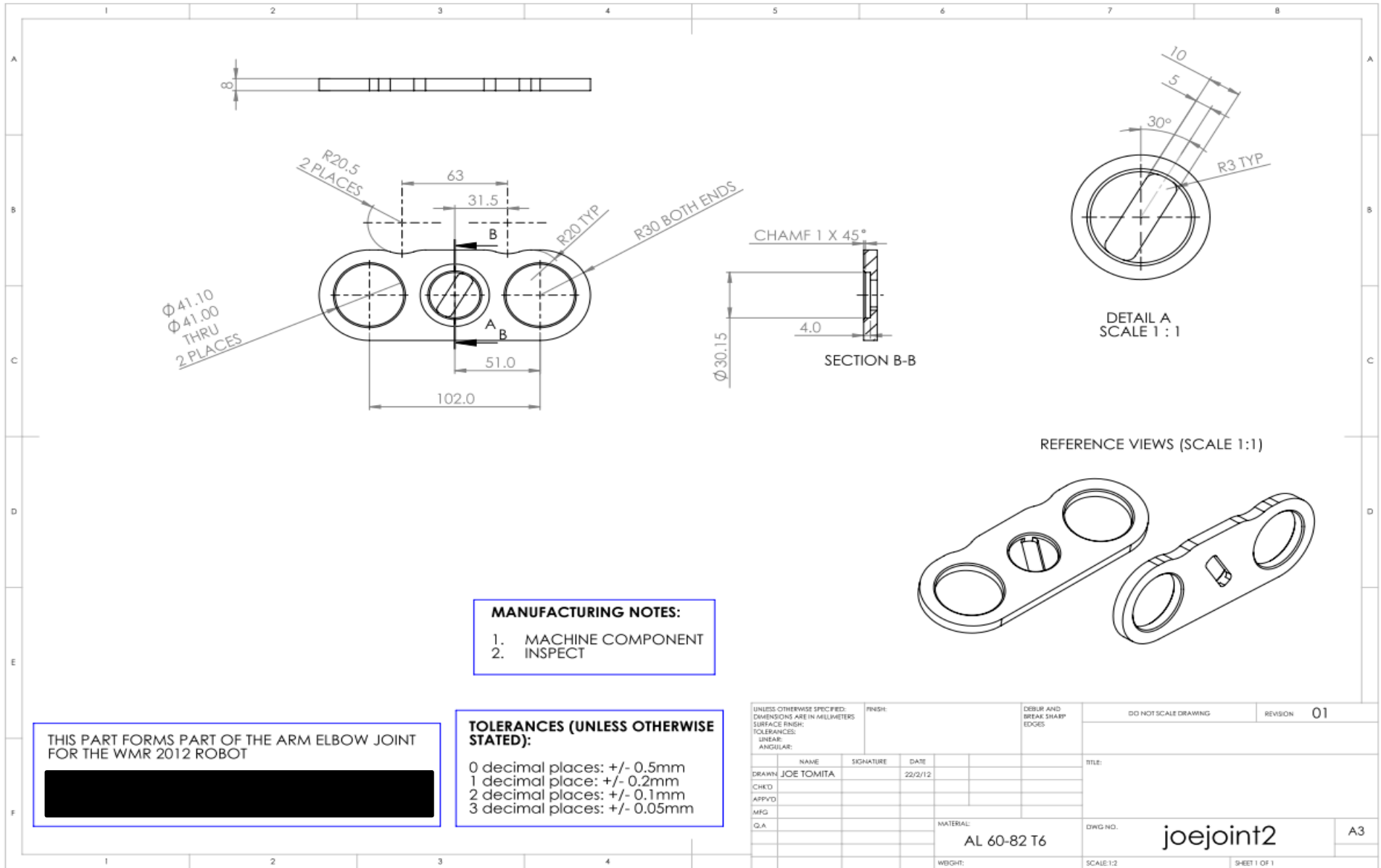












B Head

B.1 Analysis of Design

Analysis of the new head design shows the structural integrity of the design. The head assembly was tested in four different scenarios. The first scenario simulates an object falling on top of the head. To do so a force of 100N is applied on the head. This is a replication of a 10kg weight falling from a height of 1 meter onto the head. As seen from the first figure the stress acting on the head is minimal. The max displacement of 0.44 mm shows the structural soundness of the design.

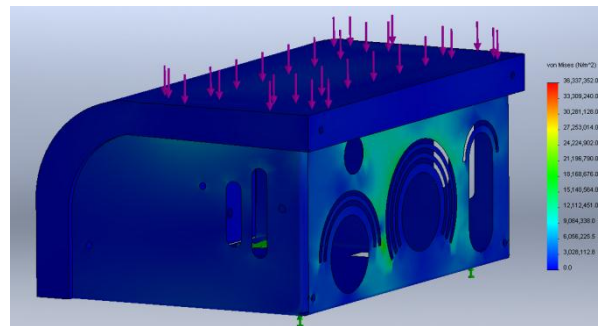


Figure 75: Stress on the head design from a 100N force

The second scenario hopes to simulate the head running into an obstacle from the side. A force of 50 N is applied to the side face of the head, which yields a maximum displacement of 0.36 mm, once again proving the effectiveness of the design. The third scenario simulates the head running into an obstacle head on. With a maximum displacement of 0.069mm, the results support the design selection.

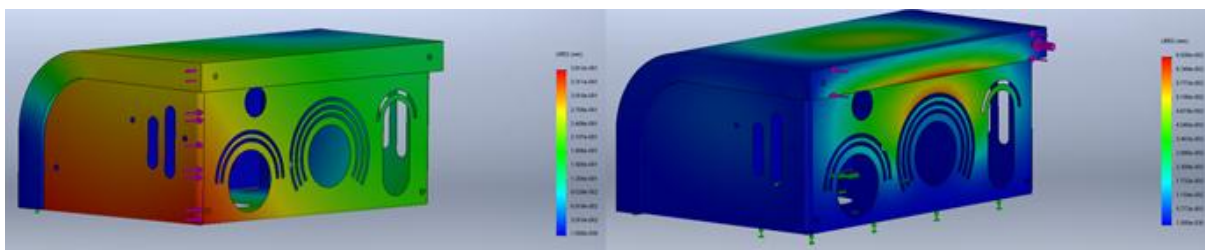


Figure 76: Displacement of head structure due to impact on side and front faces

C Flippers

C.1 Distorted Flipper Components

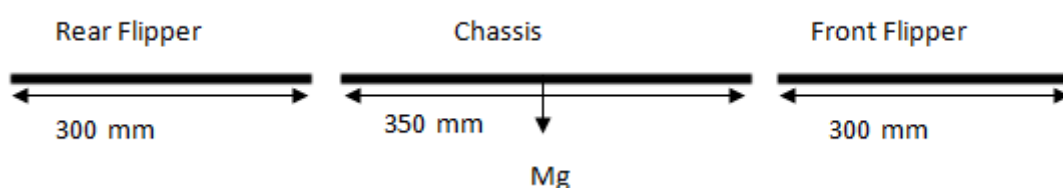
The figure below illustrates the distorted flipper motor housings.



Figure 77: Distortion in flipper motor housing

C.2 Static force exerted onto motors due to robot weight

Simple calculations were conducted on the flippers to work out an estimate of the force exerted on the motor. The first set of calculations show static loading, loading that is being applied at a certain instance, in this case the weight of the actual robot. Since the robot is lifted using the flippers regularly during the completion it is believed that a cyclic loading is experienced.



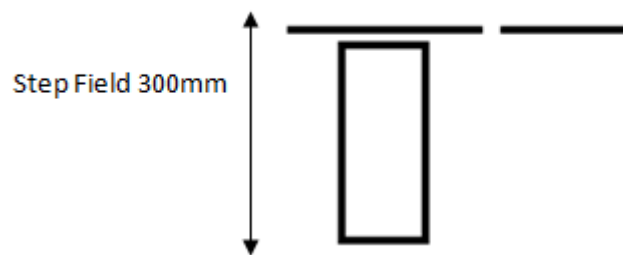
By comparing the ratio of the sprocket radii (25mm) and the length of the flipper (300mm), the force that is being exerted onto the motor can be calculated as followed:

$$F_g \times N_a = F_t$$

$$\left(\frac{45}{2} \times 10\right) \times \frac{300}{25} = 2700N$$

Where F_g is the force acting on the flipper pair (in this case $\frac{1}{2}$ of the weight of the robot) (N), N_a is the ratio between the sprocket radius and the length of the flipper and F_t is the chain tension. The worst case scenario is if the entire robot is lifted by just the flippers and if the flippers are at the same angle then the weight of the robot would be distributed evenly across the flippers. It was found that the force acting on the chain was around approximately 2.7kN.

C.3 Loading due to step field fall



By using equations of motion the time taken for the robot to reach the ground can be calculated:

$$s = ut + \frac{1}{2}at^2$$

Where S is the drop distance (m) assumed to be 0.30m, u is the initial velocity (ms^{-1}) assumed to be 0 ms^{-1} , a is the acceleration of the body (ms^{-2}) assumed to be 9.81 ms^{-2} and t is the time taken for motion (s). By rearranging the equation the time for the robot to reach the ground was found to be 0.247 seconds (3.d.p). Using this time the final velocity can be calculated using the equation:

$$s = \frac{(u + v)}{2}t$$

The velocity was found to be 2.426 ms^{-1} (3.d.p), upon impact the flippers displace by approximately 0.1m from this the acceleration can be calculated using the equation:

$$v^2 = u^2 + 2as$$

Giving an acceleration of 29.43 m/s^2 , the forces can then be calculated by multiplying this acceleration by the mass of the robot. The force was found to be approximately 1324.350N (2.d.p).

The impact force can then be calculated:

$$F_i - mg = ma$$

$$F_i = 45 \times (9.81 + 29.43)$$

Where F_i is the impact force (N), m is the mass of the robot (kg) approximately 45kg , g is the acceleration due to gravity (ms^{-2}), a is the upward acceleration experienced during impact (ms^{-2}) it was found that the impact force on the flipper was approximately 1.766 kN (3.d.p), hence the force experienced on the motor will be:

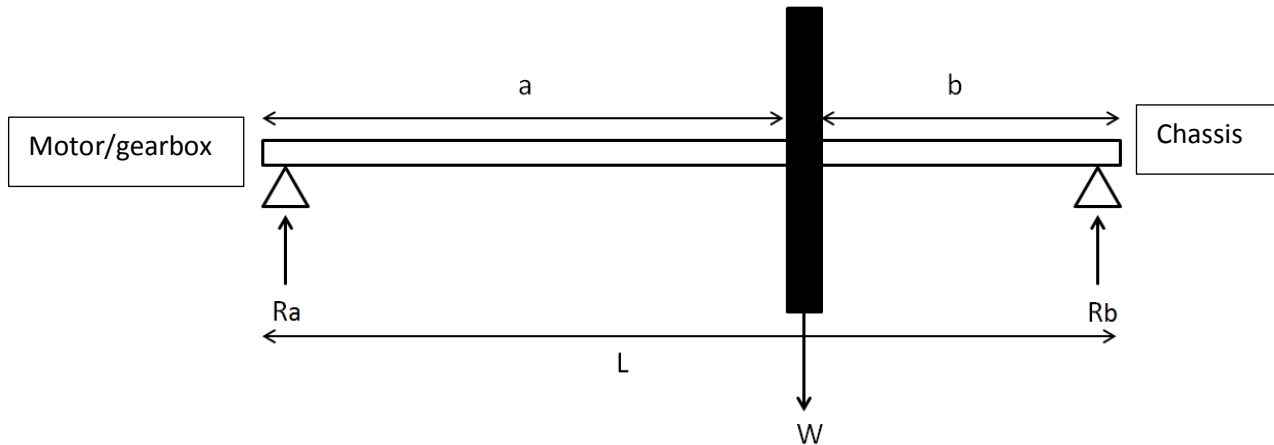
$$F_g \times N_a = F_t$$

$$1766 \times \frac{300}{25} = 21,192\text{N}$$

Hence the force acting on the motor from a step field drop is approximately 21.192kN ; this force is in effect for a very short space of time.

C.4 Analysis of force distribution on the flipper motor shaft

Due to the difficulties in measuring cyclical loading, an analysis of the forces being exerted at the end of the shafts using simple beam bending equations was carried out instead. This was to aid in gauging the dispersion of force with the new bearing system in place.



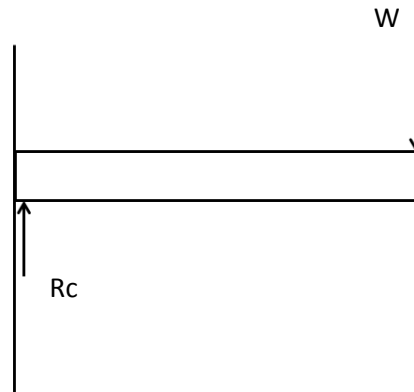
The reaction forces can be calculated from the following equations:

$$R_a = +W \times \frac{b}{L}$$

$$R_b = +W \times \frac{a}{L}$$

Where W is the Load at that particular point (N), R_a and R_b are the reaction forces at the ends of the shaft (N), b is the distance from the reaction force R_b to the load (m), a is the distance from the reaction force R_a to the load (m), L is the total length of the shaft (m).

R_a represents the end of the shaft attached to the gearbox which gave a force of approximately 900 N. R_b represents the end of the shaft attached to the housing which gave a force of approximately 1800 N. It can be seen that at this instance a vast majority of the force is being dispersed into the chassis as R_b has a force of 1800N over 66% of the total force exerted. This brings R_a to approximately 900N hence below the recommended maximum static load (1200 N). Below is a simple analysis of the shaft in its current configuration:



$$R_c = +W$$

It can be seen that with no extra support the entire force will be taken up by the motor/gearbox. On viewing the relatively large reaction force of R_b a more rigid stronger chassis may be required in order to take on the load.

D Software

D.1 Camera Pixel Mapping

The aim of this is to determine what position an object is relative to the robot based upon where it is placed in the image. This would allow the robot to determine its position within the 3D map generated by the LiDAR.

We can implement the code created by Jean-Yves Bouguet, which calibrates the camera by positioning an object of known size within the view of the camera at several different positions.

Parameter	Value
Entrance Pupil Diameter (mm)	5.25
Aperture (f/stop rating)	f/1.2
Focal Length (mm)	6.3
Resolution (pixels)	160x120
Angular Resolution (degrees)	0.1331
Detectable Light Wavelengths (microns)	8 – 14
Lens Material	Germanium

Cameras use f/stop ratings to give users an idea of what the aperture of any camera is. The aperture of a camera is a measure of how wide the entrance pupil diameter, D , is in comparison to the focal length, f , and is found using the following equation:

$$N = \frac{f}{D}$$

The theoretical angular resolution limit, θ_r , of a camera can be found using the following equation. Where λ is the wavelength of light that the camera views, in this case 8 to 14 microns, and D is the diameter of the lens.

$$\sin \theta_r = 1.22 \frac{\lambda}{D}$$

Using the given camera, the angular resolution is 0.1331 degrees.

The *Field of View* (FoV) of a camera is measured in degrees, with $\theta_{incident}$ equalling half of the field of view.

$$\theta_{\text{incident}} = \arctan\left(\frac{D}{2f}\right)$$

The theoretical angular representation of a pixel is equal to:

$$\frac{\text{Field of View}}{\text{Number of Pixels}}$$

Where *FoV* is measured in degrees, the horizontal component of the screen this gives us:

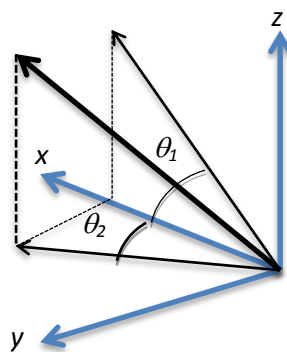
$$\frac{52}{320} = 0.1661^\circ$$

The vertical component:

$$\frac{40}{240} = 0.1667^\circ$$

This tells us that the camera is capable of reliably resolving two objects spaced 1 pixel apart.

The figure and equations below depicts the necessary maths to calculate the vector required to map the position of objects given the angles, θ_1 θ_2 , calculated by the pixel position.



$$r_1 = \frac{z}{\sin \theta_1}$$

$$r_2 = \frac{x}{\cos \theta_2}$$

$$\theta_{pix} = \arctan \left(\frac{r_1 \sin \theta_1}{r_2} \right)$$

D.2 Java centre of gravity calculation classes

Centre of gravity calculation code can be implemented due to its compartmentalised nature with regard to the rest of the robot software.

```
package cog;

/**
 *
 * @author Tim
 */
public class CoG {

    double[] ArmCoMPlanar;
    double[] ArmCoM;
    double ArmM;
    double[] CoG;

    Limb body = new Limb();
    Limb armlow = new Limb();
    Limb armhigh = new Limb();
    Limb head = new Limb();
    Limb frontflip = new Limb();
    Limb rearflip = new Limb();

    public double[] getArmCoM() {

        int i;

        for (i=0; i < armlow.MCoM.length; i++){
            ArmCoMPlanar[i] = ((armlow.MCoM[i]+armhigh.MCoM[i]+head.MCoM[i])
                / (armlow.m+armhigh.m+head.m));
        }

        ArmCoM[1] =
ArmCoMPlanar[1] * (Math.cos(armlow.gamma)+Math.sin(armlow.gamma));
        ArmCoM[2] = ArmCoMPlanar[2] * (Math.cos(armlow.gamma) -
Math.sin(armlow.gamma));
        ArmCoM[3] = ArmCoMPlanar[3];

        ArmM = armlow.m+armhigh.m+head.m;

        return ArmCoM;
    }

    public double[] getCoG() {
        int i;
        for (i=0; i < body.MCoM.length; i++){
            CoG[i] =
(ArmCoM[i]*ArmM+body.MCoM[i]+rearflip.MCoM[i]+frontflip.MCoM[i])
                / (ArmM+body.m+rearflip.m+frontflip.m);
        }
    }
}
```

```

    }
    return CoG;
}

}
package cog;

/**
 *
 * @author Tim
 */
public class Limb {
    double alpha;
    double beta;
    double gamma;
    double[] CurrentPos;
    double[] CoMRel;
    double[] CoMPos;
    double[] CoMVec;
    double[] MCoM;
    double m;
    double[] offset;
    double[] CoMAng = {alpha,beta,gamma};
    double[] JointAngles;
    int ident;

    public Limb(double[] jointAngles, double[] off,
               double[] CoMVect, double mass){
        m = mass;
        JointAngles = jointAngles;
        CoMVec = CoMVect;
        offset = off;
        CoMRel[1] = CoMVec[1]*(Math.cos(CoMAng[ident]) -
Math.sin(CoMAng[ident]));
        CoMRel[2] = CoMVec[2];
        CoMRel[3] = CoMVec[3]*(Math.cos(CoMAng[ident]) -
Math.sin(CoMAng[ident]));
        int i;
        for (i=0; i<=CoMVec.length; i++){
            CoMPos[i] = CoMRel[i]+offset[i];
        }
        int j;
        for (j=0; j<=CoMPos.length; j++){
            MCoM[j]= m*CoMPos[j];
        }
    }

    public Limb() {
        CoMRel[1] = CoMVec[1]*(Math.cos(CoMAng[ident]) -
Math.sin(CoMAng[ident]));
        CoMRel[2] = CoMVec[2];
        CoMRel[3] = CoMVec[3]*(Math.cos(CoMAng[ident]) -
Math.sin(CoMAng[ident]));
        int i;
        for (i=0; i<=CoMVec.length; i++){
            CoMPos[i] = CoMRel[i]+offset[i];
        }
        int j;
        for (j=0; j<=CoMPos.length; j++){
            MCoM[j]= m*CoMPos[j];
        }
        throw new UnsupportedOperationException("Not yet implemented");
    }
}

```

```
public double[] getMCoM(){  
    return MCoM;  
}  
}
```

E Electronics

E.1 Hall Effect Theory

When a current-carrying conductor is placed into a magnetic field, a voltage will be generated perpendicular to the current and the field. This is the principle called the Hall Effect, which is what our sensor uses to provide positional feedback.

Figure 2-1 shows a thin sheet of semi-conducting material through which a current is passed. The output connections are perpendicular to the direction of current. When no magnetic field is present current distribution is uniform and no potential difference is seen across the output.

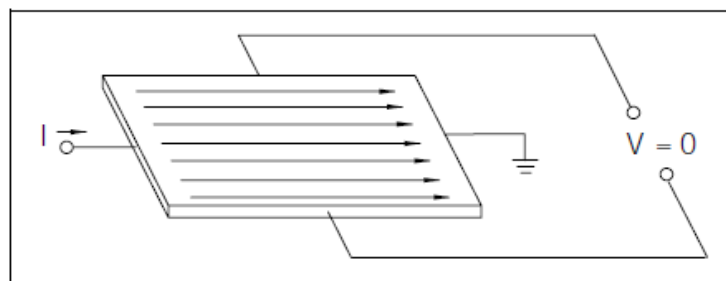


Figure 2-1 Hall effect principle, no magnetic field

When a perpendicular magnetic field is present (Fig 2-2) a Lorentz force is exerted on the current. This force disturbs the current distribution, resulting in a potential difference across the sensors outputs. The resulting voltage is usually of the order of a few tens of millivolts so IC's incorporate on-board amplifiers to boost the output voltage swing.

